EVestG-Derived Action Potential Features as Potential Biomarkers for Monitoring Patients with Alzheimer's Disease in Response to Gamma tACS Therapy

by

Omid Ehsani

A Thesis Submitted to the

Faculty of Graduate and Postdoctoral Studies of the

University of Manitoba

in partial fulfilment of the requirements of the degree of

Master of Science

Department of Electrical and Computer Engineering

University of Manitoba

Winnipeg

Abstract

Alzheimer's disease (AD) is a progressive neurodegenerative disorder for which no definitive cure currently exists. Transcranial alternating current stimulation (tACS) at gamma frequency (40 Hz), combined with cognitive exercises (CE), has emerged as a promising non-invasive neuromodulation approach, with clinical studies reporting improvements in cognitive function. The vestibular system, an evolutionarily ancient sensory system, has extensive projections to cortical regions involved in cognition, and growing evidence links vestibular dysfunction to cognitive decline in AD. Electrovestibulography (EVestG) is a non-invasive technique that records vestibulo-acoustic neural activity and enables extraction of mini action potential (AP) waveform features reflecting underlying neural dynamics. Previous studies have demonstrated that EVestG-derived features can distinguish between AD and AD with cerebrovascular symptomatology (AD-CVD), suggesting sensitivity to both disease state and cerebrovascular burden.

This study investigates whether EVestG-derived AP features can capture differential neurophysiological responses to active versus sham tACS combined with cognitive exercises, using data from a double-blind, crossover clinical trial. Participants with AD and AD-CVD were assessed at baseline, post-treatment, and follow-up sessions. The analysis comprised two parts: AP area changes across pre-selected segments, followed by multivariate decomposition of AP waveform features using Principal Component Analysis (PCA) and Independent Component Analysis (ICA) to identify dominant and independent patterns across treatment conditions.

Results suggest that active tACS+CE was associated with more structured neurophysiological patterns compared to sham tACS+CE, although most comparisons did not reach statistical significance given the limited sample size. Timing-related features, particularly depolarization and

repolarization rise times, were especially sensitive to tACS intervention. Subgroup analysis based on the modified Hachinski Ischemic Score (HIS) revealed distinct response patterns, with participants having higher cerebrovascular burden showing delayed dynamics compared to those with lower HIS. Dynamic EVestG segments were more sensitive to intervention than static segments. These exploratory findings support the potential of EVestG-derived AP features as candidate biomarkers for monitoring neurophysiological responses to neuromodulation, emphasizing the need to consider cerebrovascular status in treatment evaluation.

Table of Contents

List of Tables

List of Figures

List of Abbreviations

AD	Alzheimer's disease
AD-CVD	Alzheimer's disease with cerebrovascular disease
EVestG	Electrovestibulography
FP	Field Potential
AP	Action Potential
tACS	transcranial alternating current stimulation
CE	Cognitive Exercises
HIS	Hachinski Ischemic Score
ADAS	Alzheimer's Disease Assessment Scale-Cognitive Subscale
MOCA	Montreal Cognitive Assessment
PCA	Principal Component Analysis
ICA	Independent Component Analysis
PC1	First Principal Component
IC	Independent Component
Δpost	Change between baseline and post-treatment
Δfollow	Change between post-treatment and follow-up
Tilt	**Directions**
BAL	Backward acceleration left ear
BAR	Backward acceleration right ear
CAL	Contralateral acceleration left ear
CAR	Contralateral acceleration right ear
IAL	Ipsilateral acceleration left ear
IAR	Ipsilateral acceleration right ear
RAL	Rotation acceleration left ear
RAR	Rotation acceleration right ear
UAL	Upward acceleration left ear
UAR	Upward acceleration right ear
PUL	Prone (Supine) upward left ear
PUR	Prone (Supine) upward right ear
PRL	Prone (Supine) rotation left ear
PRR	Prone (Supine) rotation right ear
Segment	**Description**
BGi	Baseline stationary phase before motion
OnAA	Acceleration phase during movement toward the midpoint
OnBB	Deceleration phase approaching the midpoint

RTC BGi	Baseline phase during return-to-center
RTC OnAA	Acceleration phase during return motion
RTC OnBB	Deceleration phase approaching the final position

Acknowledgements

First and foremost, I thank God for giving me the strength, patience, and opportunity to complete this thesis.

I would like to express my deepest gratitude to my advisor, **Professor Zahra Moussavi**, for her guidance, support, and valuable feedback throughout this work. Her insight, encouragement, and high standards have greatly shaped both this research and my growth as a graduate student.

I am also sincerely grateful to **Professor Brian Lithgow** and **Professor Ke Peng** for their knowledge, support, and thoughtful contributions to this research.

I would like to extend special thanks to **Dr. Zeinab Dastgheib** and **Dr. Sadegh Marzban** for their guidance and generous help along this journey. Their advice and encouragement played an important role in the progress of this work.

I am deeply thankful to my **parents** for their endless love, sacrifices, and belief in me. Their unwavering support has been the foundation of everything I have achieved.

Finally, I would like to dedicate this thesis to **Iranian students** who continue their academic journeys under hardship — facing internet blackouts, limited access to knowledge and global resources, and conditions of uncertainty and insecurity. Their perseverance in the pursuit of learning, despite these barriers, is a source of deep inspiration.

Chapter 1: Introduction

1.1 Motivation and Rationale

Alzheimer's disease (AD) is a progressive neurodegenerative disorder and the most common cause of dementia, accounting for an estimated 60–80% of all cases worldwide [1, 2]. Beyond the decline in memory, AD is associated with impairments in attention, executive function, spatial orientation, and the ability to perform daily activities.

In recent years, non-invasive neuromodulation techniques have emerged as promising therapeutic approaches for AD [3]. Among these, transcranial alternating current stimulation (tACS) at gamma frequency (40 Hz), particularly when combined with cognitive exercises (CE), has shown potential for improving cognitive function in individuals with dementia [4, 5]. Clinical trials have reported cognitive improvement following active tACS + CE intervention, with effects persisting beyond the stimulation period [5]. However, while these cognitive improvements are encouraging, they provide limited insight into the underlying neurophysiological mechanisms through which tACS exerts its effects. This is particularly important given that a substantial proportion of individuals diagnosed with AD also present with concurrent cerebrovascular pathology, a condition commonly referred to as Alzheimer's disease with cerebrovascular disease (AD-CVD) [6]. The coexistence of vascular and neurodegenerative pathology may influence how the brain responds to neuromodulatory intervention, as differences in cerebral perfusion, neurovascular coupling, and neural excitability can alter both the immediate and long-term effects of stimulation. Previous work from our research group has shown that the degree of cerebrovascular burden, as quantified by the modified Hachinski Ischemic Score (HIS) [7, 8], is associated with distinct patterns and timelines of treatment response [9]. Standard cognitive assessments such as the Alzheimer's

Disease Assessment Scale–Cognitive Subscale (ADAS-Cog), an 11-item instrument where lower scores indicate better cognitive performance [10], are widely used to evaluate treatment outcomes [5]. However, such assessments cannot distinguish whether differences in treatment response reflect distinct neurophysiological trajectories shaped by underlying vascular pathology. There is therefore a clear need for objective, neurophysiology-based tools that can monitor treatment-related neural changes and capture how those changes may differ depending on cerebrovascular status in this heterogeneous population.

The vestibular system, through its extensive projections to cortical regions involved in cognition [11], offers a potential window into neural function that may be affected in AD. Electrovestibulography (EVestG) is a non-invasive technique that records vestibulo-acoustic neural activity from electrodes positioned near the tympanic membrane during controlled passive whole-body vestibular stimulation [12]. The recorded signals contain field potentials (FPs) whose action potential (AP) waveform characteristics — including amplitude, width, slope, and timing — have been shown to reflect underlying neural dynamics [12, 13]. Importantly, previous EVestG studies have demonstrated that AP waveform features can distinguish between AD and AD-CVD with high classification accuracy, with AD typically presenting narrower AP waveforms and AD-CVD presenting broader waveforms reflecting distinct neurovascular pathophysiology [6, 14]. This diagnostic sensitivity to cerebrovascular burden suggests that EVestG may also be capable of capturing differential neurophysiological responses to treatment intervention depending on vascular status. However, to date, no published study has examined EVestG-derived features as markers of treatment response to tACS. The present thesis addresses this gap by investigating whether EVestG-derived AP features can serve as candidate biomarkers for monitoring neurophysiological responses to gamma tACS in participants with AD and AD-CVD.

One further consideration is why stimulation of the left DLPFC would be expected to influence vestibular-derived measures such as EVestG. The DLPFC — the cortical target of the gamma tACS intervention in the present study [15], is a multimodal associative region central to working memory, executive function, and spatial cognition, the same higher-order domains that vestibular input helps support. The vestibular system projects, via the thalamus, to a distributed cortical network — including parietal, insular, temporal, cingulate, and hippocampal regions — that underlies these spatial and mnemonic functions [11], and the DLPFC is densely interconnected with this fronto-parietal network. Because EVestG records peripheral vestibular afferent activity that is itself modulated by descending efferent feedback from central structures [12, 13], modulation of activity within this network by left-DLPFC stimulation could propagate to the vestibular periphery and produce measurable changes in EVestG-derived AP features. This provides a mechanistic rationale for using EVestG as a vestibular-based readout of the neurophysiological effects of left-DLPFC gamma tACS and complements the laterality argument developed in the presentation of the AP feature results (Section 4.1).

EVestG provides access to vestibular-cortical neural information that appears sensitive to both disease state and intervention effects, yet its potential for longitudinal treatment monitoring has not been systematically explored. Furthermore, conventional single-feature measures such as averaged AP area may not capture the full complexity of treatment-induced neural changes. To address this, multivariate decomposition methods — specifically principal component analysis (PCA), which identifies dominant shared variance patterns, and independent component analysis (ICA), which isolates statistically independent signal sources — were applied to the EVestG feature space to identify signal patterns that may reveal structured treatment effects across specific waveform features, vestibular segments, and timepoints. This thesis applies this combined EVestG

analysis framework to data from a double-blind, crossover clinical trial [15] comparing active and sham gamma tACS, both combined with cognitive exercises, in participants with AD and AD-CVD.

1.2 Objectives of the Thesis

The primary objective of this thesis is to investigate whether EVestG-derived AP features can characterize neurophysiological responses to gamma-frequency tACS combined with cognitive exercises in participants with AD and AD-CVD, and whether these responses differ according to cerebrovascular burden.

The specific objectives are:

1. To examine changes in EVestG-derived AP features across baseline, post-treatment, and follow-up assessments under active tACS combined with cognitive exercises (tACS + CE) and sham tACS + CE conditions.
2. To compare treatment-related EVestG changes between participants with lower cerebrovascular burden (HIS < 2) and higher cerebrovascular burden (HIS ≥ 2) based on the modified HIS. (The rationale for the threshold of 2 is provided in Section 3.1)
3. To identify dominant and independent signal patterns in EVestG features using PCA and ICA, applied as segment-selection tools to determine which vestibular recording segments contribute most to treatment-related variability.
4. To determine whether specific waveform features (e.g., AP area, depolarization and repolarization slopes and rise times), tilt orientations, and temporal movement phases are particularly sensitive to intervention effects.

1.3 Organization of the Thesis

This chapter introduced the motivation, rationale, and objectives of the study. The remainder of the thesis is organized as follows. Chapter 2 provides background on AD and its mixed subtypes, non-invasive neuromodulation therapies with emphasis on gamma-frequency tACS, the relationship between the vestibular system and cognition, and the principles and capabilities of EVestG. Chapter 3 describes the study methodology, including the clinical trial design, participant characteristics, EVestG recording procedure, feature extraction, and the two-phase analytical approach comprising AP area analysis and PCA/ICA-based multivariate decomposition. Chapter 4 presents the results, organized by AP feature analysis (dynamic and static conditions), ADAS-Cog score trajectories, and the PCA- and ICA-based trend analyses across treatment conditions and cerebrovascular burden subgroups. Chapter 5 discusses the findings in relation to stimulation effects, the role of cerebrovascular burden in modulating treatment response, temporal dynamics of AP waveform changes, comparisons with previous EVestG studies, and the potential clinical relevance of EVestG-derived biomarkers. Finally, Chapter 6 summarizes the main conclusions, contributions, limitations, and directions for future research.

Chapter 2: Background

2.1 Alzheimer's Disease and mixed subtypes

Alzheimer's disease (AD) is the most common form of dementia, accounting for an estimated 60–80% of all dementia cases worldwide [1]. The global prevalence of dementia is projected to reach over 135 million by 2050, with AD representing the majority of cases, placing an enormous burden on healthcare systems and caregivers [1]. It is a progressive neurodegenerative disorder characterized by the accumulation of amyloid-beta plaques and neurofibrillary tangles composed of hyperphosphorylated tau protein, leading to synaptic dysfunction, neuronal loss, and gradual cognitive decline [2]. Clinically, AD manifests as progressive impairment in memory, language, executive function, and visuospatial abilities, ultimately affecting the ability to perform daily activities.

To date, AD can be definitively diagnosed only at autopsy. During life, it is classified as probable or possible AD based on clinical features [16]. The distinction between neuropathological changes and clinical symptoms has become increasingly blurred because of overlapping cognitive and behavioral features among dementia types [2]. Many patients present with both neurodegenerative and cerebrovascular pathology, resulting in mixed dementia, commonly referred to as Alzheimer's disease with cerebrovascular disease (AD-CVD) [6]. The clinical overlap between AD and AD-CVD complicates differential diagnosis, and existing diagnostic criteria are often insufficient to reliably distinguish between these conditions [6].

The Hachinski Ischemic Score (HIS), a 13-item clinical scale, is widely used to assess the contribution of cerebrovascular factors to cognitive impairment [7]. Scores between 4 and 7 typically indicate mixed dementia (AD-CVD), while higher scores suggest vascular dementia [7].

A modified version of the HIS, which incorporates neuroimaging information, has been proposed to improve diagnostic accuracy [6, 8, 14]. In the present study, a modified HIS with a threshold of 2 — rather than the conventional cutoff of 4 used to denote AD-CVD — was used to classify participants into subgroups with lower (HIS < 2) and higher (HIS ≥ 2) cerebrovascular burden. This lower, more conservative threshold was adopted because the aim here was not diagnostic classification but the detection of treatment-response differences associated with cerebrovascular burden: prior work [9] has shown that a cutoff of 2, compared with the conventional threshold of 4, reveals differences in treatment response between lower- and higher-burden participants that are otherwise missed. The rationale for this choice is detailed further in Section 3.1. Although the HIS provides a useful clinical framework for estimating cerebrovascular contribution, it was not designed to capture the specific neurophysiological mechanisms underlying disease progression or treatment response. This highlights the need for complementary neurophysiological measures that can detect subtle neural alterations linked to cognitive decline and differentiate underlying disease mechanisms at the physiological level.

2.2 Neuromodulation Therapies for Alzheimer's Disease

Despite decades of research, pharmacological treatments for AD remain limited in their ability to arrest or reverse disease progression, with most available medications offering only symptomatic relief [3]. This therapeutic gap has driven growing interest in non-invasive brain stimulation (NIBS) techniques as complementary or alternative approaches to modulating neural function in AD [3]. Among the most widely investigated NIBS methods are repetitive transcranial magnetic stimulation (rTMS), transcranial direct current stimulation (tDCS), and transcranial alternating current stimulation (tACS). rTMS uses brief magnetic pulses to induce electrical currents in targeted cortical regions and has shown some promise in improving memory and language function

in AD, although the results remain inconsistent across studies [3]. tDCS delivers a constant low-intensity current to modulate cortical excitability, with anodal stimulation generally enhancing neuronal firing rates; however, its effects in AD populations have been modest and variable [3]. In contrast, tACS delivers oscillatory electrical currents to the brain, enabling modulation of neural activity in a frequency- and phase-specific manner, making it uniquely suited to target specific neural oscillation patterns that are disrupted in AD [17, 18].

Among these approaches, tACS at gamma frequencies (approximately 40 Hz) has attracted particular attention because gamma oscillations play a critical role in cognitive processes including attention, memory encoding, and sensory binding [19]. In AD, gamma band activity is known to be disrupted, and restoring these oscillations through external stimulation has been proposed as a potential therapeutic mechanism [3]. Preclinical studies in animal models of AD have demonstrated that gamma frequency entrainment can reduce amyloid-beta deposition and promote microglial activation, providing a biological rationale for clinical translation [3].

At the cellular level, tACS is thought to modulate neural activity through subthreshold polarization of neuronal membranes [19]. Unlike direct current stimulation, which shifts the resting membrane potential in a polarity-dependent manner, tACS induces rhythmic fluctuations in membrane potential that can synchronize endogenous neural oscillations to the frequency of the applied current [17, 19]. When the stimulation frequency matches the brain's intrinsic oscillatory activity, tACS can enhance the amplitude and temporal coherence of these oscillations through resonance-like mechanisms [19]. In the context of AD, where gamma oscillations are weakened and desynchronized, 40 Hz tACS aims to restore this oscillatory activity by re-engaging the neural circuits responsible for gamma-band synchronization. Additionally, the after-effects of tACS — changes in neural activity that persist beyond the stimulation period — have been linked to

synaptic plasticity mechanisms, including long-term potentiation-like processes, suggesting that repeated sessions may produce cumulative neurophysiological effects [17, 18]. These mechanisms provide the theoretical basis for using gamma tACS as a tool to modulate cortical excitability and potentially improve cognitive function in neurodegenerative populations. To maximize therapeutic benefit, tACS has been combined with concurrent cognitive exercises (CE), based on the rationale that engaging cognitive networks during stimulation may enhance the neuroplastic effects of the intervention [4].

To evaluate the cognitive effects of neuromodulatory interventions in AD, the ADAS-Cog [10] is widely used as a primary outcome measure [5]. Clinical studies applying gamma-frequency tACS alongside cognitive training have reported improvements in ADAS-Cog scores, with some studies showing sustained effects beyond the stimulation period [3, 4, 5]. These findings suggest that tACS may modulate neural circuits involved in cognition, potentially offering therapeutic benefits in neurodegenerative conditions.

2.3 Vestibular System and Cognition

The vestibular system is an evolutionarily ancient sensory system that plays a fundamental role in maintaining balance and spatial orientation. Through reflex pathways such as the vestibulo-ocular reflex, which stabilizes vision during head movement, and vestibulo-spinal reflexes, which maintain postural alignment, the vestibular system provides continuous information about head motion and position [20]. Beyond these reflexive functions, vestibular inputs project through the brainstem to subcortical and cortical regions, contributing to higher-order cognitive processes including spatial memory, navigation, and orientation [11]. Vestibular projections reach multiple cortical areas, including the parieto-insular vestibular cortex, the temporoparietal junction, the

hippocampus, and the prefrontal cortex — regions that are critically involved in spatial processing, memory consolidation, and executive function, and that are among the earliest affected in AD [11]. With aging, vestibular performance declines, and accumulating evidence suggests that reduced vestibular performance in older adults is associated with impairments in spatial cognition, including mental rotation and navigation abilities [21]. Emerging evidence from both population studies and neurophysiological investigations links vestibular decline — encompassing peripheral loss and central processing deficits — to cognitive impairment and AD [11, 21]. The mechanisms linking vestibular decline to cognitive impairment are not fully understood but may involve reduced hippocampal input due to deafferentation of vestibular pathways, leading to hippocampal atrophy and impaired spatial memory formation [11]. Such deficits also characterize individuals with AD. Furthermore, patients with AD exhibit greater vestibular impairment compared to age-matched healthy controls, and vestibular dysfunction has been linked to disproportionately greater cognitive deficits [22, 23]. These findings suggest that vestibular-related neural pathways may play a critical role in the progression and manifestation of cognitive decline in dementia.

2.4 Electrovestibulography (EVestG) as a tool for Neurophysiological Changes

Electrovestibulography (EVestG) is an emerging, non-invasive technique that records vestibulo-acoustic neural activity using electrodes positioned near the tympanic membrane. During EVestG recordings, participants undergo controlled passive whole-body movements administered via a hydraulic chair, which elicits vestibular responses under standardized conditions. These responses are recorded across multiple movement directions and phases, generating a comprehensive profile of vestibular neural activity [12, 13]. The detailed recording protocol is described in Section 3.2. The recorded signals contain neural mini field potentials (FPs) — short, synchronized extracellular voltages produced by the collective firing of vestibular and acoustic afferent fibers — which appear

as compound action potential–like waveforms when averaged [12]. Because FPs are typically buried in physiological and environmental noise, a neural event extraction algorithm, known as NEER, is used to isolate and average these FPs along with their firing time intervals, providing a representation of underlying neural activity [12].

EVestG has demonstrated considerable promise in identifying neurophysiological alterations associated with neurodegenerative conditions, including AD [12, 13]. These alterations likely reflect disruptions within vestibulo-cortical circuits that contribute to cognitive processing [12, 13]. In EVestG recordings, the action potential (AP) (Figure 2.d) appears as the steep, V-shaped component of the averaged field potential waveform, corresponding to the rapid depolarization–repolarization cycle generated by synchronized firing of vestibular afferent neurons [12, 13]. Based on prior EVestG studies [12, 14], changes in the depolarization phase of the averaged FP waveform have been attributed to or interpreted as reflecting alterations in Na^+ channel dynamics, although direct measurement of ion channel activity was not performed. These interpretations are based on analogy with known intracellular AP physiology and observed waveform differences between clinical populations. In AD, alterations such as up-regulation of Na^+ channels can lead to a narrower and steeper AP waveform, whereas cerebrovascular pathology and altered K^+ channel expression may result in a broader AP with slower repolarization [6]. Consequently, quantitative differences in AP waveform characteristics — such as amplitude, width, and slope — serve as non-invasive proxies for ion channel dynamics and offer mechanistic insights into neurodegenerative pathophysiology [6, 14].

Importantly, EVestG has also demonstrated the ability to distinguish between AD and AD-CVD, with classification studies reporting high accuracy based on differences in the averaged field potential (FPave) AP waveform shape [6]. Specifically, AD typically presents with a narrower AP

waveform, whereas AD-CVD shows broader waveforms, reflecting distinct neurovascular pathophysiology [6]. In addition, EVestG-derived biomarkers have shown potential in predicting response to neuromodulatory interventions. For instance, baseline EVestG features, including firing interval dynamics, have been associated with differential responses to 40 Hz tACS combined with cognitive exercises, with variations depending on the cerebrovascular burden as quantified by the modified Hachinski Ischemic Score [7, 8] — a version of the original HIS that incorporates neuroimaging data to improve classification of vascular contributions to dementia [6, 14, 33]. The application of the modified HIS in the present study is described in detail in Section 3.1. These findings suggest that EVestG not only captures disease-specific neural alterations but also provides a sensitive and objective measure for evaluating and predicting treatment-related neurophysiological changes [6, 14].

Combining these EVestG-derived neurophysiological features with the modified HIS-based classification [7, 8] provides a framework for analyzing how neuronal changes in different patient subgroups — distinguished by cerebrovascular burden — relate to treatment response and clinically significant cognitive outcomes. This approach forms the basis of the present study.

Chapter 3: Methodology

This chapter describes the study design, data acquisition, and analytical methods used to investigate the effects of Real/Sham tACS combined with cognitive exercises on EVestG-derived neural activity. Section 3.1 outlines the clinical trial design and participant characteristics. Section 3.2 describes the EVestG recording procedure and signal extraction. Section 3.3 details the two sets of data analysis: AP feature extraction and statistical comparison (Section 3.3.1), followed by multivariate decomposition using PCA and ICA for segment selection and trend analysis (Section 3.3.2).

3.1 Study Design

Thirty-four out of the 42 individuals with AD or AD-CVD, who participated in the clinical trial [15] receiving real and/or sham tACS paired with cognitive exercises in a cross-over study design, were also assessed by EVestG pre- and post-intervention. All participants signed an informed consent approved by the Biomedical Research Ethics Board of the University of Manitoba. The study experiments were conducted in accordance with the Declaration of Helsinki. This EVestG study was a sub-study of the main clinical trial [15]. Participants were randomly assigned to two treatment sequences: one group first received active tACS combined with CE (real tACS + cognitive exercises) followed by a washout period and then sham tACS + cognitive exercises, while the other group received the treatments in the reverse order [15]. Each treatment block consisted of 4 weeks of intervention followed by an assessment, with a washout period of around two months between the two treatment blocks. For the purposes of the present EVestG substudy, analyses focused on comparing the neurophysiological outcomes between the active tACS + cognitive exercises condition and the sham tACS + cognitive exercises condition using three

assessment timepoints: baseline (week 0), post-intervention (week 5), and follow-up (two months post-intervention) (Figure 1).

The number of this study's participants (34) was smaller than the number of total participants (42) of the main clinical trial [15] because not everyone was eligible for EVestG recording at the allotted time for baseline recording due to earwax buildup or ear inflammation. In addition, several of the 34 participants missed the last assessment due to earwax, attrition, and/or scheduling difficulties. As a result, complete EVestG data across all crossover timepoints were not available for most participants, and the analysis was therefore limited to the first three assessments (baseline, post-intervention, and follow-up) rather than the full crossover sequence. This implies that the EVestG data was not analyzed as a crossover design. Instead, each treatment condition was treated independently across a consistent set of three assessment timepoints, which also has the advantage of avoiding potential carryover confounds between treatment blocks.

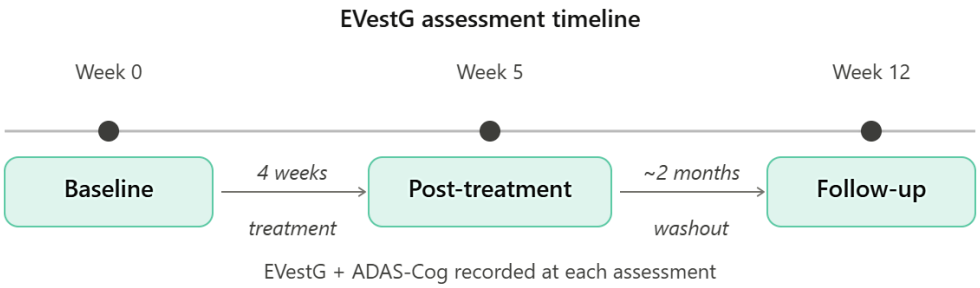

Figure 1. EVestG assessment timeline. Three assessment timepoints were used in the present study: baseline (week 0), post-treatment (week 5), and follow-up (week 12), with EVestG and ADAS-Cog recordings obtained at each session.

Participants (aged 50–90 years) were proficient in English or Spanish and had no history of neurological or mental illnesses. They were either not receiving medication for AD or were on a stable dose for at least three months before enrollment. They were enrolled if their Montreal

Cognitive Assessment (MoCA) [24] score was between 5 and 25. Additional exclusion criteria, described in the main clinical study [15], included any history of major neurological disorders. The demographic and baseline characteristics of the EVestG study participants, including mean age, sex distribution, and MoCA scores for each group, are summarized in Table 1.

Each real/sham treatment block included 4 weeks of intervention (five days per week; two 30-minute sessions per day), followed by an assessment and with a protocol-specified washout of at least 8 weeks between blocks [5, 15]. The realized washout averaged 11.3 weeks for the real-first sequence and 10.7 weeks for the sham-first sequence [5]; adherence to the planned schedule was affected by participant health, weather-related transportation difficulties, and travel [5]. The gamma tACS stimulation utilized a sinusoidal waveform at 40 Hz with a current amplitude of 1.5 mA peak-to-peak, targeting the left dorsolateral prefrontal cortex (DLPFC), while the reference electrode was on the contralateral supraorbital region [15]. For the sham condition, the same electrode configuration was used. The Soterix device delivered a brief ramp-up of current intensity over 30 seconds followed by a ramp-down to 0 mA over another 30 seconds at the beginning of each session, and a similar ramp-up and ramp-down within the final minute, with no current delivered during the remainder of the session [5]. This protocol ensured that participants experienced the initial and final skin sensations associated with stimulation. Participants engaged in cognitive tasks during all stimulation sessions using the MindTriggers app [4, 25] on an iPad.

To provide additional context for EVestG analysis, data from 19 healthy control participants from a previous study [6] were included as descriptive reference only. The healthy controls did not receive treatment and underwent only a single-session EVestG recording. Table 1 also presents the demographic information of the participants.

To account for the effect of CVD on patients' treatment response, we calculated the modified Hachinski Ischemic Score [7, 8, 14], based on a 13-item scale, which is commonly used to assess cerebrovascular contributions to cognitive decline [7]. Specifically, participants were categorized into subgroups with low CVD (HIS<2) and higher CVD (HIS≥2). This classification was used to evaluate potential effects of cerebrovascular pathology and vascular-related medical history, as CVD and impaired cerebral blood flow may influence neural firing properties and treatment responsiveness. Previous studies indicate that lower HIS values are more consistent with AD, whereas increasing HIS values reflect AD with cerebrovascular involvement [7, 8, 14]. In particular, using a lower HIS threshold has been shown to improve discrimination between AD and mixed-AD populations, with improved classification accuracy when scores below 3 are considered representative of only AD pathology [6, 14]. Accordingly, a HIS cutoff of 2 was selected in this study to conservatively separate participants with minimal cerebrovascular burden from those with CVD. A pilot study [9] demonstrated that using a lower HIS threshold of 2, compared to the conventional threshold of 4, revealed significant differences in treatment response between AD and AD-CVD subgroups that were not apparent at the higher threshold [9]. Another study [6] used a modified HIS with a threshold of 3 as the highest acceptable score for AD classification, and a range of ≥ 4 to ≤ 7 for AD-CVD, with mean HIS scores of 1.8 ± 1.2 and 5.6 ± 1.4 for the AD and AD-CVD groups, respectively. In contrast, the present study adopted a more conservative threshold of 2, based on [9], which demonstrated that this lower cutoff reveals significant treatment response differences not apparent at higher thresholds. This finding supports the use of a more conservative cutoff to capture cerebrovascular contributions that may otherwise be missed. The present study adopts this threshold of 2 to enable comparison with that work and to maximize sensitivity to cerebrovascular effects on neurophysiological treatment response.

Groups	BASELINE CHARACTERISTICS			
	Number	***Sex***	***Age (μ ± SD)***	***MoCA (μ±SD)***
Real tACS+CE	17	9 Females/ 8 Males	71.13 ± 8.43	15.76 ± 6.23
Sham tACS+CE	17	5 Females/ 12 Males	75.44 ± 9.81	15.67 ± 4.79
Control	19	10 Females/ 9 Males	65.50 ± 4.9	26.75 ± 1.88

Table 1. DEMOGRAPHIC AND BASELINE CHARACTERISTICS OF STUDY PARTICIPANTS

3.2 Electrovestibulography (EVestG) Recording

EVestG recordings were conducted in a controlled environment within a sound-attenuated and electromagnetically shielded chamber to minimize external noise and interference. Participants were seated in a hydraulic chair designed to deliver precise, controlled passive whole-body movement stimuli. To minimize muscle artifacts, participants were instructed to remain relaxed, keep their eyes closed, with their heads supported throughout the recording session. Gelled electrodes were positioned near the tympanic membranes to capture vestibular-driven neural signals. Reference electrodes were placed at the outer ear canal, and a common ground electrode was positioned on the forehead. To ensure good signal quality and reduce thermal and biological noise, custom cotton-wool-tipped electrodes were used [26] (Figure 2.e).

During each EVestG session, participants experienced a series of passive body movements administered via the hydraulic chair to elicit vestibular responses under controlled conditions (Figure. 2a–c). These movements included:

1. Vertical Translation: 15 cm upward and downward movements while participants were seated upright.
2. Supine up: 15 cm upward and downward movements while participants were lying supine.

3. Lateral rotation: 40° rotation to the right side and return to the starting position while seated upright.
4. Supine rotation: 40° rotation to the right side and return to the starting position while seated supine.
5. Forward and Backward tilts: 40° tilts in the sagittal plane while in an upright seated posture.
6. Lateral tilts: Ipsilateral right and contralateral left tilts from an upright sitting position, followed by a return-to-center (RTC) and tilts to the opposite side (ipsilateral left and contralateral right).

Each tilt consists of three primary movement phases: stationary (Figure 2. BGi, 1.5 seconds prior to motion), acceleration (OnAA), and deceleration (OnBB) to the midpoint, lasting 3 seconds in total. These phases were repeated during the return-to-center (RTC) phase, capturing a total of six segments for each directional movement (BGi, OnAA, OnBB, RTC BGi, RTC OnAA, and RTC OnBB). Each phase lasted approximately 1.5 seconds, ensuring consistency and control across trials to facilitate reliable analysis of vestibular-driven neural signals [12, 13].

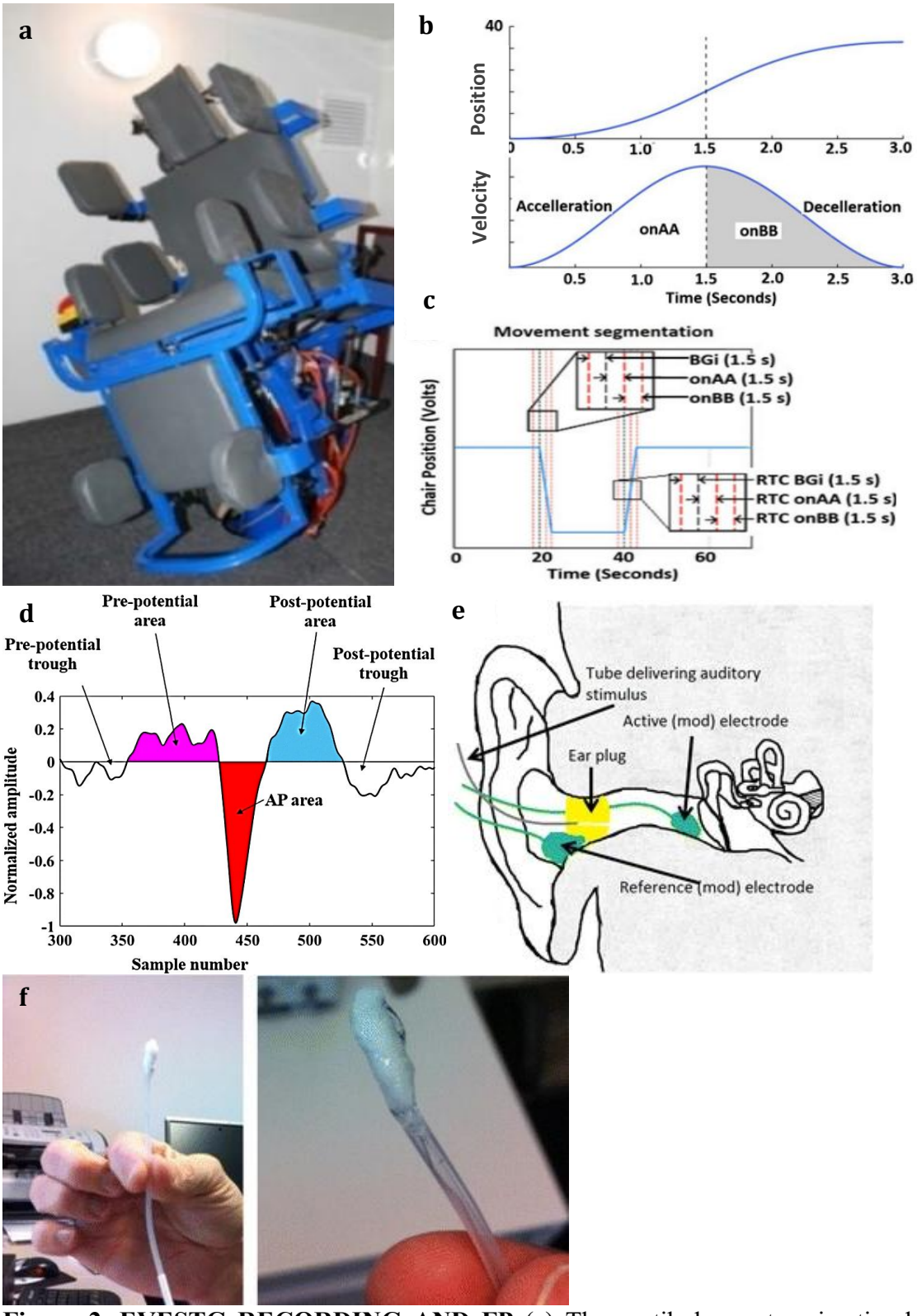

Figure 2. EVESTG RECORDING AND FP (a) The vestibular system is stimulated in the bed/chair's sitting and supine positions [12]. (b) The bed motion's positional and velocity

characteristics [12]. (c) A 20-second motionless period followed by 3-second motion, 17 seconds of stationary motion make up the full stimulus (bed movement pattern). The three movement phases are onAA (the first 1.5 seconds of motion, or the acceleration phase), onBB (the latter 1.5 seconds of the 3-second movement phase, or the deceleration phase), and BGi (the 1.5 seconds just before movement) [12]. (d) The sketch of an averaged FP. (e) Electrode placement: active electrode positioned proximal to the tympanic membrane; reference electrode at the base of the ipsilateral ear canal (incisura) [26]. (f) Custom cotton-wool-tipped electrode [26].

The NEER algorithm [12] was employed to analyze the EVestG signals. The NEER algorithm applies a complex Morlet wavelet transform and matching filter to detect FPs that are hidden within noise. FPs are extracellular electrical signals produced by the overlapping activity of groups of neurons activated by hair-cell stimulation [12]. Each FP has a V-shaped waveform – action potential (AP) – that begins near baseline, reaches a negative peak, and returns toward baseline (Figure 2.d). The NEER algorithm efficiently extracts these FPs, averaging them to generate characteristic waveforms that represent the underlying neural activity.

3.3 EVestG Data Analysis

The analysis in this study was conducted by two approaches. First, we focused on extracting features from action potential (AP) using predefined segments similar to those identified in earlier pilot studies [6, 14]. Second, the analysis was extended to include additional AP characteristics, particularly time- and magnitude-based measures of the AP waveform, such as depolarization and repolarization rise times, slopes, and peak index. Principal Component Analysis (PCA) and Independent Component Analysis (ICA) were then applied to identify the most informative features. Subsequently, the temporal trends of segments identified as dominant by PCA and ICA were assessed by averaging their corresponding feature values across sessions.

3.3.1 Action Potential (AP) Feature Analysis

After the initial extraction of the averaged FP curve, several preprocessing steps were applied to ensure the quality and consistency of the data. These steps included normalization of the signals

and the application of three quality-control criteria based on the original EVestG methodology [6]. A recording segment was excluded if any of the following conditions were met: (1) more than one action-potential notch was detected between the pre-potential and post-potential waveforms, indicating a noisy or ambiguous signal; (2) the absolute peak value of either the pre-potential or the post-potential exceeded two-thirds of the absolute AP peak amplitude, suggesting disproportionate non-AP activity; or (3) the AP width measured at the baseline (zero-voltage line) was 25 samples or fewer, indicating a signal too brief to be physiologically plausible. Segments failing any of these criteria were excluded before subsequent normalization and further analysis. In this work, the focus was on the AP region of the FP signals (Figure 2.d), as this portion is key to understanding the underlying neural dynamics [6, 14]. Accordingly, the steepness and narrowness of the AP's ascending and descending arms have been associated with Na+/K+ channel activity and possible GABA-related firing-pattern alterations [12, 14]. Pilot studies have shown significant changes in the AP region in response to vestibular-motion stimulation. In addition, the narrowness of the AP part may represent changes in the number of ion channels [6, 14]. Therefore, the steepness of the AP's arms–both the ascending and descending phases–can reflect changes in ion channel activation within neurons [12, 14]; hence, the area above the action potential, measured relative to the zero baseline, was used as a feature to capture the overall characteristics of the AP. The averaged AP area (i.e., the 84 segments of both ears' EVestG signal) for each participant was compared across the groups and assessments. Statistical analysis was conducted using a two-way ANOVA with treatment sequence as the between-subject factor and assessment session as the within-subject factor, followed by Bonferroni post-hoc correction to determine significant differences across treatment conditions. Since each participant provided a single measurement per condition at each session, no within-cell replication was available.

The EVestG feature-selection procedure was not performed in a post-hoc manner and did not include any information from the present treatment outcome analysis. Instead, segment selection was based on an independent, previously established study [6]. Although the feature selection was based on the prior study [6] conducted independently of the current treatment analysis, both studies were conducted within the same research group using the same EVestG recording system. Of the 34 participants in the present study, 26 also contributed baseline EVestG recordings to the classification study [6], along with the same 19 healthy controls used as a descriptive reference. However, the features selected in [6] were derived solely from baseline diagnostic classification between AD, AD-CVD, and healthy controls, and did not incorporate any treatment-related or longitudinal data from the present study. While this separation reduces the risk of direct circularity, the substantial overlap in participants means that the pre-specified segments may be optimized for this particular cohort. Full external validation with an independent cohort would be needed to confirm the generalizability of these biomarkers.

In the previous classification study [6], 84 segments (6 motion phases × 7 tilts × both ears) were analyzed using a step-by-step feature-extraction framework. Features were initially filtered based on statistical significance ($p<0.05$) and subsequently reduced using a linear support vector machine (SVM) with repeated 10-fold cross-validation. The feature-selection process was repeated across multiple random training-test splits (with 20% held out in each iteration) and only features consistently selected in more than 50% of repetitions were retained as stable biomarkers [6]. The high-performing segments identified in that independent study (OnBB, RTC-OnAA, BGi, RTC-BGi) were pre-specified prior to the present tACS analysis. Importantly, no information regarding the current part 1 of this study's cognitive outcomes was incorporated into the feature-selection process. Additionally, another pilot study found that specific segments yielded higher

classification accuracy and were most relevant for capturing AP dynamics associated with tACS effects [12, 27].

Therefore, the onBB and RTC-onAA segments from the Supine-up tilt, and the BGi and RTC-BGi segments from the Up/Down tilt, were selected as pre-specified biomarkers for the feature-selection process in the first phase of this study. A pilot study demonstrated that tACS effects on cortical excitability are complex: stimulating an identical cortical area with the same waveform does not always yield the same outcome, as these effects depend on the existing balance between cortical excitation and inhibition [28].

To further reduce the dataset, the AP areas from the onBB and RTC-onAA segments (the deceleration and return-to-center acceleration phases, as described in Section 3.2) of the Supine-up tilt signals were averaged together and defined as dynamic condition. The averaged AP area from the BGi and RTC-BGi segments (the stationary phases before and during return-to-center) of the Up/Down translation was used as the static condition. By segmenting the data into dynamic and static conditions, we could examine how tACS influenced neural activity under different movement conditions. The dynamic segments (OnBB and RTC-onAA) capture evoked vestibular response to motion and therefore can show larger, more phase-locked AP changes, whereas the static segments (BGi and RTC-BGi) are recorded without head movement and serve as a baseline representation of spontaneous vestibular neural activity [6, 14].

3.3.2 PCA/ICA Analysis

For this analysis, features were extracted from the characteristics of the AP waveform as illustrated in Figure 3. These features were selected to quantify the shape, timing, and magnitude of the neural response reflected in the EVestG signal. Because the AP waveform contains distinct phases of activation and recovery, measurements obtained from this waveform can provide meaningful descriptors of the underlying neural activity.

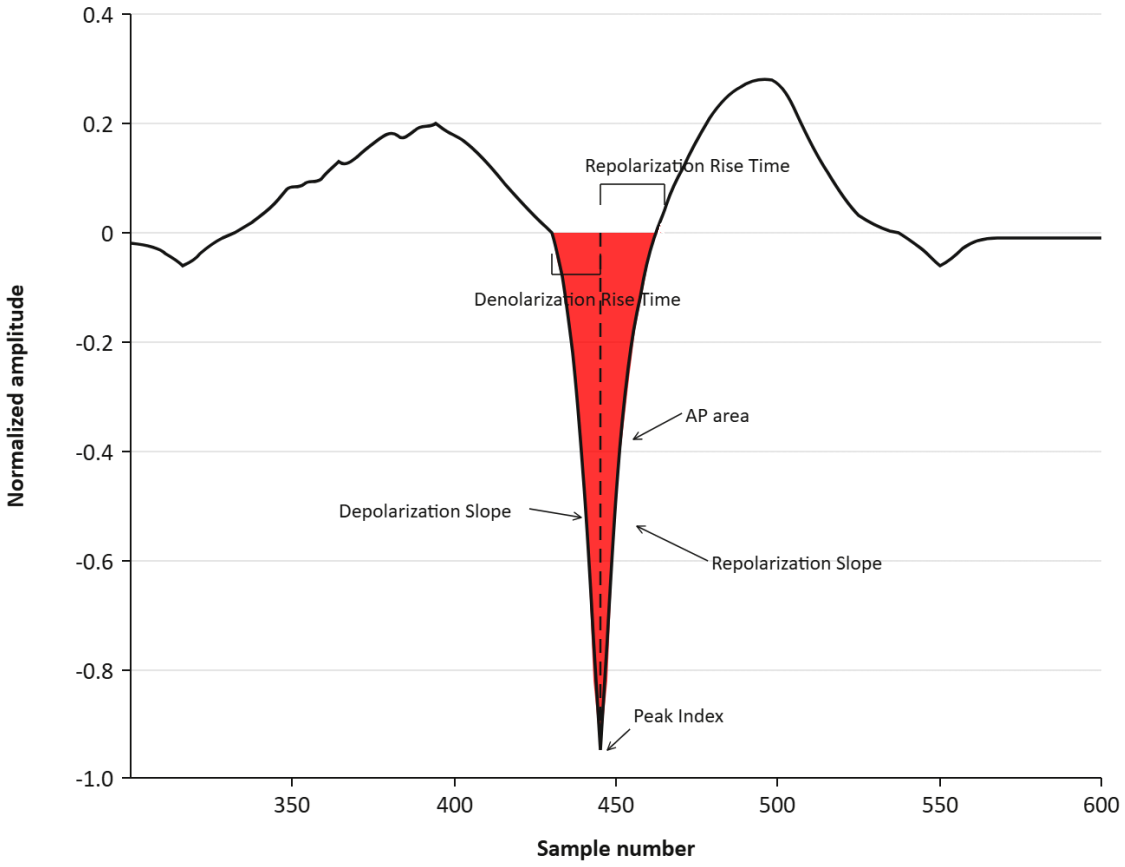

Figure 3. Averaged field potential (FP) waveform and extracted EVestG features. The schematic illustrates the key descriptors, including depolarization and repolarization slopes, rise times, AP area, and peak index, which together quantify the waveform's amplitude, timing, and shape characteristics. The depolarization and repolarization slopes are estimated over defined segments of their respective phases (e.g., between onset and peak for depolarization, and between peak and return to baseline for repolarization), representing the overall rate of change in each phase rather than a single-point derivative.

The depolarization slope describes the steepness of the descending part of the AP waveform as the signal moves from the pre-potential region toward the main negative peak. It is estimated as the overall rate of change in amplitude over the depolarization phase — that is, the amplitude difference between the onset of the main negative deflection and the AP peak, divided by the duration of that interval — rather than a single-point derivative. A steeper depolarization slope indicates a more rapid drop in amplitude and therefore a faster activation-related change in the recorded neural signal. The depolarization rise time represents the duration of this phase, measured as the time interval between the onset of the main negative deflection and the AP peak. In other words, it reflects how long the waveform takes to travel from the beginning of depolarization to its maximum negative amplitude.

The repolarization slope describes the steepness of the recovery phase after the AP peak. It is estimated as the overall rate of change in amplitude between the AP peak and the point where the waveform returns toward baseline, divided by the duration of that interval. This feature reflects the speed of recovery of the recorded neural response. The repolarization rise time represents the duration of the repolarization phase and is measured as the time interval between the AP peak and the point where the waveform returns toward baseline after the main negative peak. Together, the repolarization slope and repolarization rise time characterize how quickly and over what duration the signal recovers following the peak response.

The peak index identifies the temporal location of the AP peak, which corresponds to the maximum negative deflection of the waveform. In this study, it is defined as the sample-index at which the minimum amplitude occurs within the AP waveform. This feature provides information about the timing of the main neural response and can reflect changes in temporal synchronization across

conditions. A shift in peak-index indicates that the strongest part of the response occurs earlier or later in the waveform.

The AP area was used to quantify the overall magnitude of the action potential. It is measured as the area under the main AP waveform, specifically around the negative-peak relative to baseline. This feature reflects the integrated strength of the neural response, rather than only its instantaneous amplitude at one point. Unlike the peak-index, which captures timing, or slopes, which capture the rate of change, the AP area summarizes the cumulative size of the response over the duration of the AP.

These features were selected because they capture complementary aspects of the waveform. The slope measures describe the rate of change, the rise time measures describe the duration of the main activation and recovery phases, the peak index describes the timing of the maximum response, and the AP area describes the overall magnitude of the signal. Taken together, these features provide a comprehensive set of descriptors for characterizing both the FP wave and the underlying AP-related neural dynamics reflected in EVestG recordings.

To explore underlying data patterns and reduce dimensional redundancy among the extracted EVestG features, two complementary multivariate decomposition methods —principal component analysis (PCA) and independent component analysis (ICA)— were applied. These two methods were selected because they capture different aspects of the data structure: PCA identifies dominant shared variance patterns, while ICA isolates statistically independent source components that may reflect distinct physiological processes [29, 30]. PCA was first employed to identify dominant directions of variance across participants and features, enabling visualization of which waveform characteristics contributed most to the overall variability and to treatment-related changes [29]. This unsupervised method transforms correlated variables (e.g., AP area, slopes, and rise

times) into orthogonal principal components that capture the maximal variance in the dataset, thereby highlighting dominant patterns without assuming prior knowledge of class labels [29]. Subsequently, ICA was used to separate statistically independent source patterns within the same feature space [30]. While PCA emphasizes variance maximization, ICA focuses on statistical independence, which can isolate physiologically distinct response processes that may exist within the EVestG signals [29, 30]. It should be noted that ICA assumptions (statistical independence) may not be perfectly met in biological signals; however, the method still provides valuable insights into potentially distinct physiological contributors to the recorded EVestG patterns. Applying both methods allows differentiation between dominant (shared) and independent (feature-specific) neural response components, providing a more complete characterization of vestibular-related electrophysiological dynamics. A similar PCA-based approach has been applied to EVestG data for identifying meaningful biomarker segments [26]. The addition of ICA in the present study extends this framework by providing a complementary perspective based on statistical independence rather than variance.

For each AP feature (e.g., AP Area, Depolarization Rise Time), a data matrix was constructed in which rows represented participants and columns represented the 84 EVestG segments (6 movement phases × 7 tilt directions × 2 ears). Each entry in the matrix contained the change in that feature's value between two consecutive assessment timepoints — specifically, the difference between post-treatment and baseline (Δpost), or the difference between follow-up and post-treatment (Δfollow). Separate matrices were constructed for each feature, each treatment condition (active tACS+CE and sham tACS+CE), and each time interval.

PCA was applied to each matrix by computing the covariance structure across segments and extracting the principal components. The first principal component (PC1) was examined as it

captures the direction of maximum variance across the 84 segments. The PC1 loadings — which quantify how strongly each segment contributes to this dominant variance pattern — were used to identify the most influential segments. Segments with the highest absolute PC1 loadings were selected for subsequent trend analysis. The percentage of total variance explained by PC1 was also recorded to assess how concentrated the variance structure was.

ICA was applied to the same data matrices to identify statistically independent source components rather than variance-maximizing components. While PCA decomposes the data based on orthogonality and maximum variance, ICA seeks components that are as statistically independent as possible, which can reveal feature-specific or subgroup-specific patterns that may be obscured by the dominant variance captured by PCA. The dominant independent component (IC1) loadings were extracted, and the segments with the highest absolute IC1 loadings were selected for trend analysis, analogous to the PCA procedure.

In both cases, PCA and ICA were used solely as segment-selection tools. The selected segments' original, non-transformed feature values were then averaged for each HIS subgroup and plotted across the three assessment timepoints to visualize temporal trends.

Chapter 4: Results

4.1 Action Potential (AP) Feature Analysis Results

The following sections present the EVestG-derived AP feature results across baseline, post-treatment, and follow-up assessments for both treatment conditions, classified by HIS subgroup. ADAS-Cog score trajectories from the main clinical trial [15] are presented alongside the EVestG results to provide cognitive context for interpreting the neurophysiological changes.

In the following sections, the area under the AP curve was calculated as the AP feature and averaged among the different segments for each participant at each assessment. The box-whisker plots show the minimum, maximum, median, and mean-values. In this study, tACS was applied using a sinusoidal 40 Hz waveform with the active electrode placed over the left dorsolateral prefrontal cortex (DLPFC) and the return electrode on the contralateral supraorbital region. Because vestibular afferent pathways project ipsilaterally from the peripheral vestibular organs through the brainstem to cortical regions, stimulation of the left DLPFC is expected to preferentially modulate left-sided vestibulo-cortical circuits [4, 15]. Consistent with this, the left ear EVestG results showed stronger treatment-related effects and are therefore presented in this section. Moreover, the ANOVA analysis for both groups confirmed the left-ear results (real tACS + CE (cognitive exercises): $F(1, 125) = 5.19$, $p = 0.007$ & sham tACS + CE: $F(1, 125) = 2.90$, $p = 0.06$) were more significant, compared to the non-significant right-ear results (real tACS + CE: $F(1, 125) = 2.17$, $p = 0.12$ & sham tACS + CE: $F(1, 125) = 2.15$, $p = 0.13$). The denominator degrees of freedom (125) reflect the 42 EVestG segments per ear evaluated across three assessment sessions.

a

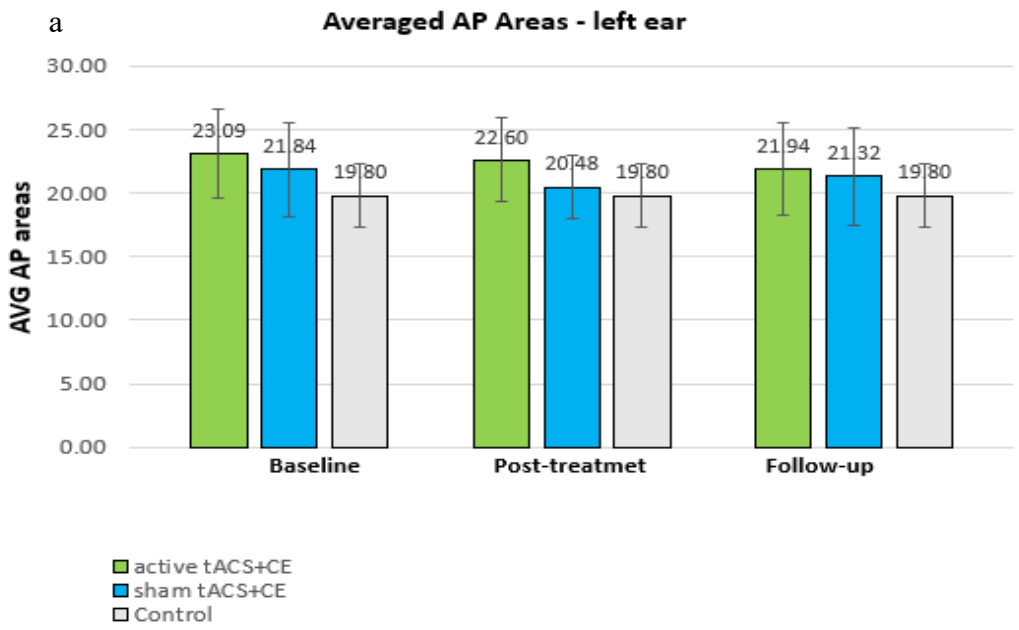
Averaged AP Areas - left ear
AVG AP areas
30.00
25.00
20.00
15.00
10.00
5.00
0.00
23.09
21.84
19.80
22.60
20.48
19.80
21.94
21.32
19.80
Baseline
Post-treatmet
Follow-up
active tACS+CE
sham tACS+CE
Control

b

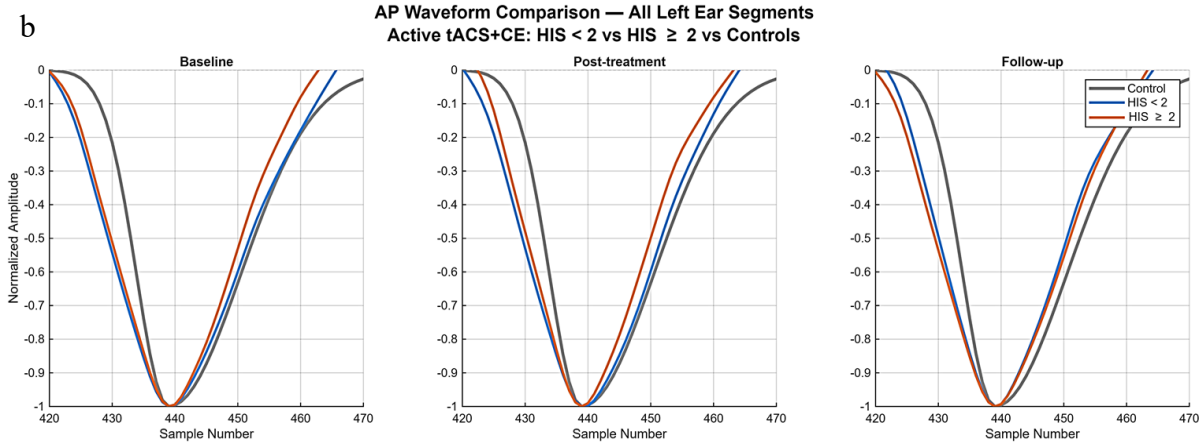
AP Waveform Comparison — All Left Ear Segments
Active tACS+CE: HIS < 2 vs HIS ≥ 2 vs Controls
Baseline
Post-treatment
Follow-up
Normalized Amplitude
Sample Number
Control
HIS < 2
HIS ≥ 2

c

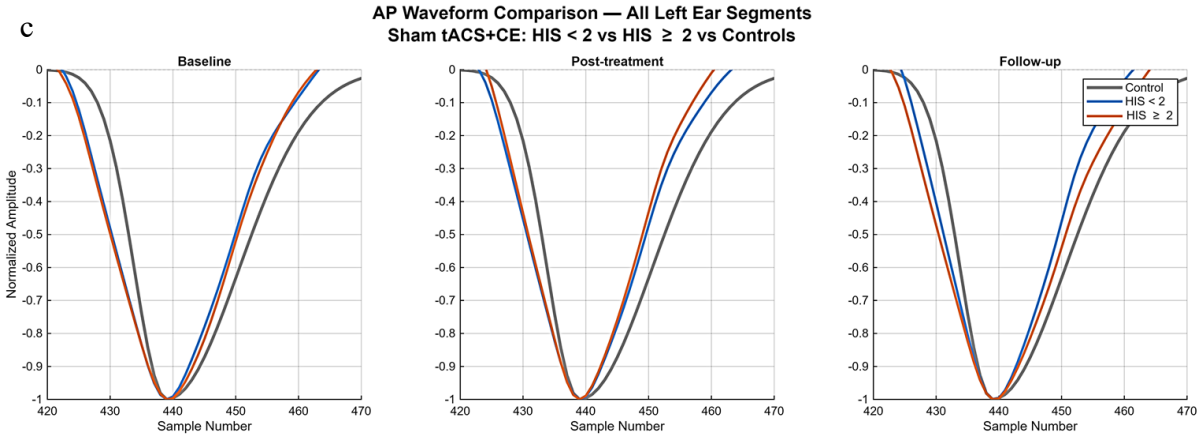
AP Waveform Comparison — All Left Ear Segments
Sham tACS+CE: HIS < 2 vs HIS ≥ 2 vs Controls
Baseline
Post-treatment
Follow-up
Normalized Amplitude
Sample Number
Control
HIS < 2
HIS ≥ 2

Figure 4. Averaged AP areas across all 42 segments (left ear). (a) For active tACS+CE (N = 17), sham (N = 17) tACS+CE, and healthy control groups (N = 19) at baseline, post-treatment, and follow-up. Error bars represent standard deviation. (b) & (c) Averaged left-ear AP waveforms for controls, HIS < 2, and HIS ≥ 2 groups at baseline, post-treatment, and follow-up during active tACS+CE and sham tACS+CE conditions.

Figure 4 shows the averaged AP areas across all 42 segments for the left ear, comparing active tACS+CE and sham tACS+CE conditions with healthy controls across the three assessment sessions. When all participants were considered together regardless of cerebrovascular status, AP area showed no clear session-to-session pattern, and the overall left-ear effect reported above (real tACS + CE: $p = 0.007$; sham tACS + CE: $p = 0.06$) was driven by ear-side and segment differences rather than by a uniform across-session change. This suggests that group-level averaging across all segments may obscure subgroup-specific treatment effects. Furthermore, because different vestibular segments capture distinct neural processes — with motion-evoked (dynamic) segments reflecting active vestibular responses and stationary (static) segments reflecting baseline neural activity — the 42 segments were separated into dynamic (OnBB and RTC-OnAA from the Supine-up tilt) and static (BGi and RTC-BGi from the Up/Down tilt) conditions, based on segments identified as most informative in prior EVestG classification studies [6, 14, 27]. To investigate whether distinct response patterns emerge when both cerebrovascular burden and segment type are accounted for, participants were subsequently stratified by HIS threshold (HIS < 2 vs HIS ≥ 2) and analyzed separately for dynamic and static conditions, as presented in the following sections. In addition to the AP area trends shown in Figure 4.a, the averaged AP waveforms in Figure 4.b and 4.c illustrate distinct response patterns between the HIS < 2 and HIS ≥ 2 subgroups. In both the active tACS+CE and sham tACS+CE conditions, the HIS < 2 group showed a mild decreasing trend across assessments, whereas the HIS ≥ 2 group showed an initial reduction from baseline to

post-treatment followed by a rebound at follow-up. These differences in AP waveform morphology between the HIS subgroups suggest that cerebrovascular burden may influence EVestG-derived treatment responses. The observed waveform differences are discussed further in chapter 5 in relation to findings from recent EVestG classification studies [6, 13].

4.1.1 AP Dynamic

The calculated AP-dynamic features were averaged across the onBB and RTC-onAA segments (deceleration and return-to-center acceleration phases) of the Supine-up tilt for each participant at each assessment. The box-and-whisker plots in Figure 5 display the distribution of averaged AP-dynamic areas for each subgroup at each session. The horizontal line within each box indicates the median, the × symbol marks the mean (with numerical value annotated), and the box edges represent the interquartile range. The -•- markers indicate the minimum and maximum values. Significance levels from post-hoc comparisons are indicated above the boxes, where * denotes $p < 0.05$ and ns denotes non-significant. Given the small subgroup sizes — particularly for HIS ≥ 2 — and the overlapping error bars, the patterns described below are reported as non-significant trends only and should be interpreted as indicative rather than conclusive.

In the real tACS + cognitive exercises group (Figure 5a), the results showed the following non-significant trends. Participants with HIS < 2 showed a decrease in mean AP-dynamic area from baseline (26.24) to post-treatment (20.33) and a further slight decrease at follow-up (20.15), consistent with a trend toward sustained reduction across sessions. For participants with HIS ≥ 2, the mean AP-dynamic area also decreased from baseline (21.08) to post-treatment (19.49) and then rose at follow-up (20.15), consistent with a partial-rebound trend. Both subgroups trended toward the healthy control mean over time. None of these pairwise comparisons reached statistical

significance, and the HIS ≥ 2 subgroup in particular (N = 6) is too small to support more than a tentative description.

In contrast, the sham tACS + cognitive exercises group (Figure 5b) showed a different pattern. Participants with HIS < 2 exhibited a slight increase in mean AP-dynamic area from baseline (18.24) to post-treatment (20.25), followed by a rebound decrease at follow-up (18.72). For those with HIS ≥ 2, the trend ran in the opposite direction: the mean decreased from baseline (17.96) to post-treatment (16.63), then rebounded at follow-up (21.30), diverging from the control value (19.84). None of the pairwise comparisons in the sham tACS + cognitive exercises group reached statistical significance.

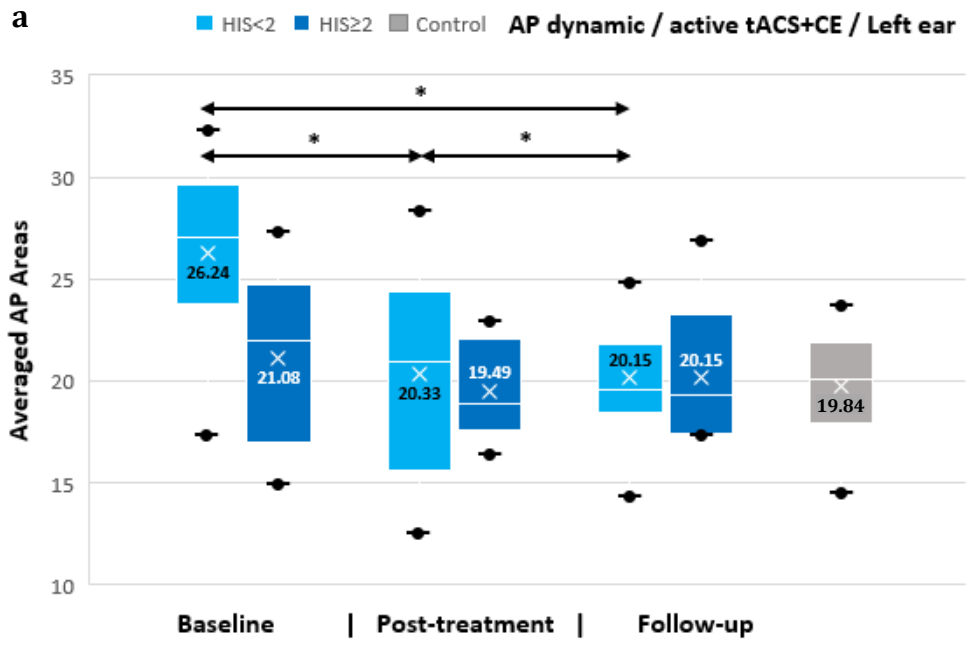

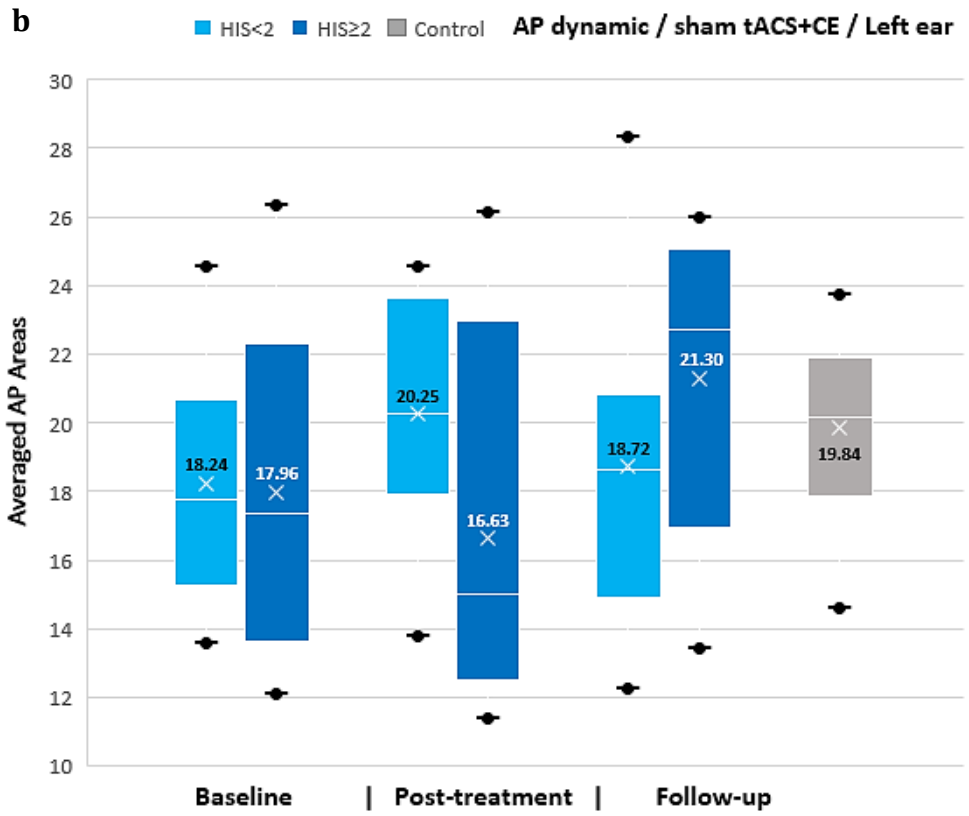

Figure 5. AP-DYNAMIC AREA CHANGES ACROSS STUDY PHASES CLASSIFIED BY TREATMENT GROUP AND HIS SCORES. EVestG-derived AP-dynamic area change measures, extracted from the left ears, are shown at baseline, post-treatment, and follow-up. -•- marks stand for minimum and maximum values of each data range. In addition, the intensity of changes based on the p-values were shown as * (p-value<0.05). No marks (*) means not significant. (a) All participants in the first group (active tACS + CE (cognitive exercises)), classified by HIS < 2 (N=11) and HIS ≥ 2 (N =6). (b) All participants in the second group (sham tACS + CE (cognitive exercises)), classified by HIS < 2 (N=10) and HIS ≥ 2 (N =7).

4.1.2 AP static

Across all participants, AP-static areas showed smaller changes from baseline to post-intervention and follow-up compared with AP-dynamic features, with group-specific and HIS-dependent differences. The box-and-whisker plots in Figure 6 follow the same format as Figure 5, with × indicating the mean, the horizontal line indicating the median, and -•- marking minimum and maximum values. As with the dynamic condition, all subgroup patterns below are non-significant

trends given the small cell sizes and overlapping distributions, except where a significant pairwise comparison is explicitly noted.

In the real tACS + cognitive exercises group (Figure 6a), participants with HIS < 2 showed an increase in mean AP-static area from baseline (22.96) to post-treatment (24.93), followed by a decrease at follow-up (20.91). Conversely, participants with HIS ≥ 2 exhibited a slight decrease from baseline (23.46) to post-treatment (22.37), followed by an increase at follow-up (24.46). A significant difference was observed between post-treatment and follow-up for the HIS < 2 group ($p < 0.05$), while other comparisons were non-significant. The HIS subgroups showed opposing directional trends during the wash-out period, which may indicate that the static condition reflects different aspects of neural modulation than the dynamic condition. Given the small subgroup sizes, this contrast is offered as a trend to be confirmed in larger samples rather than an established effect; the single significant pairwise comparison should likewise be interpreted cautiously in the context of multiple comparisons.

In the sham tACS + cognitive exercises group (Figure 6b), both subgroups showed a decrease from baseline to post-treatment, with HIS < 2 declining from 22.19 to 19.56 and HIS ≥ 2 from 21.25 to 19.64, both trending toward the control mean (19.77). During follow-up, participants with HIS < 2 remained near the post-treatment level (19.60), while those with HIS ≥ 2 increased to 21.68, diverging from the control value. None of the pairwise comparisons reached statistical significance.

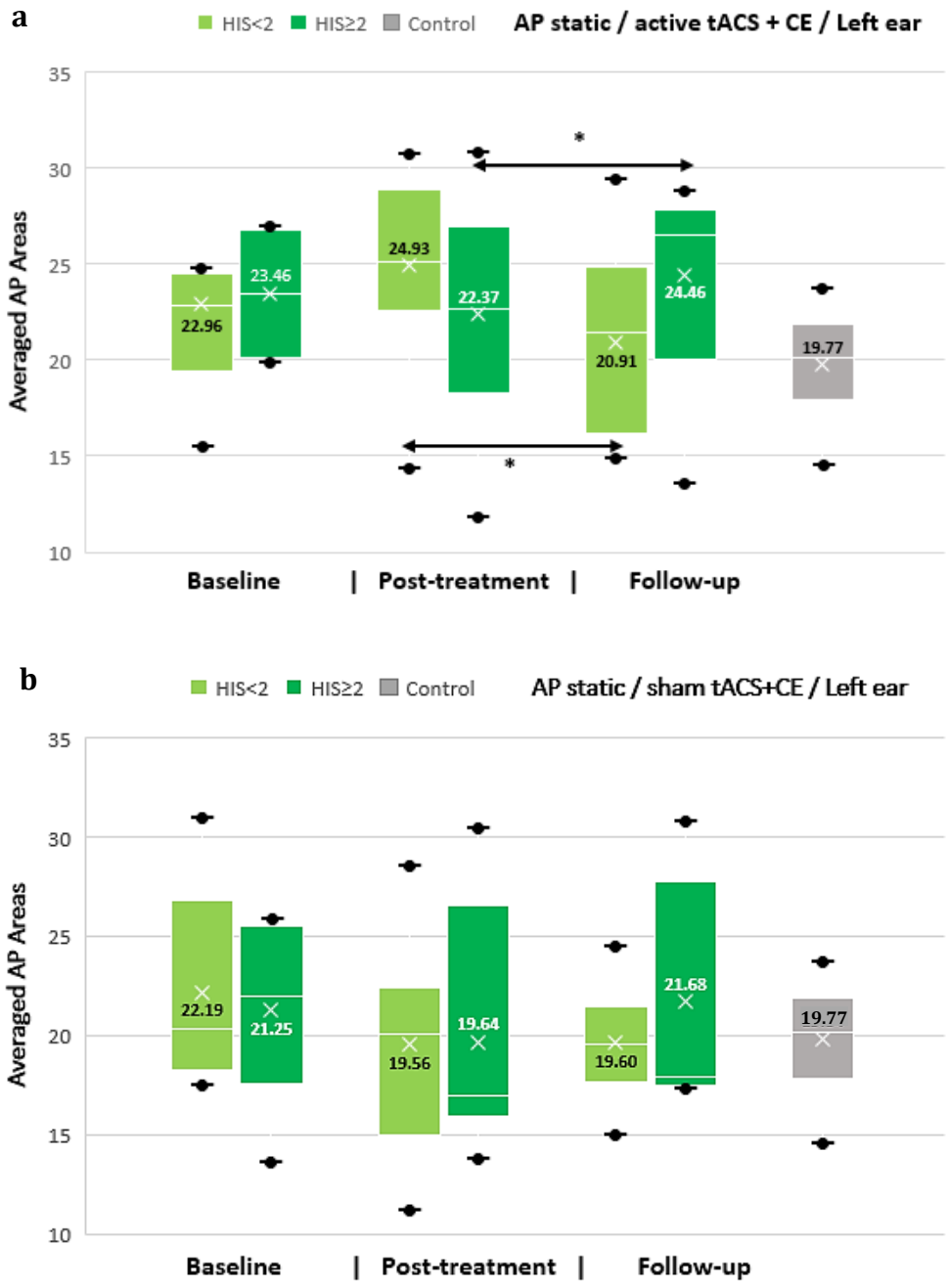

Figure 6. AP-STATIC AREA CHANGES ACROSS STUDY PHASES CLASSIFIED BY TREATMENT GROUP AND HIS SCORES. EVestG-derived AP-static area change measures, extracted from the left ears, are shown at baseline, post-treatment, and follow-up. -•- marks stand for minimum and maximum values of each data range. In addition, the intensity of changes based on the p-values were shown as * (p-value<0.05). No marks (*) means not significant. (a) All participants in the first group (real tACS + CE (cognitive exercises)), classified by HIS < 2 (N=11) and HIS ≥ 2 (N =6). (b) All participants in the second group (sham tACS+CE (cognitive exercises)), classified by HIS < 2 (N=10) and HIS ≥ 2 (N =7).

To provide cognitive context for the neurophysiological changes described above, ADAS-Cog score trajectories of the first 3 assessments of the main cross-over clinical trial [5] for the participants of this study are summarized below.

Across all participants (Figure. 7a), mean ADAS-Cog scores showed a general reduction (indicating cognitive improvement) over time in both real tACS + cognitive exercises and sham tACS + cognitive exercises groups. The first group demonstrated a consistent decrease from baseline to post-intervention and follow-up, whereas the second one shows a similar decreasing trend post-intervention followed by a rise at follow-up. This is consistent with a trend toward a longer-lasting effect.

In the subgroup of participants classified as HIS<2 (Figure. 7b), both groups showed a reduction in ADAS-Cog scores from baseline to follow-up. Those who received sham tACS + cognitive exercises exhibited higher ADAS-Cog scores, specifically at follow-up. One confounding factor is that participants with HIS < 2 who received sham tACS combined with cognitive exercises began the study with an average higher baseline cognitive impairment.

For the participants with HIS ≥ 2 (Figure. 7c), ADAS-Cog scores reduced from baseline to post-intervention and then rose at follow-up, a trend that — with only 13 participants split across conditions — should be read as indicative only.

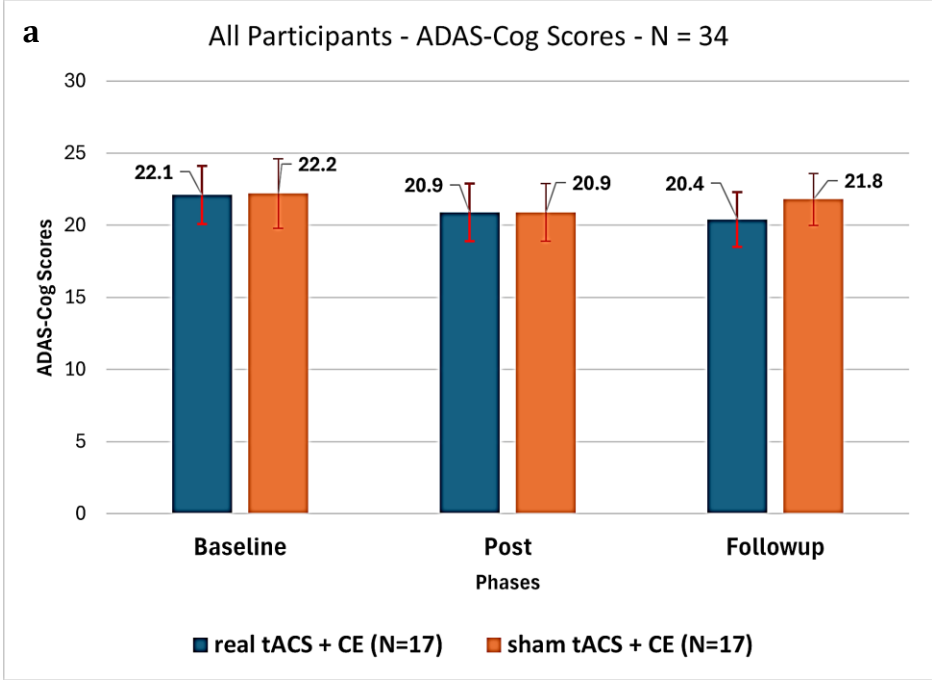
a
All Participants - ADAS-Cog Scores - N = 34
ADAS-Cog Scores
30
25
20
15
10
5
0
22.1
22.2
20.9
20.9
20.4
21.8
Baseline
Post
Followup
Phases
real tACS + CE (N=17)
sham tACS + CE (N=17)

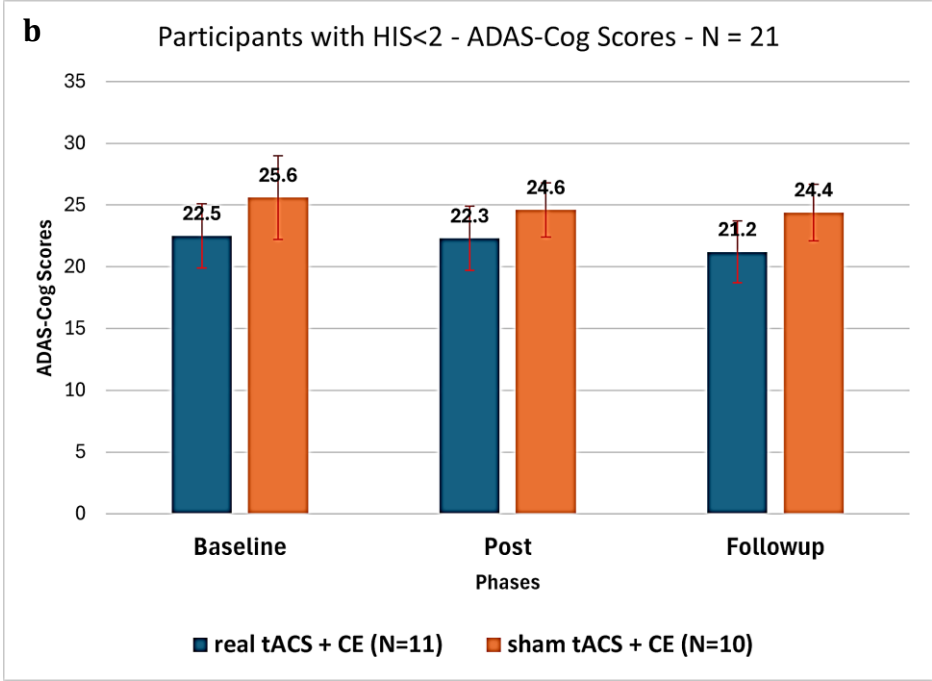
b
Participants with HIS<2 - ADAS-Cog Scores - N = 21
ADAS-Cog Scores
35
30
25
20
15
10
5
0
22.5
25.6
22.3
24.6
21.2
24.4
Baseline
Post
Followup
Phases
real tACS + CE (N=11)
sham tACS + CE (N=10)

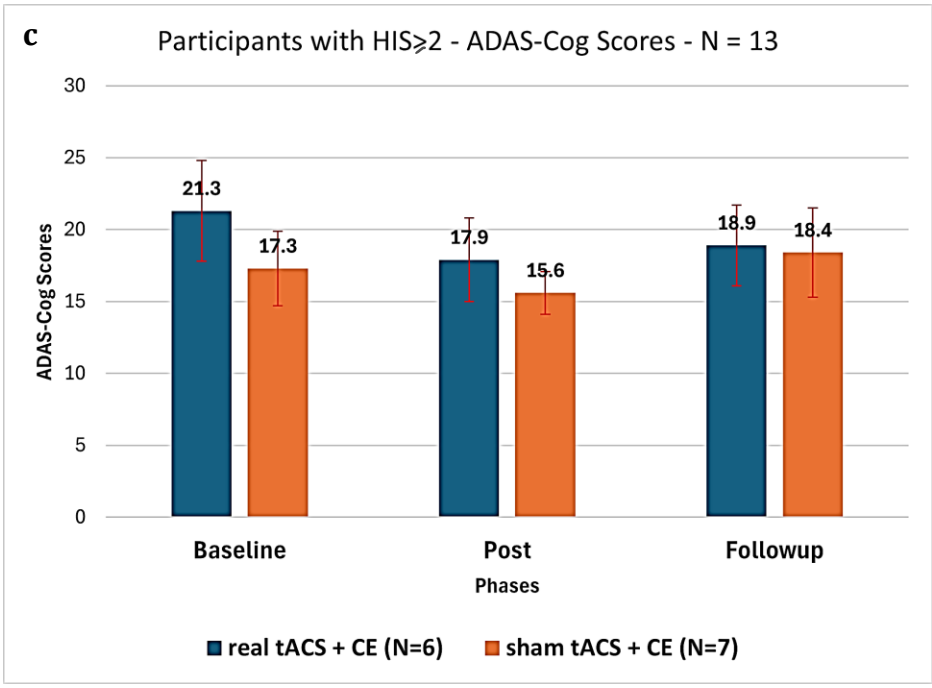

Figure 7. CHANGES IN ADAS-COG SCORES ACROSS STUDY PHASES FOR ALL PARTICIPANTS AND CLASSIFIED PARTICIPANTS BY HIS SCORES. Mean ADAS-Cog scores are shown at baseline, post-intervention, and follow-up for participants who received active tACS+CE (cognitive exercises) and sham tACS+CE (cognitive exercises). Lower ADAS-Cog scores indicate better cognitive performance. (a) ADAS-Cog trends for all participants (n=34). (b) Participants classified as HIS < 2 (n=21). (c) Participants classified as HIS ≥ 2 (n=13).

4.2 PCA/ICA Results

Principal component analysis (PCA) was performed on the EVestG-derived AP features to identify dominant patterns of segment contributions associated with treatment-related changes. The first principal component (PC1) was examined because it captures the dominant variance pattern across the EVestG segments. Participants who first received active tACS + cognitive exercises were further classified by the cerebrovascular burden severity based on their HIS scores. The analysis was conducted separately for the change between baseline and post-treatment (Δpost) and the change between post-treatment and follow-up (Δfollow). The baseline-to-follow-up interval was not analyzed separately, as the trends frequently showed a rebound toward baseline values at

follow-up, particularly in the HIS ≥ 2 group, resulting in minimal net change over the full interval that would obscure the distinct post-treatment and follow-up dynamics captured by the two shorter intervals. The first principal component (PC1) was examined because it captures the dominant variance pattern across the EVestG segments.

4.2.1 PCA results for Real tACS + cognitive exercises treatment in low and high HIS scores

PCA was performed separately for Δpost and Δfollow intervals across both HIS subgroups. In participants with HIS < 2, PC1 explained a moderate proportion of variance (16–22% across features), with Depolarization Rise Time and Peak Index showing the highest contributions. Most features exhibited negative correlations between Δpost and Δfollow PC1 scores (e.g., Repolarization Slope: $r = -0.72$; Depolarization Rise Time: $r = -0.67$), indicating that the dominant AP patterns underwent substantial reorganization during the follow-up period. The most frequently contributing tilts included Upward Acceleration Left (UAL) (8 occurrences), Supine Rotation Right (PRR), and Supine Upward Right (PUR) (7 occurrences each). The tilt and segment abbreviations used in the result sections are defined in the List of Abbreviations and described in Section 2.2.

In contrast, participants with HIS ≥ 2 showed substantially higher PC1 variance (33–39%), suggesting stronger dominance of a single underlying AP pattern. Unlike the low HIS group, most features demonstrated moderate to strong positive correlations between Δpost and Δfollow (e.g., Repolarization Rise Time: $r = 0.76$; Depolarization Rise Time: $r = 0.69$), indicating greater temporal consistency. The most frequent tilts were Ipsilateral Acceleration Left (IAL) and Supine Upward Right (PUR) (9 occurrences each), followed by Backward Acceleration Right (BAR) and Upward Acceleration Right (UAR) (7 occurrences each). Full details of variance explained, PC1 score magnitudes, correlations, and dominant segment tables are provided in Appendix A.

The higher proportion of variance explained in the HIS ≥ 2 group suggests that cerebrovascular burden may influence the structure and stability of the dominant AP patterns following stimulation. Based on these PCA results, the segments with the strongest PC1 contributions were selected for the trend analyses presented below.

4.2.2 PCA trend results for Real tACS + cognitive exercises

Following the PCA component analysis presented above, temporal trend analyses were performed to examine how the AP features evolved across sessions under the active tACS+CE condition. PCA was used as a segment-selection tool rather than a feature-combination method. Specifically, for each AP feature (e.g., AP Area, Depolarization Rise Time), PCA was applied across the 84 EVestG segments to identify which segments contributed most strongly to the dominant variance pattern (PC1). The segments with the highest PC1 loadings were then selected, and the original (non-transformed) feature values from these segments were averaged and plotted across baseline, post-treatment, and follow-up sessions for both HIS < 2 and HIS ≥ 2 groups. These plots therefore illustrate the temporal trends of each individual feature based on the most influential segments identified by PCA, rather than the principal component scores themselves. Because these analyses are based on a selective subset of segments rather than the full dataset, the absolute values may differ from overall group-level patterns reported in the literature. The primary purpose of these trend plots is to compare the direction and pattern of change across sessions between the two HIS subgroups, rather than to compare absolute values between groups at any given session.

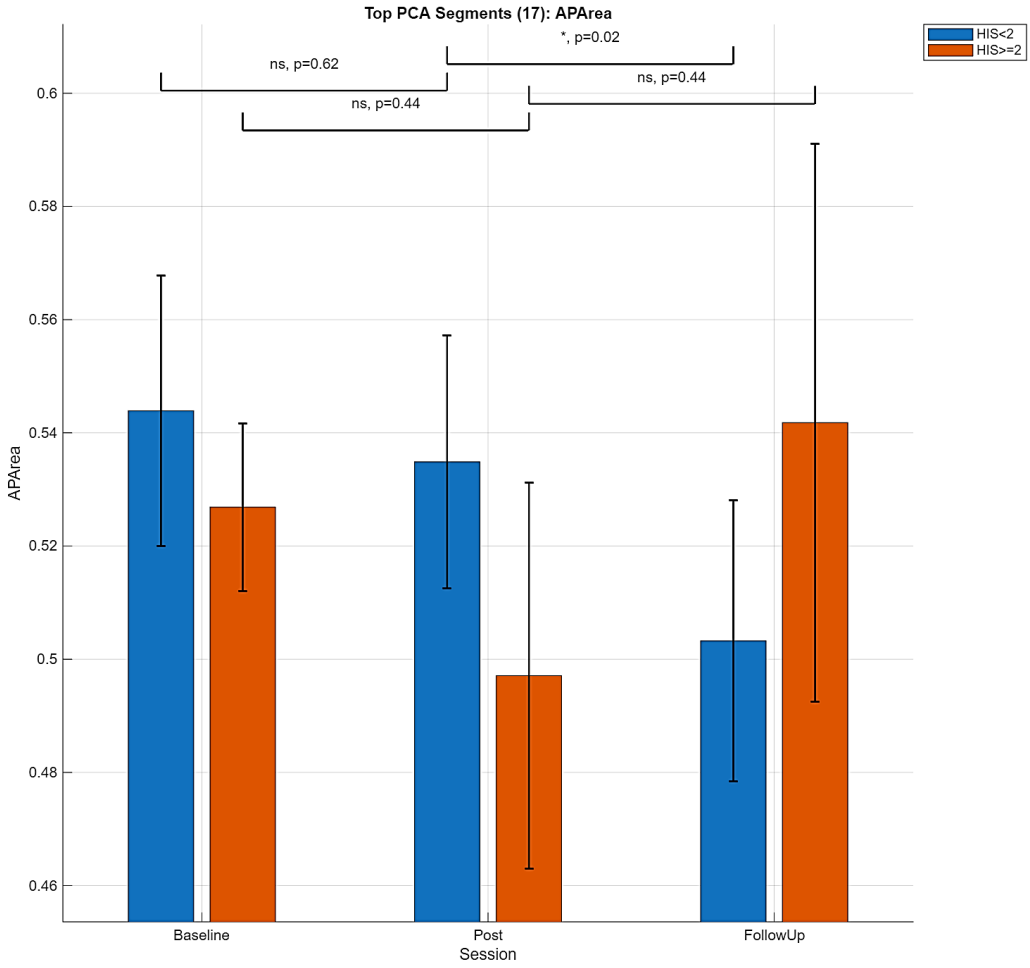

Figure 8. AP Area. PCA trend analysis of AP Area under active tACS+CE. Mean AP Area values from the top 17 PCA-selected segments are shown across baseline, post-treatment, and follow-up sessions for HIS < 2 and HIS ≥ 2 groups. Error bars represent standard error. The list of selected segments and their PC1 loadings are provided in Appendix A, Table A.1.

The trend of AP area across sessions is shown in Figure 8. For the HIS < 2 group, the AP area showed a gradual decrease from baseline to follow-up. The mean value decreased slightly after treatment and continued to decrease at follow-up.

In contrast, the HIS ≥ 2 group showed a different pattern. The AP area decreased from baseline to post-treatment but rebounded again during the follow-up session, resulting in a higher mean value at follow-up compared with the post-treatment measurement.

A statistically significant difference was observed between the post-treatment and follow-up sessions ($p = 0.02$) for the HIS < 2 group, supporting a change in AP area during the follow-up interval. Other comparisons did not show significant differences.

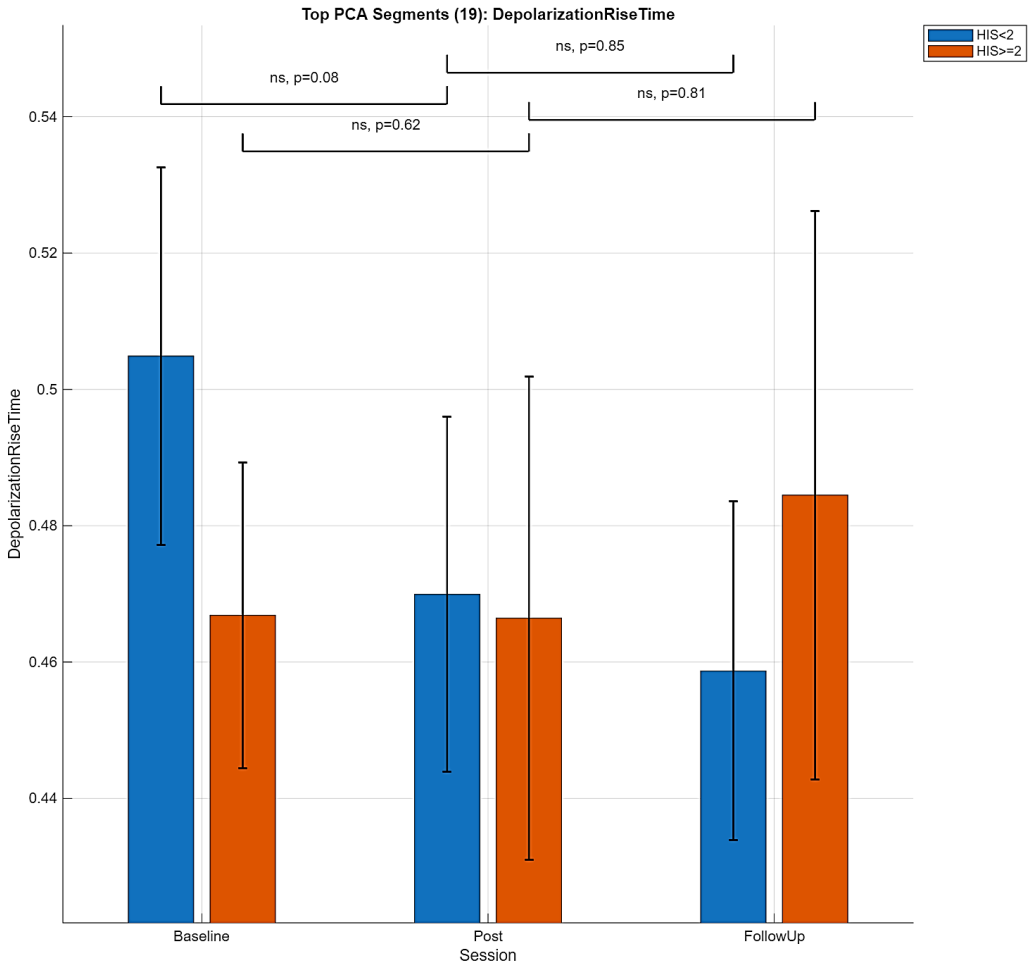

Figure 9. Depolarization Rise Time. PCA trend analysis of Depolarization Rise Time under active tACS+CE. Mean Depolarization Rise Time values from the top 19 PCA-selected segments

are shown across baseline, post-treatment, and follow-up sessions for HIS < 2 and HIS ≥ 2 groups. Error bars represent standard error. The list of selected segments and their PC1 loadings are provided in Appendix A, Table A.1.

The depolarization rise time trends are presented in Figure 9. For the HIS < 2 group, the mean depolarization rise time decreased consistently across the sessions, showing a progressive reduction from baseline to follow-up.

For the HIS ≥ 2 group, the pattern differed slightly. The mean value remained relatively stable between baseline and post-treatment but increased during the follow-up session. None of the above comparisons between sessions reached statistical significance.

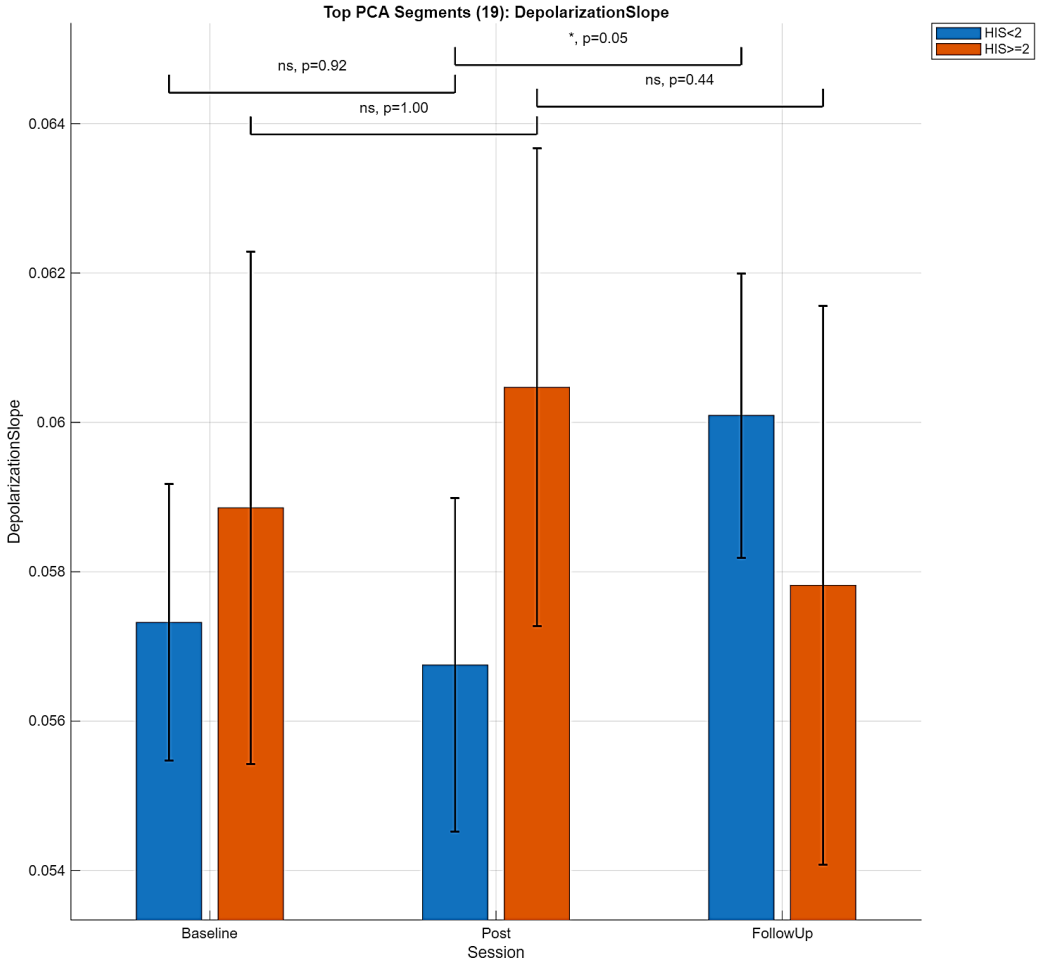

Figure 10. Depolarization Slope. PCA trend analysis of Depolarization Slope under active tACS+CE. Mean Depolarization Slope values from the top 19 PCA-selected segments are shown across baseline, post-treatment, and follow-up sessions for HIS < 2 and HIS ≥ 2 groups. Error bars represent standard error. The list of selected segments and their PC1 loadings are provided in Appendix A, Table A.1.

Figure 10 illustrates the changes in depolarization slope across sessions. For the HIS < 2 group, the depolarization slope decreased slightly from baseline to post-treatment but increased again during follow-up.

In contrast, the HIS ≥ 2 group showed an increase (getting steeper) from baseline to post-treatment followed by a rebound decrease at follow-up. This pattern indicates different trends between the two groups after treatment.

A marginally significant difference was observed between the post-treatment and follow-up sessions ($p = 0.05$) for the HIS < 2 group, suggesting a potential treatment-related effect on depolarization slope in the segments contributing most strongly to PC1.

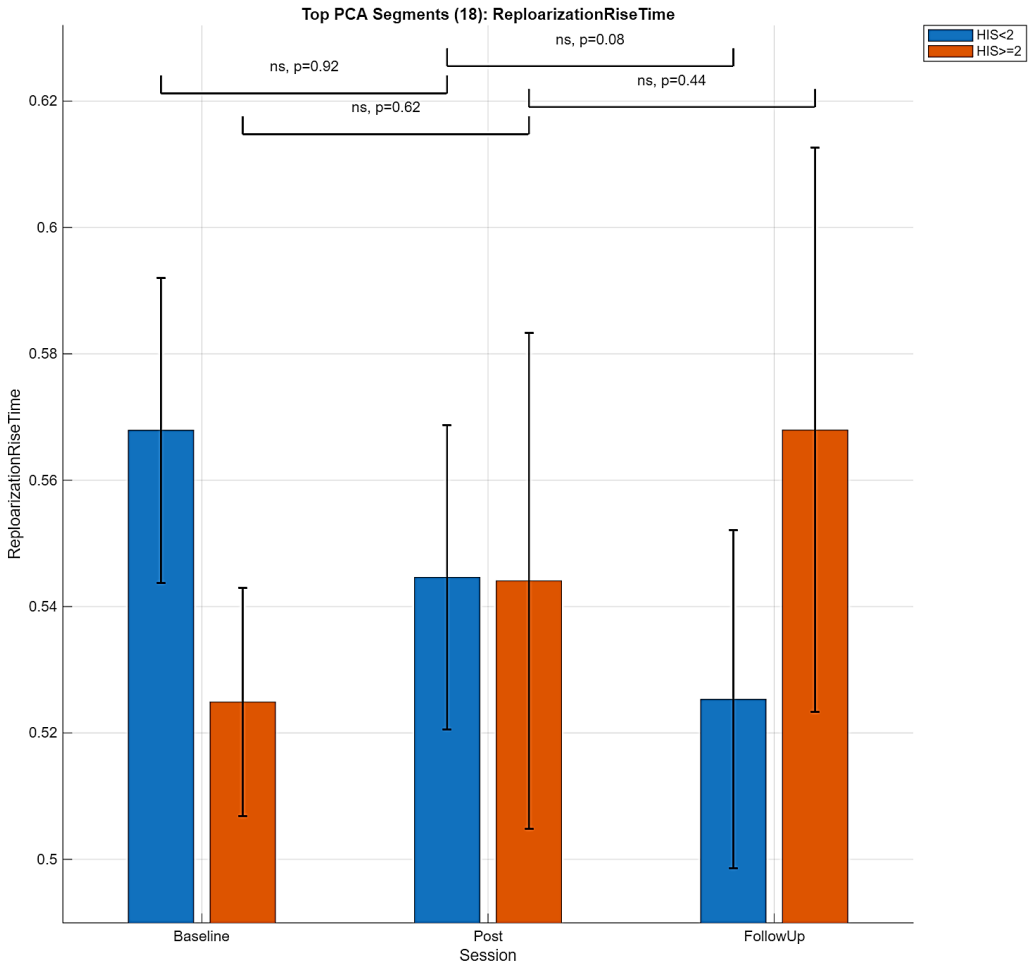

Figure 11. Repolarization Rise Time. PCA trend analysis of Repolarization Rise Time under active tACS+CE. Mean Repolarization Rise Time values from the top 18 PCA-selected segments

are shown across baseline, post-treatment, and follow-up sessions for HIS < 2 and HIS ≥ 2 groups. Error bars represent standard error. The list of selected segments and their PC1 loadings are provided in Appendix A, Table A.1.

The repolarization rise time trends are shown in Figure 11. For the HIS < 2 group, the repolarization rise time decreased from baseline to post-treatment and remained slightly lower at follow-up.

The HIS ≥ 2 group exhibited a different pattern, with a lower value at baseline followed by an increase (getting steeper) toward the follow-up session.

Although these patterns suggest opposite trends between groups, the statistical tests did not reveal significant differences between sessions.

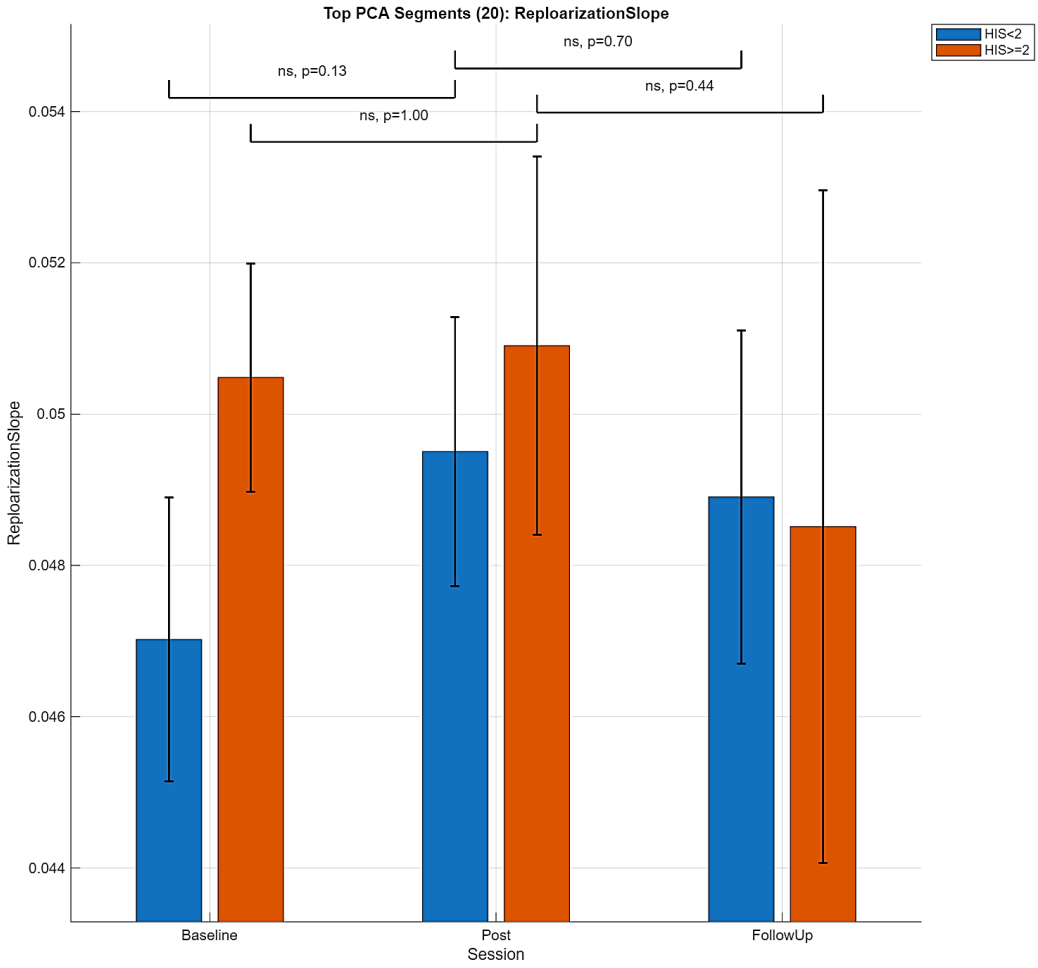

Figure 12. Repolarization Slope. PCA trend analysis of Repolarization Slope under active tACS+CE. Mean Repolarization Slope values from the top 20 PCA-selected segments are shown across baseline, post-treatment, and follow-up sessions for HIS < 2 and HIS ≥ 2 groups. Error bars represent standard error. The list of selected segments and their PC1 loadings are provided in Appendix A, Table A.1.

Figure 12 presents the repolarization slope across the three sessions. The HIS < 2 group demonstrated an increase (getting steeper) from baseline to post-treatment followed by a slight decrease at follow-up. The HIS ≥ 2 group showed a similar trend across the sessions. However, the statistical comparisons between sessions were not significant.

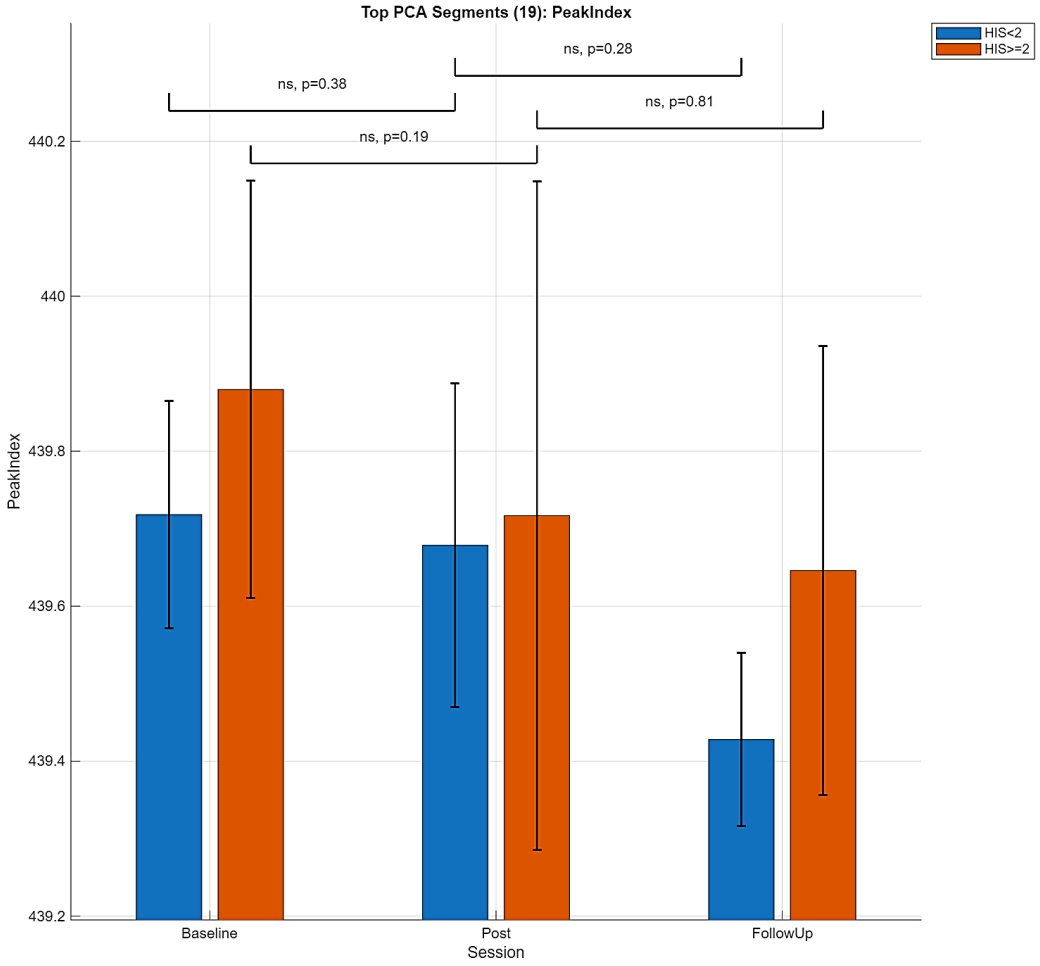

Figure 13. Peak Index. PCA trend analysis of Peak Index under active tACS+CE. Mean Peak Index values from the top 19 PCA-selected segments are shown across baseline, post-treatment, and follow-up sessions for HIS < 2 and HIS ≥ 2 groups. Error bars represent standard error. The list of selected segments and their PC1 loadings are provided in Appendix A, Table A.1.

The peak index values across sessions are presented in Figure 13. Both groups demonstrated relatively small changes in peak index across sessions with a slight decrease from baseline to follow-up. The statistical comparisons between sessions were not significant, indicating that peak index remained relatively stable across the measurement intervals.

Across the EVestG-derived AP features, extracted from the dominant PCA segments, several general patterns were observed:

1. The HIS < 2 group often showed gradual decreases across sessions for several features, in particular, depolarization rise time and repolarization rise time.
2. The HIS ≥ 2 group frequently exhibited recovery or increases at follow-up, especially in AP area and depolarization rise time. Although this pattern may appear counterintuitive — given that AD-CVD is typically associated with broader AP waveforms that would be expected to narrow with treatment — the initial post-treatment narrowing followed by a rebound widening at follow-up is consistent with a delayed re-emergence of the underlying vascular-constrained neural dynamics. This pattern is discussed further in Discussion subsection 5.3.
3. Most session-to-session comparisons did not reach statistical significance, indicating that some of the observed changes may represent subtle trends rather than large treatment-induced shifts.

Overall, these results suggest that the AP features derived from the most influential PCA segments demonstrate different patterns between the two HIS groups. Notably, the HIS ≥ 2 group exhibited a substantially higher proportion of variance explained by PC1 compared with the HIS < 2 group, indicating a stronger dominance of a single AP pattern in participants with greater cerebrovascular burden.

In addition, these temporal patterns are consistent with previous findings from our research, where changes in EVestG-derived features were associated with variations in cognitive performance measured by ADAS-Cog. In particular, features related to signal timing and recovery dynamics, such as peak index and repolarization characteristics, demonstrated stronger relationships with

cognitive changes. The present results extend these observations by showing that such feature-level dynamics are also reflected in the dominant segments identified by PCA and evolve differently depending on cerebrovascular burden and stimulation condition.

While PCA identifies dominant variance patterns in the data, ICA was additionally applied to separate statistically independent pattern sources underlying the EVestG-derived AP features.

Independent component analysis (ICA) was applied to the EVestG-derived AP features to identify statistically independent patterns underlying the AP characteristic changes for participants with HIS < 2 and HIS ≥ 2 who received real tACS combined with cognitive exercises first. In contrast to PCA, which identifies orthogonal patterns of maximal variance, ICA separates statistically independent pattern sources contributing to the AP features.

Similar to the PCA analysis, ICA was performed separately for the changes between baseline and post-treatment (Δpost) and post-treatment and follow-up (Δfollow). The dominant independent component (IC) extracted from each feature was examined to assess its contribution to the AP features variability.

4.2.3 ICA results for Real tACS + cognitive exercises treatment in low and high HIS scores

ICA was applied to separate statistically independent source patterns within the EVestG-derived AP features for both HIS subgroups. In participants with HIS < 2, the dominant IC accounted for 13–20% of variability across features, with rise-time features showing the largest increases during the follow-up interval (e.g., Depolarization Rise Time: 14.1% to 20.4%). The correlations between Δpost and Δfollow IC scores were generally weaker and more variable than those observed in PCA, with Peak Index showing the strongest negative correlation ($r = -0.96$), indicating substantial

reorganization of independent patterns over time. The most frequently contributing tilts included PUR (8 occurrences) and RAR (6 occurrences).

In participants with HIS ≥ 2, the dominant IC captured a substantially larger proportion of variability (29–38%), consistent with the PCA finding of stronger single-pattern dominance in this group. Several features showed negative correlations between Δpost and Δfollow (e.g., AP Area: r = −0.86; Depolarization Rise Time: r = −0.63), suggesting that the independent patterns associated with treatment-related changes reversed or evolved during follow-up. The most frequent tilts were Backward Acceleration Right (BAR), Rotation Acceleration Right (RAR), and Supine Upward Right (PUR), with a notable shift from BAR_RTConBB (Backward Acceleration Right ear, return-to-center deceleration phase) dominance during Δpost to PUR_onBB (Supine Upward Right ear, deceleration phase) dominance during Δfollow. Compared with PCA, ICA revealed greater variability in temporal stability across features, indicating that multiple independent neural processes contribute to the EVestG response structure. Based on these ICA results, the segments with the strongest IC contributions were selected for the trend analyses presented below.

4.2.4 ICA trend results for Real tACS + cognitive exercises

Following the ICA component analysis presented above, temporal trend analyses were performed to examine how the EVestG-derived AP features evolved across sessions. ICA was used as a segment-selection tool, analogous to the PCA approach described above. For each AP feature, ICA was applied across the 84 EVestG segments to identify which segments contributed most strongly to the dominant independent component. The segments with the highest IC loadings from both participant groups were then selected, and the original (non-transformed) feature values from these segments were averaged and plotted across Baseline, Post-treatment, and Follow-up sessions,

calculated separately for the HIS < 2 and HIS ≥ 2 groups. These plots therefore illustrate the temporal trends of each individual feature based on the most influential segments identified by ICA, rather than the independent component scores themselves. It should be noted that the baseline AP area values for the HIS ≥ 2 group appear lower than those for the HIS < 2 group in these trend plots. This differs from the overall pattern reported in the literature, where AD-CVD patients typically exhibit broader AP waveforms [6, 14]. This discrepancy arises because the trend analyses are based on a subset of segments selected by ICA for their independent signal contributions, rather than the full set of 84 segments. The ICA-selected segments capture statistically independent patterns rather than overall amplitude differences, which may result in different baseline relationships between groups. Accordingly, the purpose of these trend plots is to compare the direction and pattern of change across sessions between the two HIS subgroups, rather than to compare absolute values between groups at any given session.

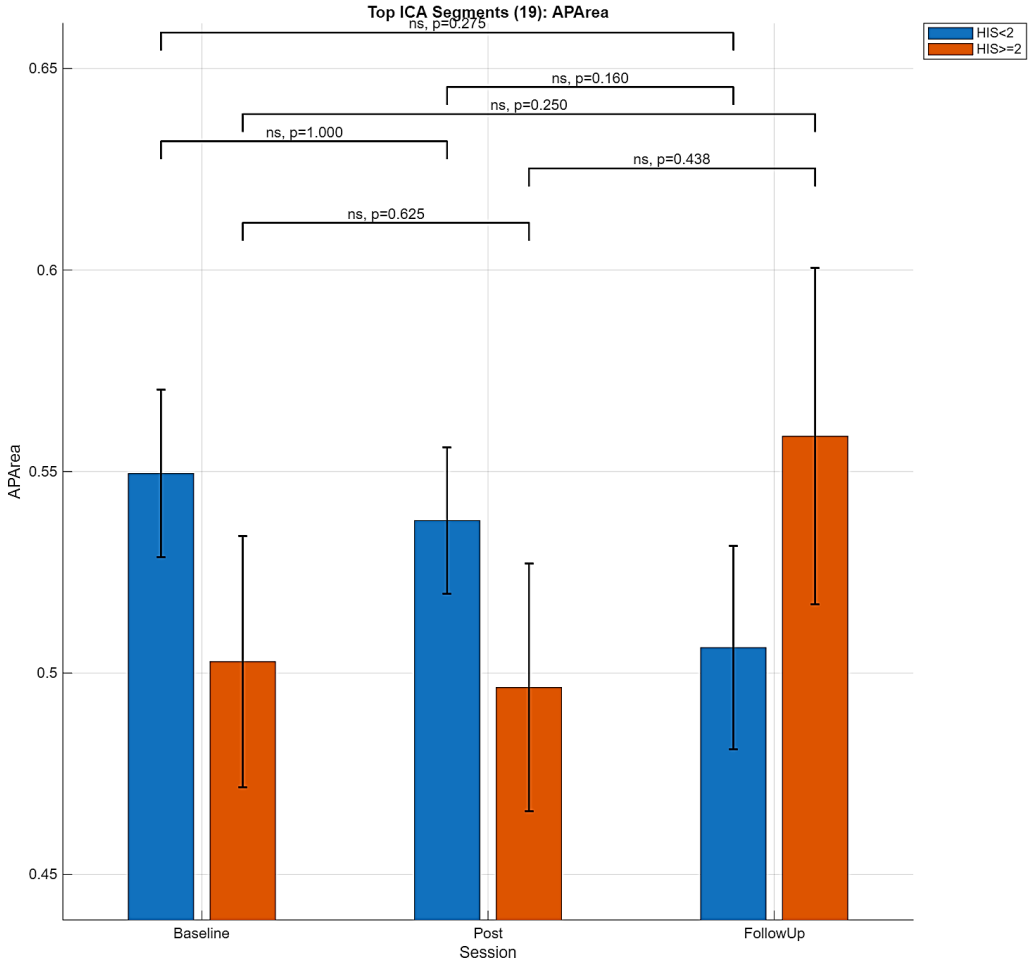

Figure 14. AP Area. ICA trend analysis of AP Area under active tACS+CE. Mean AP Area values from the top 19 ICA-selected segments are shown across baseline, post-treatment, and follow-up sessions for HIS < 2 and HIS ≥ 2 groups. Error bars represent standard error. The list of selected segments and their IC1 loadings are provided in Appendix B, Table B.1.

The AP Area trends are shown in Figure 14. For participants with HIS < 2, the mean AP Area exhibited a gradual decrease across sessions, declining from baseline to post-treatment and further at follow-up. In contrast, the HIS ≥ 2 group showed a different pattern, with slightly lower values at baseline and post-treatment followed by a marked increase at follow-up.

Despite these differing trends between groups, the statistical comparisons between sessions did not reveal significant differences within either group ($p > 0.05$). These results indicate that although AP area exhibited temporal variations, the changes were not statistically significant across the measured intervals.

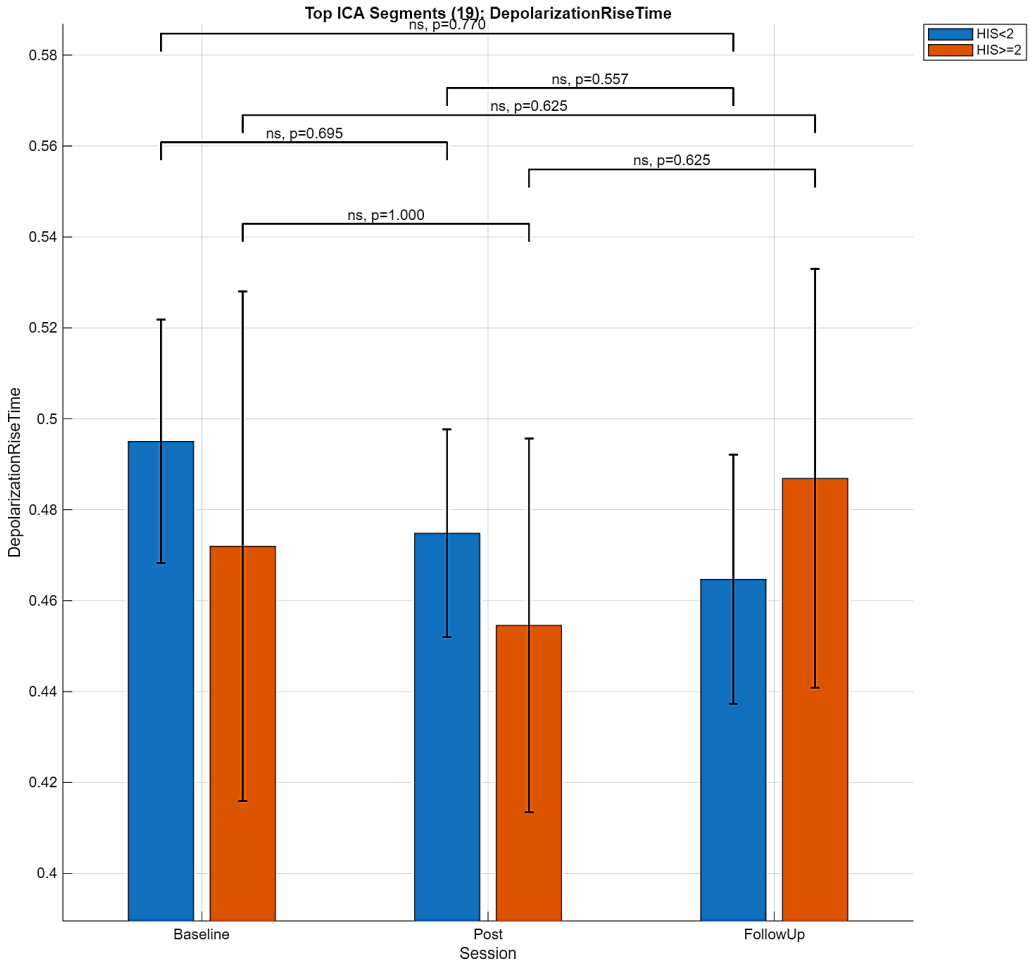

Figure 15. Depolarization Rise Time. ICA trend analysis of Depolarization Rise Time under active tACS+CE. Mean Depolarization Rise Time values from the top 19 ICA-selected segments are shown across baseline, post-treatment, and follow-up sessions for HIS < 2 and HIS ≥ 2 groups. Error bars represent standard error. The list of selected segments and their IC1 loadings are provided in Appendix B, Table B.1.

The trend of Depolarization Rise Time is illustrated in Figure 15. In the HIS < 2 group, the mean value decreased slightly from baseline to post-treatment and continued to decline modestly at follow-up. In contrast, participants with HIS ≥ 2 demonstrated a decrease from baseline to post-treatment followed by an increase during the follow-up session.

All comparisons between sessions were statistically non-significant ($p > 0.05$). Overall, these results suggest that the temporal changes in Depolarization Rise Time were modest and did not reach statistical significance in either participant group.

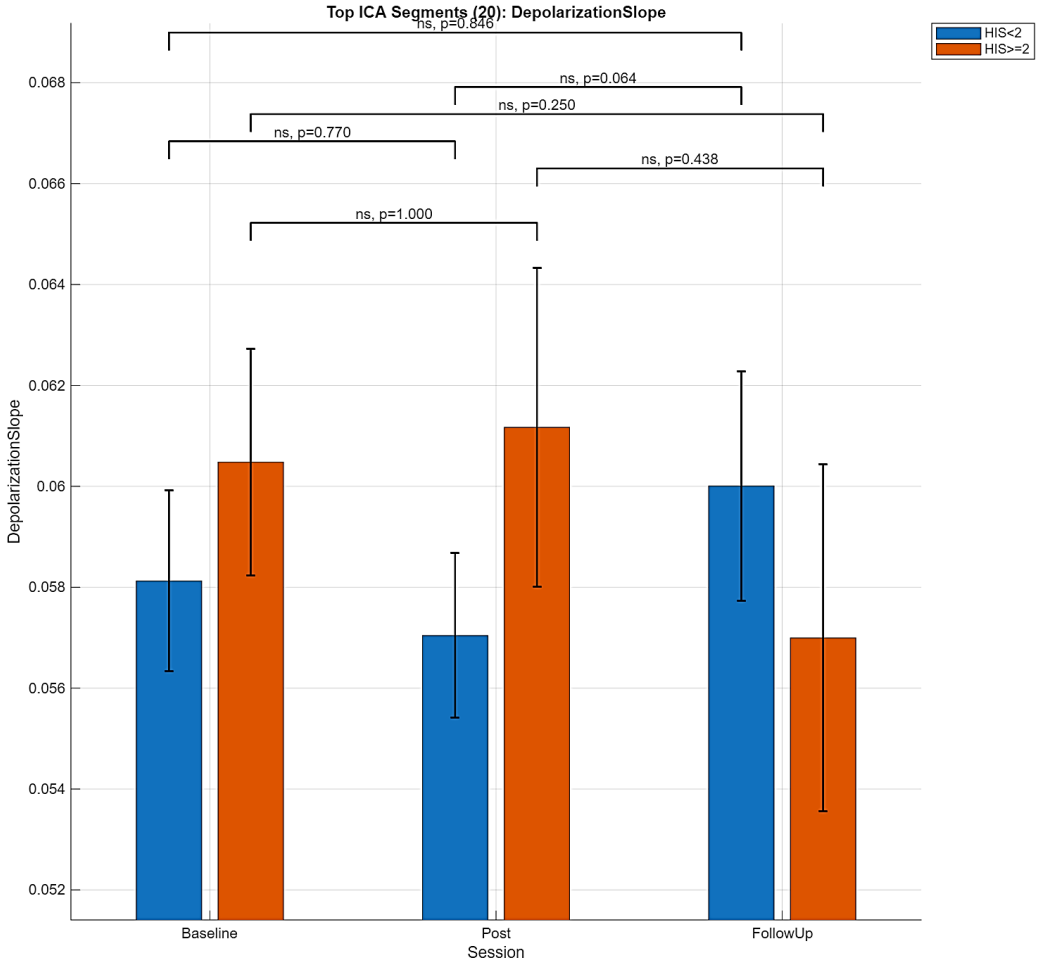

Figure 16. Depolarization Slope. ICA trend analysis of Depolarization Slope under active tACS+CE. Mean Depolarization Slope values from the top 20 ICA-selected segments are shown across baseline, post-treatment, and follow-up sessions for HIS < 2 and HIS ≥ 2 groups. Error bars represent standard error. The list of selected segments and their IC1 loadings are provided in Appendix B, Table B.1.

The trends for Depolarization Slope are presented in Figure 16. For the HIS < 2 group, the slope decreased slightly from baseline to post-treatment and then increased at follow-up. The HIS ≥ 2 group showed a slight increase from baseline to post-treatment, followed by a decrease at follow-up. Although the HIS ≥ 2 group exhibited higher baseline values, the two groups converged at

follow-up. None of the comparisons between sessions reached statistical significance ($p > 0.05$).

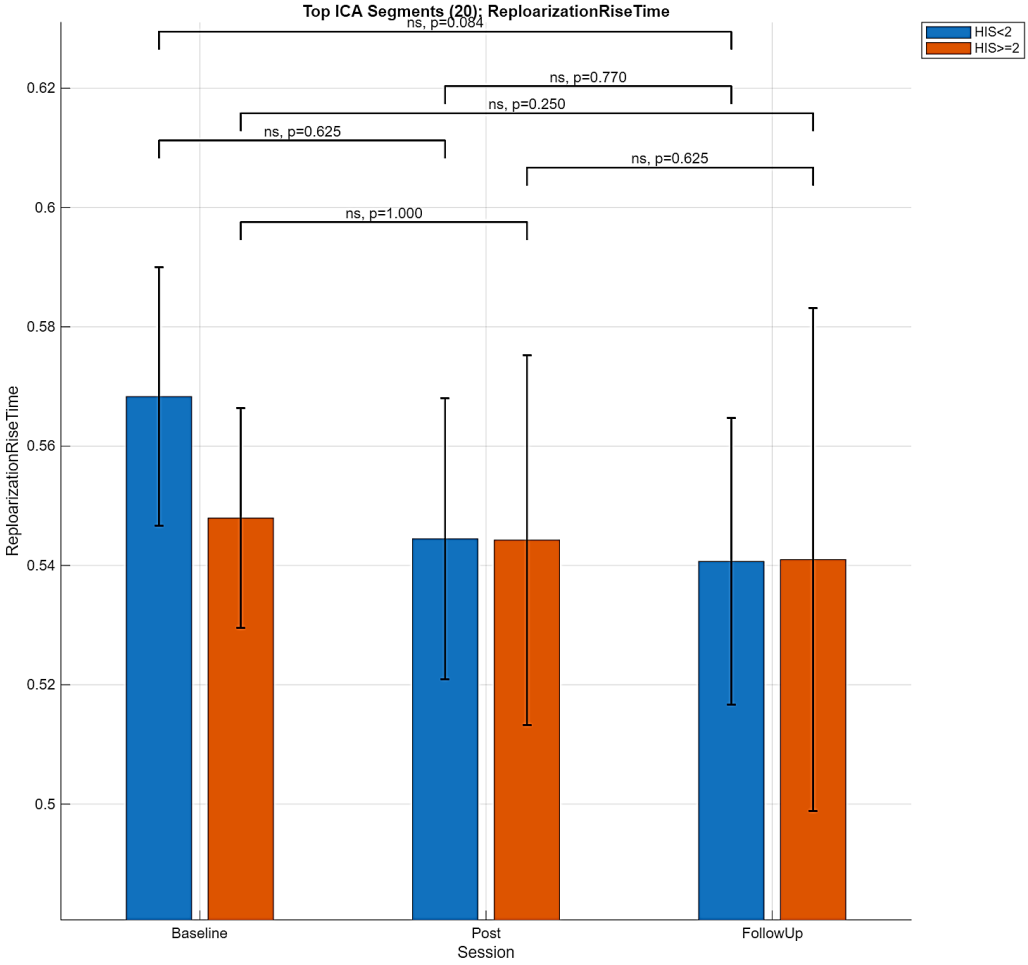

Figure 17. Repolarization Rise Time. ICA trend analysis of Repolarization Rise Time under active tACS+CE. Mean Repolarization Rise Time values from the top 20 ICA-selected segments are shown across baseline, post-treatment, and follow-up sessions for HIS < 2 and HIS ≥ 2 groups. Error bars represent standard error. The list of selected segments and their IC1 loadings are provided in Appendix B, Table B.1.

Figure 17 illustrates the trends for Repolarization Rise Time. For participants with HIS < 2, Repolarization Rise Time showed a gradual decrease across sessions. However, the HIS ≥ 2 group

demonstrated relatively stable values between post-treatment and follow-up after a slight reduction from baseline.

All comparisons between sessions were statistically non-significant ($p > 0.05$), indicating that the variations in Repolarization Rise Time were relatively small over time.

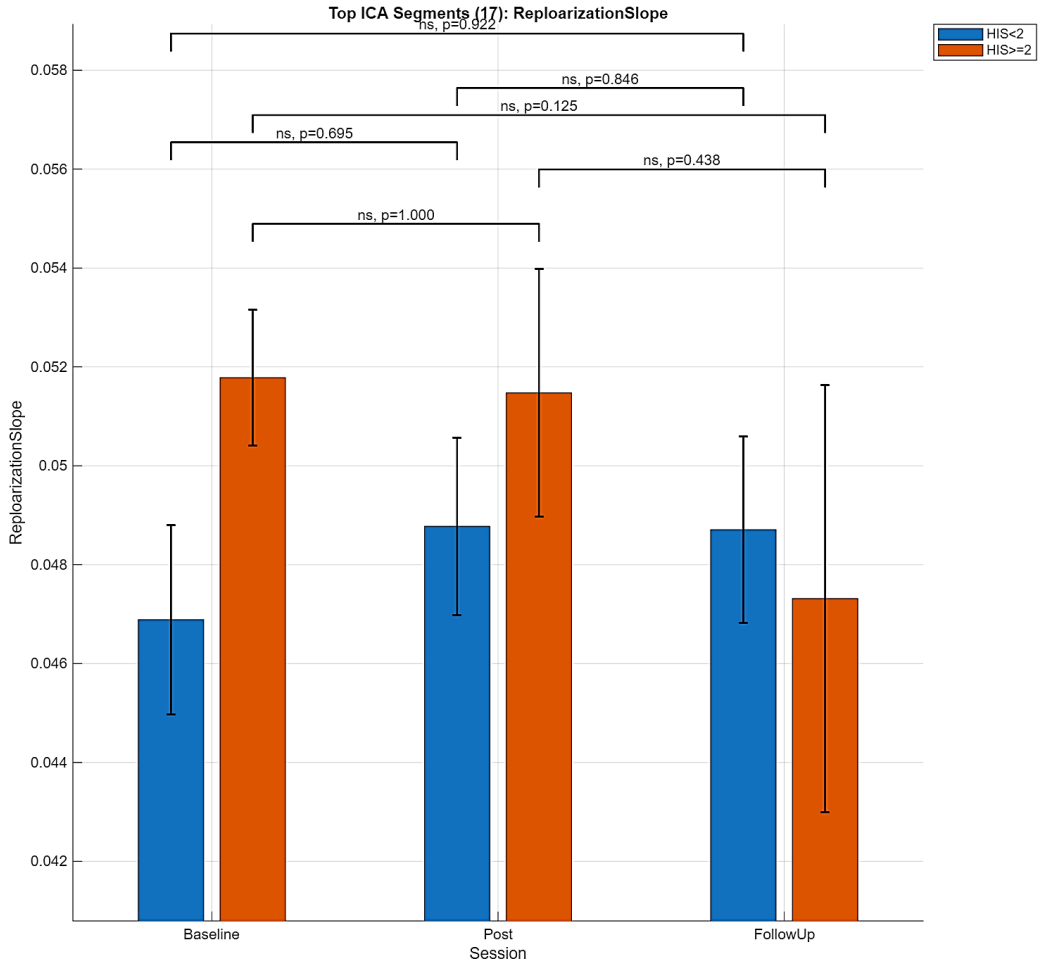

Figure 18. Repolarization Slope. ICA trend analysis of Repolarization Slope under active tACS+CE. Mean Repolarization Slope values from the top 17 ICA-selected segments are shown across baseline, post-treatment, and follow-up sessions for HIS < 2 and HIS ≥ 2 groups. Error bars represent standard error. The list of selected segments and their IC1 loadings are provided in Appendix B, Table B.1.

The trends for Repolarization Slope are shown in Figure 18. Participants with HIS < 2 demonstrated a slight increase from baseline to post-treatment followed by relatively stable values at follow-up. In contrast, the HIS ≥ 2 group showed a gradual decrease from baseline to follow-up.

As with most of the analyzed features, none of the comparisons between sessions reached statistical significance ($p > 0.05$), suggesting that the observed changes were relatively subtle.

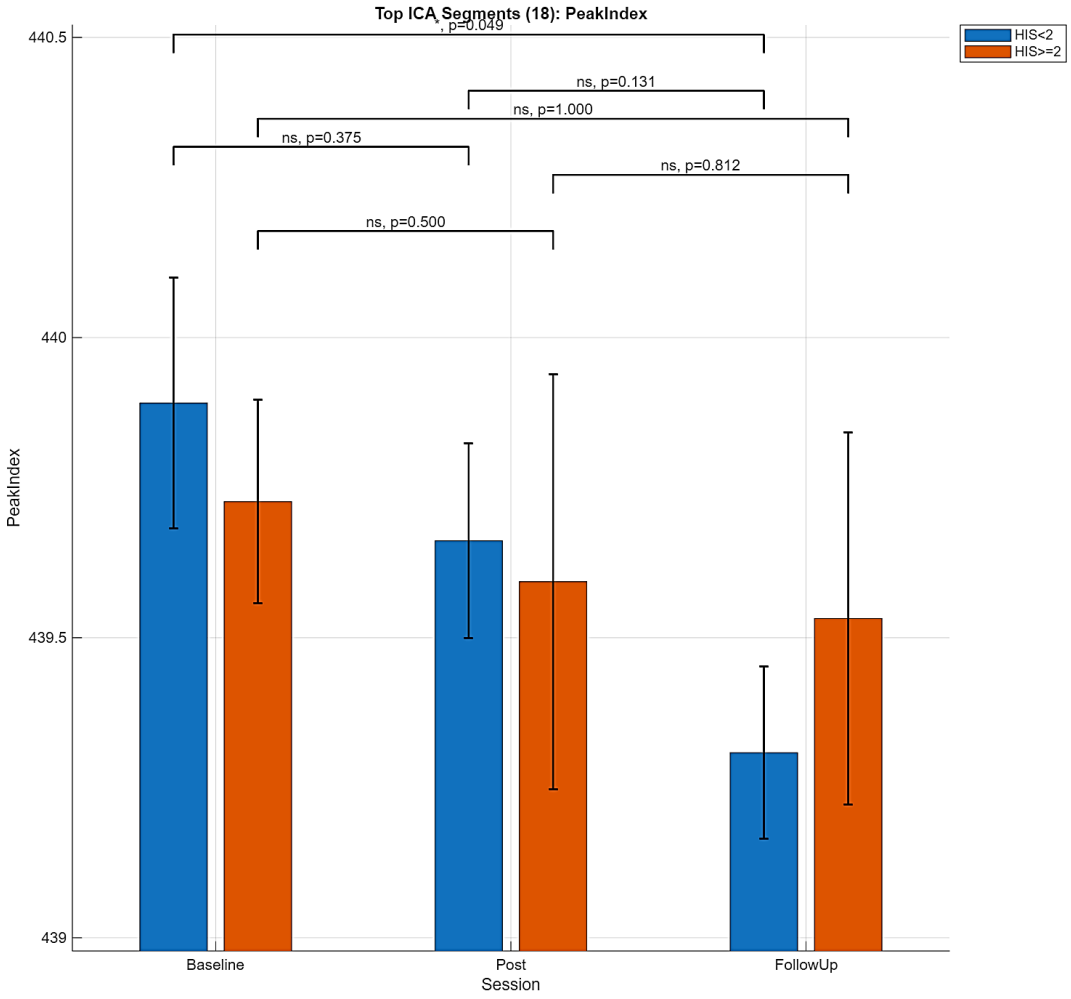

Figure 19. Peak Index. ICA trend analysis of Peak Index under active tACS+CE. Mean Peak Index values from the top 18 ICA-selected segments are shown across baseline, post-treatment, and follow-up sessions for HIS < 2 and HIS ≥ 2 groups. Error bars represent standard error. The list of selected segments and their IC1 loadings are provided in Appendix B, Table B.1.

The Peak Index trends are shown in Figure 19. Both participants with HIS < 2 and HIS ≥ 2 displayed a steady decrease across sessions from baseline to follow-up. The comparison between baseline and follow-up sessions across groups showed a marginal effect ($p \approx 0.049$), while other comparisons remained non-significant ($p > 0.05$).

These ICA-based temporal patterns are consistent with prior EVestG work relating feature changes to ADAS-Cog performance [33], and with the left–right asymmetry observed in the present study (Section 4.1), where left-ear responses showed stronger treatment-related effects.

In particular, features related to signal timing and recovery dynamics, such as peak index and repolarization characteristics, demonstrated stronger associations with cognitive changes. The present results extend these observations by showing that these relationships are not only reflected in overall signal trends but also emerge at the level of independent neural components and evolve differently depending on both stimulation condition and cerebrovascular burden.

Overall, the ICA-based trend analysis revealed modest temporal variations across EVestG-derived AP features for both participant groups. Several features showed gradual decreases in the HIS < 2 group, whereas participants with HIS ≥ 2 often exhibited partial recovery or increases at follow-up. However, no significant differences were observed between sessions, indicating that the magnitude of these changes remained limited.

Compared with the PCA results, the ICA analysis revealed greater variability in the temporal stability of the dominant patterns, suggesting that multiple independent pattern sources contribute to the neurophysiological vestibular responses over time.

PCA was also performed on the EVestG-derived AP features from the second treatment-sequence of participants, who only had sham tACS + cognitive exercises, to identify dominant patterns of segment contributions associated with sham tACS treatment-related changes. The analysis was conducted separately for the change between baseline and post-treatment (Δpost) and the change between post-treatment and follow-up (Δfollow). PC1 was examined because it captures the dominant variance pattern across the EVestG segments. Similar to group 1 (tACS + cognitive

exercises), participants from group 2 (sham tACS + cognitive exercises) were further classified by the cerebrovascular burden severity based on their HIS scores.

4.2.5 PCA results for Sham tACS + cognitive exercises treatment in low and high HIS scores

PCA was performed separately for Δpost and Δfollow intervals across both HIS subgroups in participants who received sham tACS + cognitive exercises. In participants with HIS < 2, PC1 explained 16.7–19.9% of variance during Δpost, increasing to 24.4–27.1% during Δfollow, indicating that the dominant signal pattern became more pronounced over time even in the absence of active stimulation. PC1 score magnitudes also increased consistently from Δpost to Δfollow across all features. Correlations between Δpost and Δfollow varied across features, with Repolarization Rise Time showing stability (r = 0.77) while Depolarization Rise Time showed reversal (r = −0.64). The most frequently contributing tilts included CAR, IAR, and PRR.

In participants with HIS ≥ 2, PC1 explained a higher proportion of variance (22.6–30.2%), consistent with the pattern observed in the tACS + cognitive exercises group where higher cerebrovascular burden was associated with stronger single-pattern dominance. However, the correlation analysis revealed mixed temporal stability, with Repolarization Slope showing consistency (r = 0.58) while Depolarization Slope exhibited near-complete reversal (r = −0.99). The most frequent tilts selections included RAR, UAL, and UAR. Full details of variance explained, PC1 score magnitudes, correlations, and dominant segment tables are provided in Appendix C.

A notable difference from the tACS+ cognitive exercises group was the consistent increase in PC1 variance and score magnitudes during follow-up in the low HIS subgroup, suggesting that sham tACS + cognitive exercises effects may consolidate over time differently than those observed

under active stimulation. Based on these PCA results, the segments with the strongest PC1 contributions were selected for the trend analyses presented below.

4.2.6 PCA trend results for Sham tACS + cognitive exercises

Following the PCA component analysis presented above, temporal trend analyses were performed to examine how the AP features evolved across sessions under the sham tACS+CE condition. PCA was again used as a segment-selection tool. For each feature, the segments with the highest PC1 loadings were selected, and their original (non-transformed) feature values were plotted across baseline, post-treatment, and follow-up sessions for both HIS < 2 and HIS ≥ 2 groups. These plots illustrate the temporal trends of each individual feature based on the most influential segments identified by PCA, rather than the principal component scores themselves. Overall, the trends differed between the two groups, although most comparisons did not reach statistical significance.

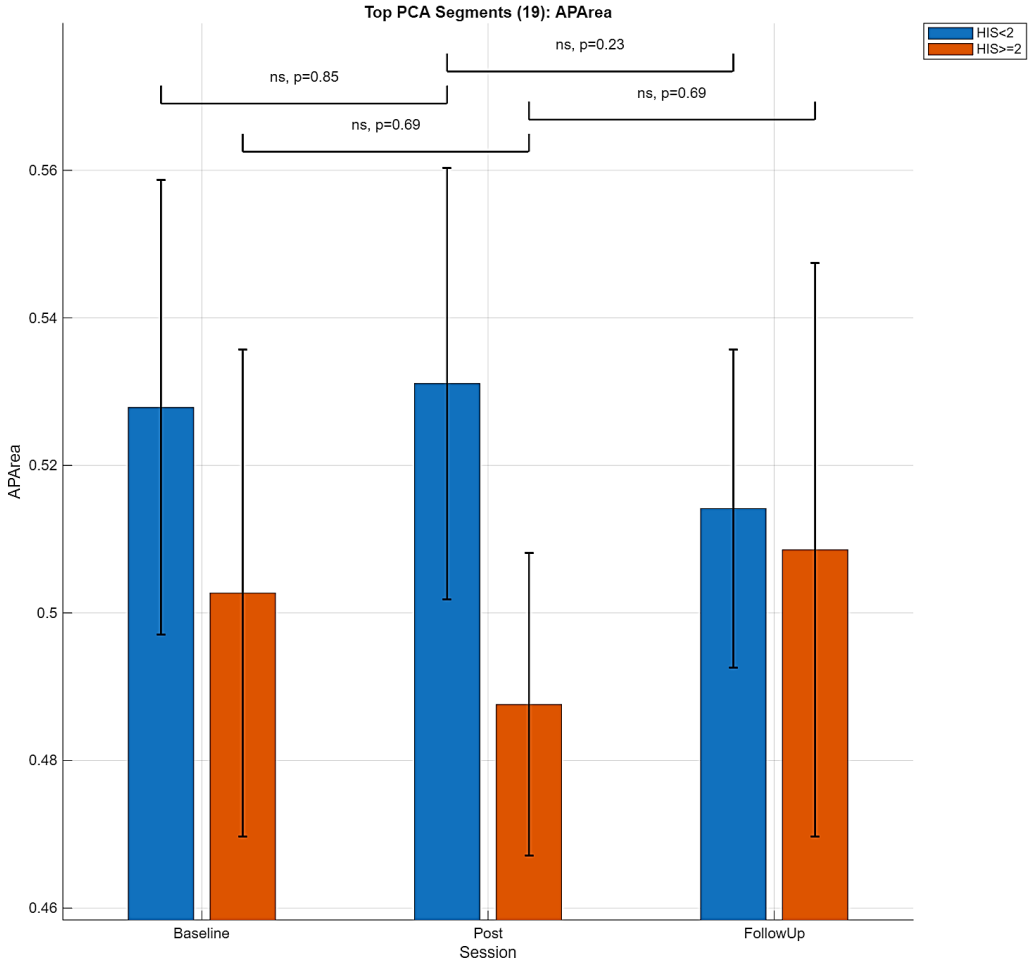

Figure 20. AP Area. PCA trend analysis of AP Area under sham tACS+CE. Mean AP Area values from the top 19 PCA-selected segments are shown across baseline, post-treatment, and follow-up sessions for HIS < 2 and HIS ≥ 2 groups. Error bars represent standard error. The list of selected segments and their PC1 loadings are provided in Appendix C, Table C.1.

In the AP area, participants with HIS < 2 showed a slight increase from baseline to post-treatment followed by a decrease at follow-up, whereas the HIS ≥ 2 group exhibited relatively stable values across sessions. However, all pairwise comparisons were non-significant, indicating that the observed changes were modest.

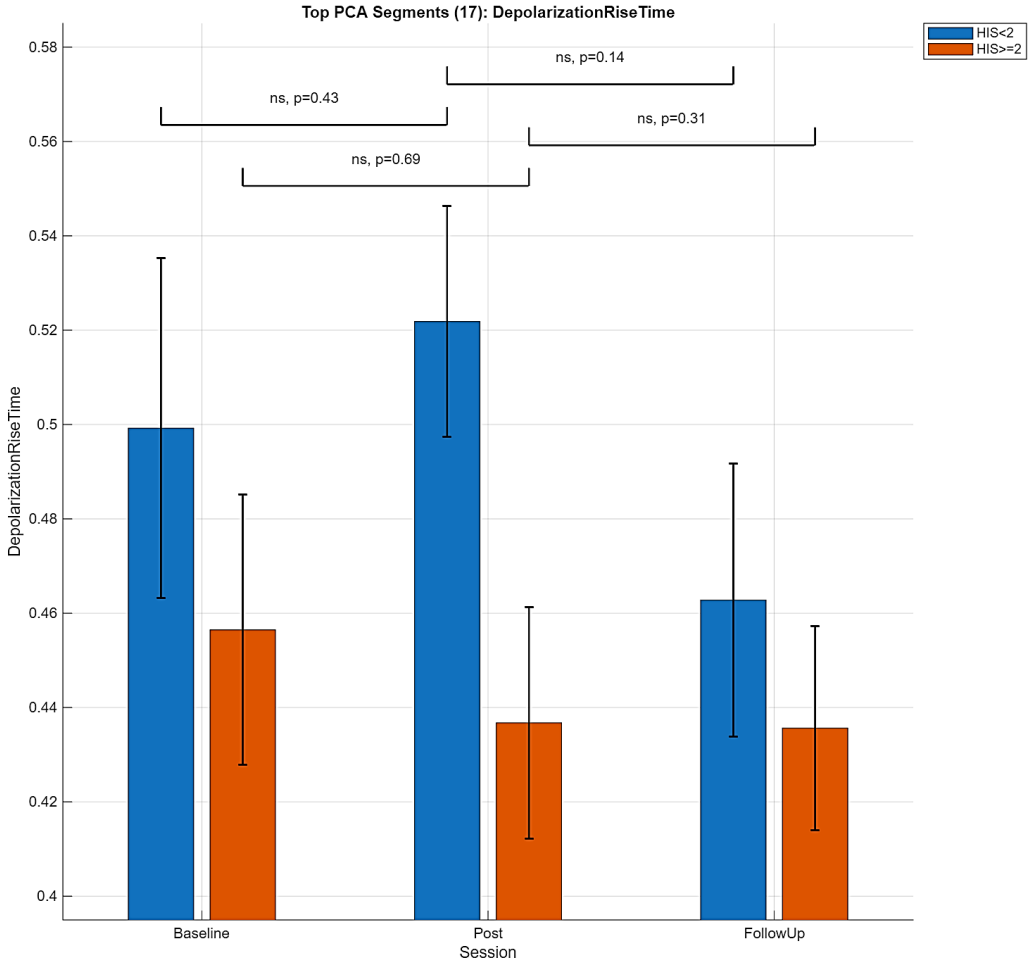

Figure 21. Depolarization Rise Time. PCA trend analysis of Depolarization Rise Time under sham tACS+CE. Mean Depolarization Rise Time values from the top 17 PCA-selected segments are shown across baseline, post-treatment, and follow-up sessions for HIS < 2 and HIS ≥ 2 groups. Error bars represent standard error. The list of selected segments and their PC1 loadings are provided in Appendix C, Table C.1.

For depolarization rise time, the HIS < 2 group demonstrated an increase at post-treatment followed by a decrease at follow-up, while the HIS ≥ 2 group showed a gradual reduction from baseline to post-treatment with minimal change thereafter. Despite these differing patterns, no statistically significant differences were observed.

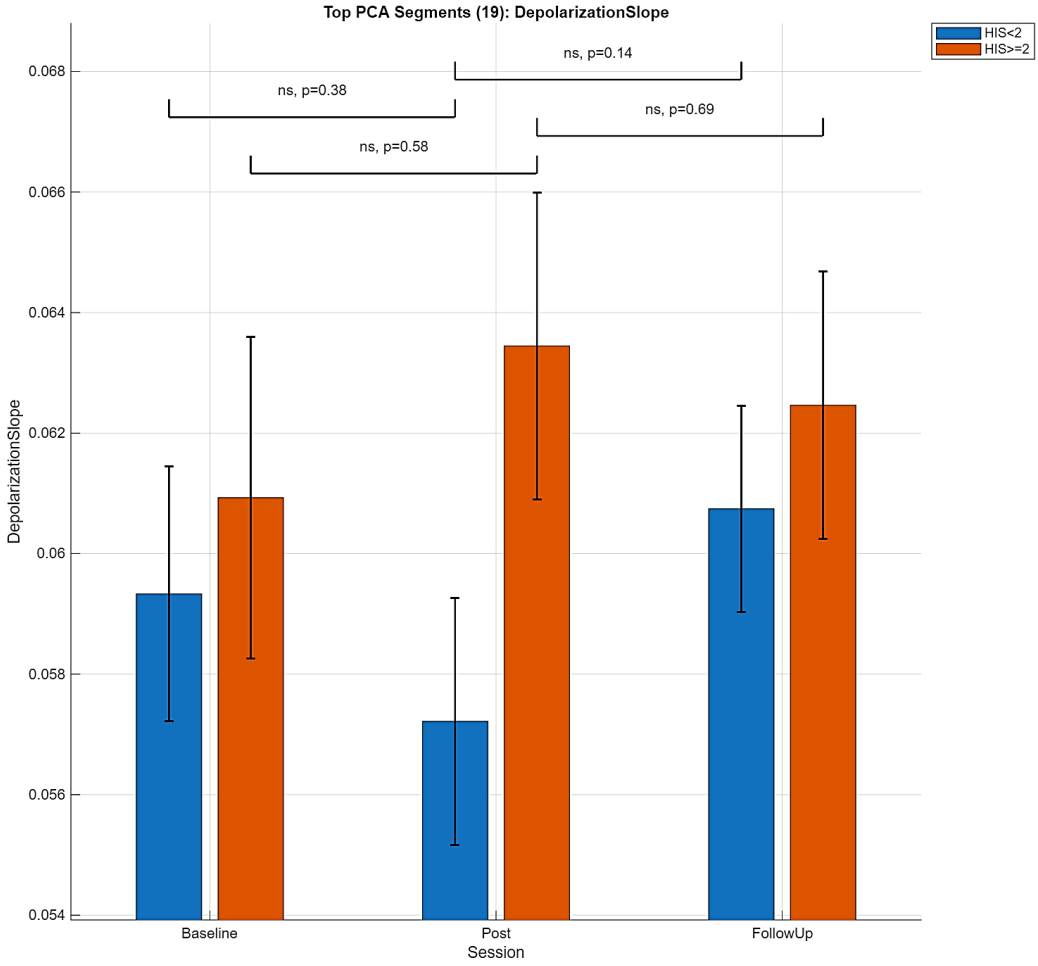

Figure 22. Depolarization Slope. PCA trend analysis of Depolarization Slope under sham tACS+CE. Mean Depolarization Slope values from the top 19 PCA-selected segments are shown across baseline, post-treatment, and follow-up sessions for HIS < 2 and HIS ≥ 2 groups. Error bars represent standard error. The list of selected segments and their PC1 loadings are provided in Appendix C, Table C.1.

In the case of depolarization slope, the HIS ≥ 2 group exhibited higher values at post-treatment compared with baseline, followed by a slight decrease at follow-up. In contrast, the HIS < 2 group showed a reduction at post-treatment and a recovery at follow-up. These opposite trends suggest

different underlying response dynamics between the groups, although again, the differences were not statistically significant.

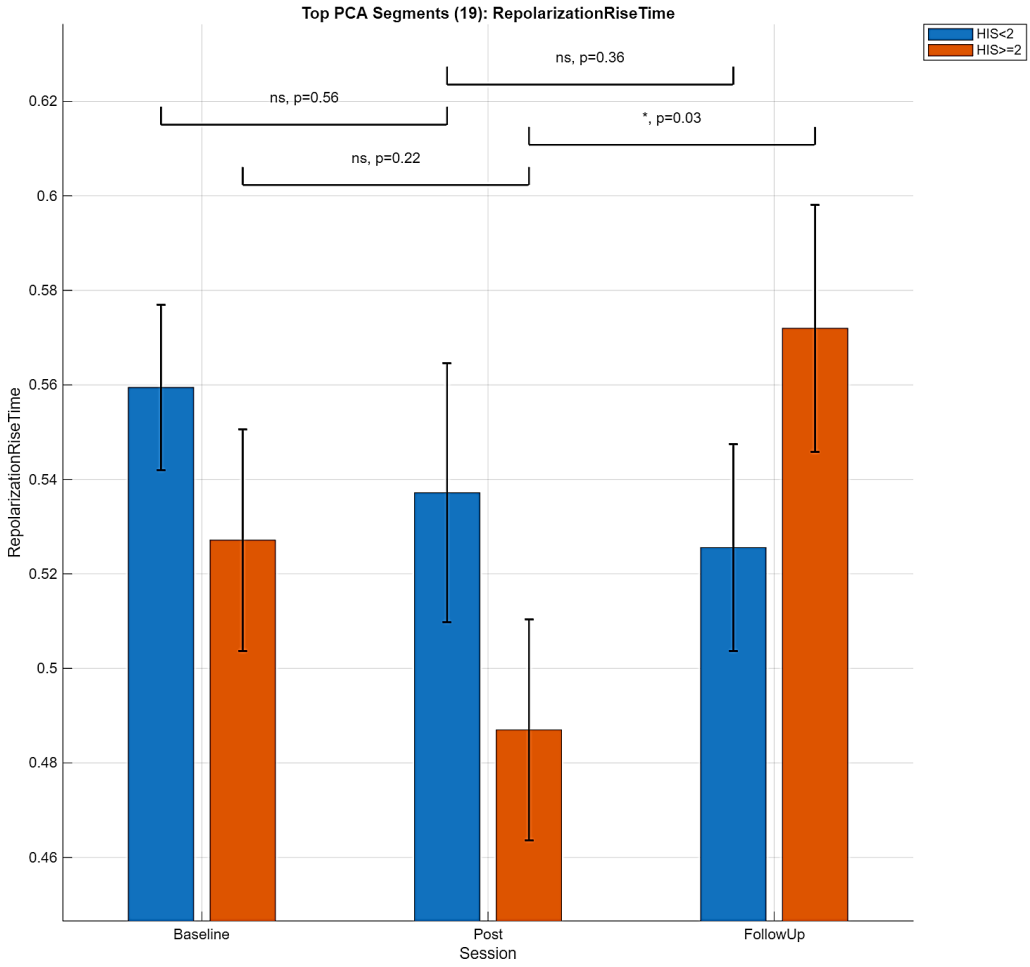

Figure 23. Repolarization Rise Time. PCA trend analysis of Repolarization Rise Time under sham tACS+CE. Mean Repolarization Rise Time values from the top 19 PCA-selected segments are shown across baseline, post-treatment, and follow-up sessions for HIS < 2 and HIS ≥ 2 groups. Error bars represent standard error. The list of selected segments and their PC1 loadings are provided in Appendix C, Table C.1.

For repolarization rise time, a distinct pattern was observed. The HIS ≥ 2 group showed a decrease at post-treatment followed by a marked increase at follow-up, whereas the HIS < 2 group

demonstrated a gradual decline across sessions. Notably, a significant difference ($p = 0.03$) was observed between post-treatment and follow-up in the HIS ≥ 2 group, indicating a meaningful change in this feature over time.

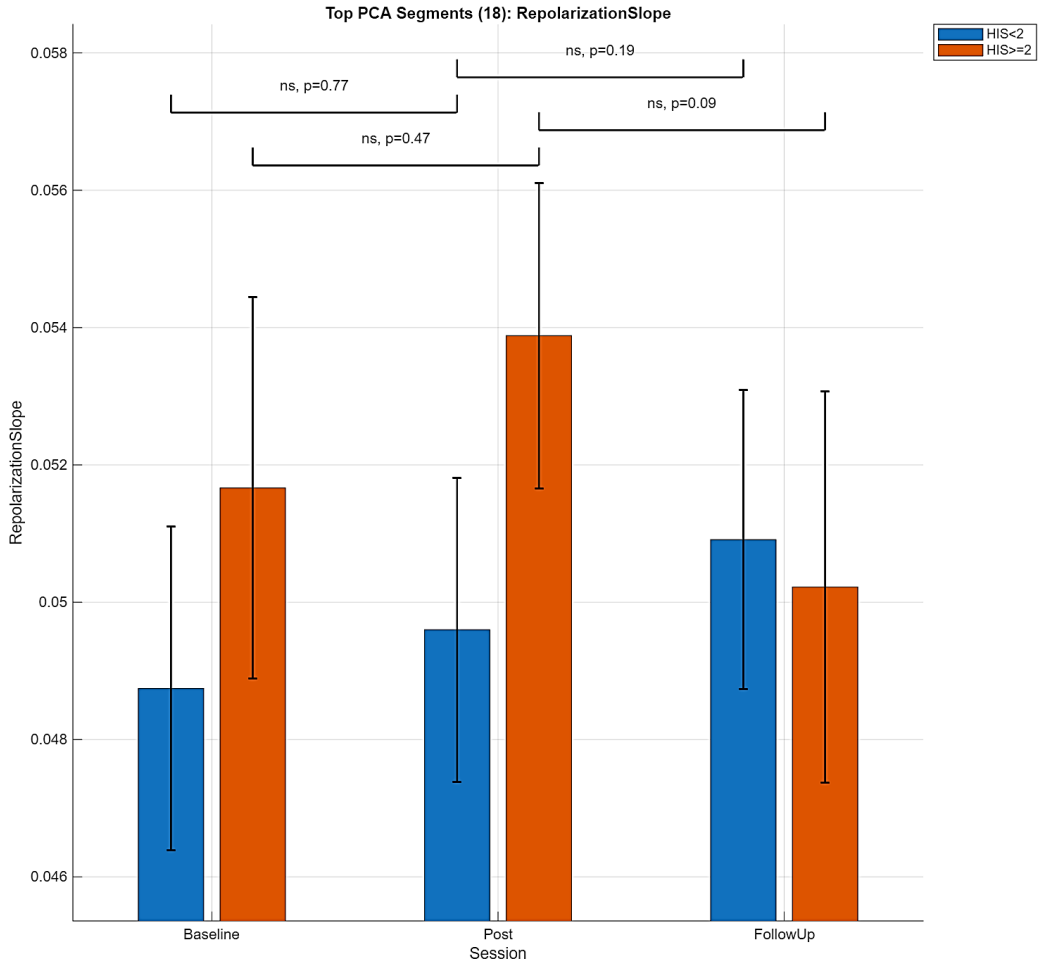

Figure 24. Repolarization Slope. PCA trend analysis of Repolarization Slope under sham tACS+CE. Mean Repolarization Slope values from the top 18 PCA-selected segments are shown across baseline, post-treatment, and follow-up sessions for HIS < 2 and HIS ≥ 2 groups. Error bars represent standard error. The list of selected segments and their PC1 loadings are provided in Appendix C, Table C.1.

The repolarization slope showed a general increase from baseline to post-treatment in the HIS ≥ 2 group, followed by a slight decrease at follow-up. The HIS < 2 group displayed a more modest increase across sessions. However, none of these changes reached statistical significance.

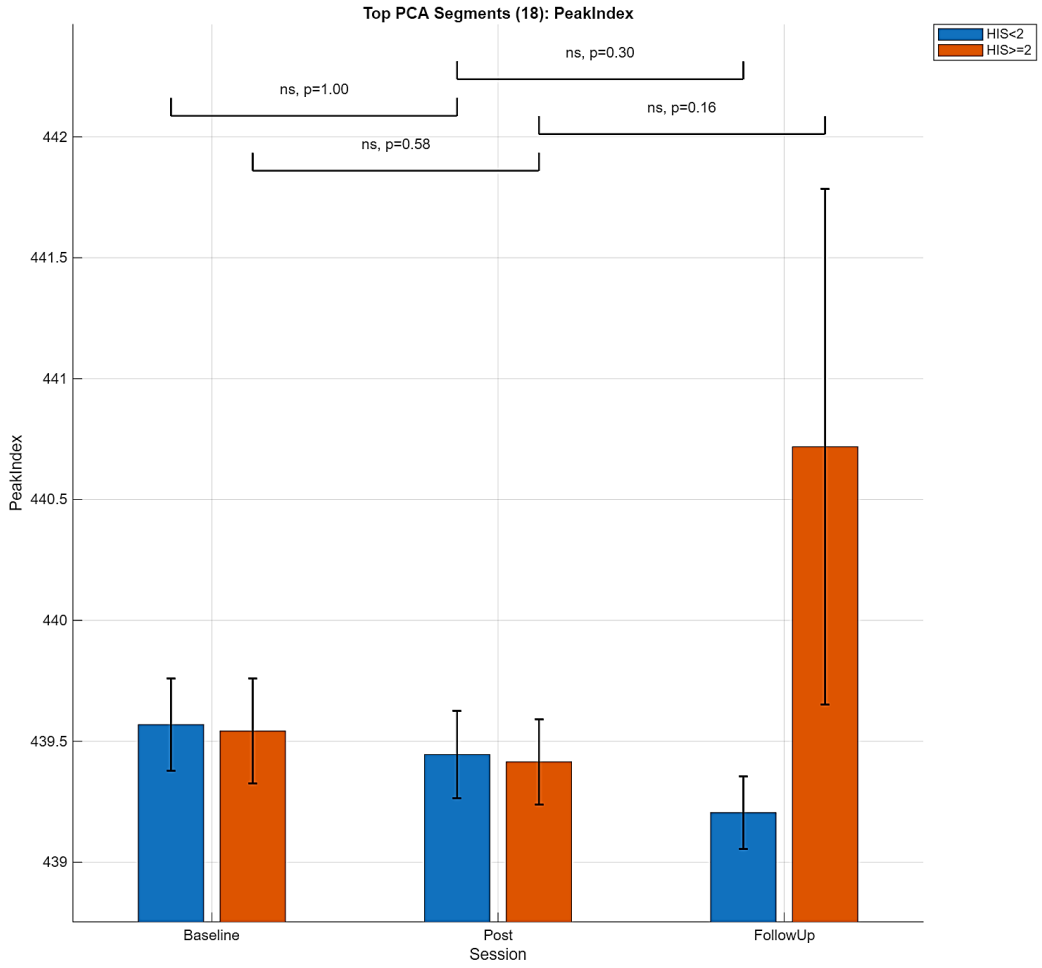

Figure 25. Peak Index. PCA trend analysis of Peak Index under sham tACS+CE. Mean Peak Index values from the top 18 PCA-selected segments are shown across baseline, post-treatment, and follow-up sessions for HIS < 2 and HIS ≥ 2 groups. Error bars represent standard error. The list of selected segments and their PC1 loadings are provided in Appendix C, Table C.1.

Finally, the peak index remained relatively stable across sessions for the HIS < 2 group, whereas the HIS ≥ 2 group showed a marked increase at follow-up. Despite this apparent divergence, statistical testing indicated no significant differences across sessions.

Afterwards, ICA was applied to the EVestG features to identify statistically independent patterns underlying the signal changes in participants with HIS < 2 and HIS ≥ 2 who received sham tACS + cognitive exercises. The analysis was performed separately for the changes between baseline and post-treatment (Δpost) and between post-treatment and follow-up (Δfollow). The IC for each feature was examined in terms of its contribution, magnitude, and temporal consistency.

4.2.7 ICA results for Sham tACS + cognitive exercises treatment in low and high HIS scores

ICA was applied to identify statistically independent source patterns in participants who received sham tACS + cognitive exercises. In participants with HIS < 2, the dominant IC accounted for 15–18% of variability during Δpost, increasing to 20–24% during Δfollow, with IC score magnitudes also increasing consistently across all features. This indicates that independent signal structures became more pronounced over time even without active stimulation. Correlations between Δpost and Δfollow were predominantly negative, with Peak Index showing the strongest reversal ($r = -0.96$) and Repolarization Slope also showing substantial change ($r = -0.67$). The most informative segments were associated with RTC phases and posterior/vertical tilts (PUL, BAL, PRR).

In participants with HIS ≥ 2, the dominant IC captured a larger proportion of variability (20–27%), with a more uniform distribution across features compared to the low HIS group. A strong negative correlation was observed for Depolarization Slope ($r = -0.98$), while Repolarization Rise Time and AP Area showed weak positive correlations, indicating mixed temporal stability. Compared

to the low HIS group, there was a stronger representation of supine position tilts (PUL, PRR), suggesting a shift toward posterior vestibular dominance in participants with higher cerebrovascular burden. Full details of IC contributions, score magnitudes, correlations, and dominant segment tables are provided in Appendix D.

Overall, both HIS subgroups showed increasing IC strength over time, but limited temporal stability of the independent patterns — a finding consistent with the ICA results from the tACS + cognitive exercises group and supporting the interpretation that independent component structures are inherently more dynamic than the dominant variance patterns captured by PCA. Based on these ICA results, the segments with the strongest IC contributions were selected for the trend analyses presented below.

4.2.8 ICA trend results for Sham tACS + cognitive exercises

Following the ICA component analysis presented above, temporal trend analyses were performed to examine how the EVestG features evolved across sessions under the sham tACS+CE condition. ICA was again used as a segment-selection tool. For each feature, the segments with the highest IC loadings were selected, and their original (non-transformed) feature values were examined across baseline, post-treatment, and follow-up sessions for both HIS < 2 and HIS ≥ 2 groups. Overall, the ICA-based trends revealed feature-dependent temporal dynamics, with clear differences between the two groups in both magnitude and direction of change.

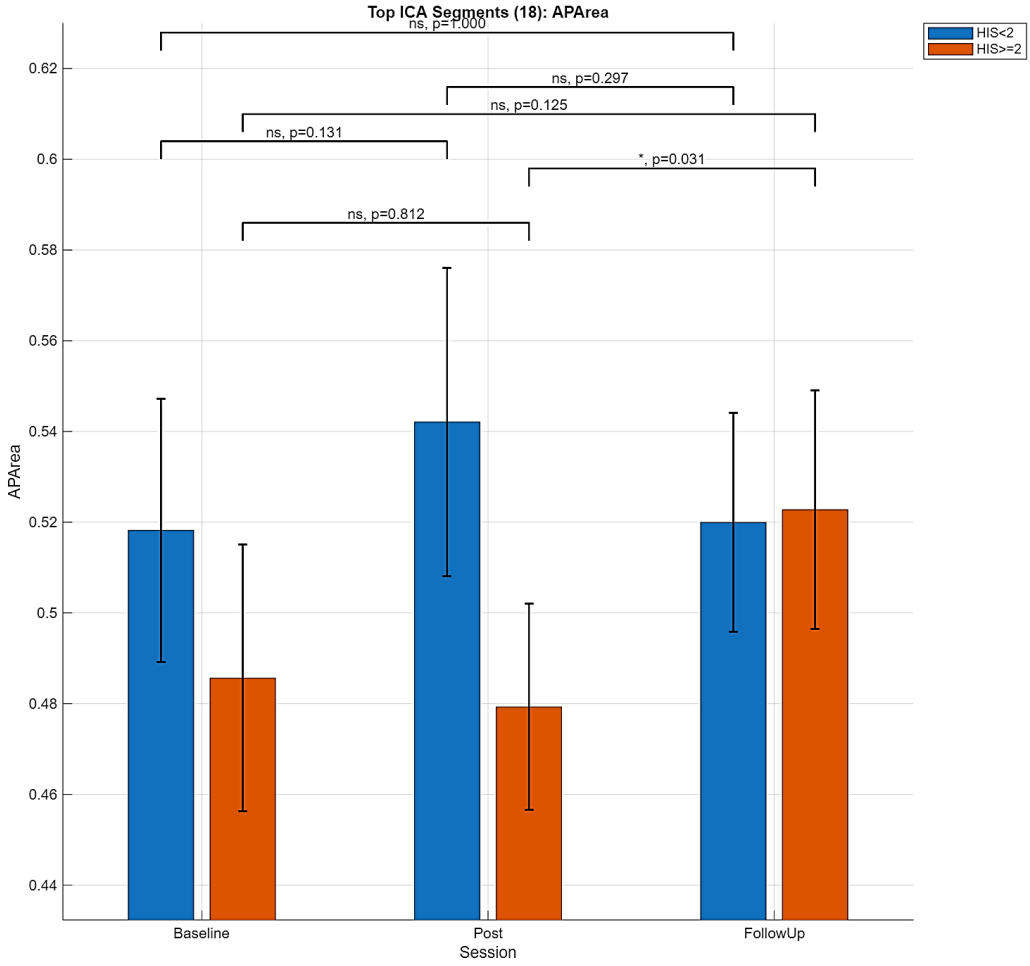

Figure 26. AP Area. ICA trend analysis of AP Area under sham tACS+CE. Mean AP Area values from the top 18 ICA-selected segments are shown across baseline, post-treatment, and follow-up sessions for HIS < 2 and HIS ≥ 2 groups. Error bars represent standard error. A significant difference was observed between post-treatment and follow-up for the HIS ≥ 2 group ($p = .031$). The list of selected segments and their IC1 loadings are provided in Appendix D, Table D.1.

For AP area, participants with HIS < 2 exhibited a modest increase from baseline to post-treatment followed by stabilization at follow-up. In contrast, the HIS ≥ 2 group showed a relatively lower value at baseline and post-treatment but demonstrated an increase at follow-up, resulting in convergence between the two groups. A statistically significant difference was observed between

post-treatment and follow-up in the HIS ≥ 2 group ($p \approx 0.031$), suggesting delayed changes in signal magnitude in this group.

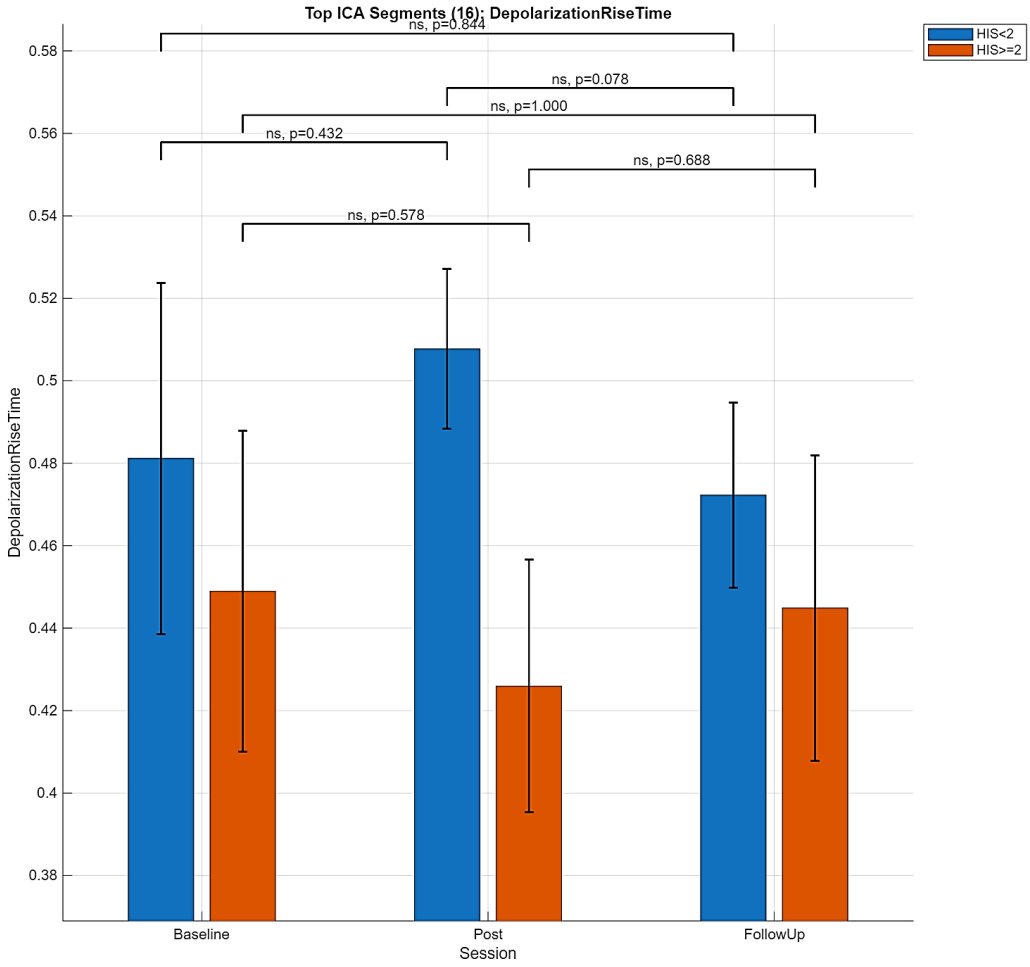

Figure 27. Depolarization Rise Time. ICA trend analysis of Depolarization Rise Time under sham tACS+CE. Mean Depolarization Rise Time values from the top 16 ICA-selected segments are shown across baseline, post-treatment, and follow-up sessions for HIS < 2 and HIS ≥ 2 groups. Error bars represent standard error. The list of selected segments and their IC1 loadings are provided in Appendix D, Table D.1.

For depolarization rise time, the two groups exhibited distinct temporal patterns rather than a common trend. The HIS < 2 group showed an increase from baseline to post-treatment followed

by a decrease at follow-up. In contrast, the HIS ≥ 2 group demonstrated a decrease from baseline to post-treatment and a recovery at follow-up, without returning to baseline levels. Across all sessions, the HIS ≥ 2 group consistently exhibited lower values than the HIS < 2 group, suggesting an overall attenuated depolarization response. Despite these opposing trajectories, no statistically significant between-session differences were observed.

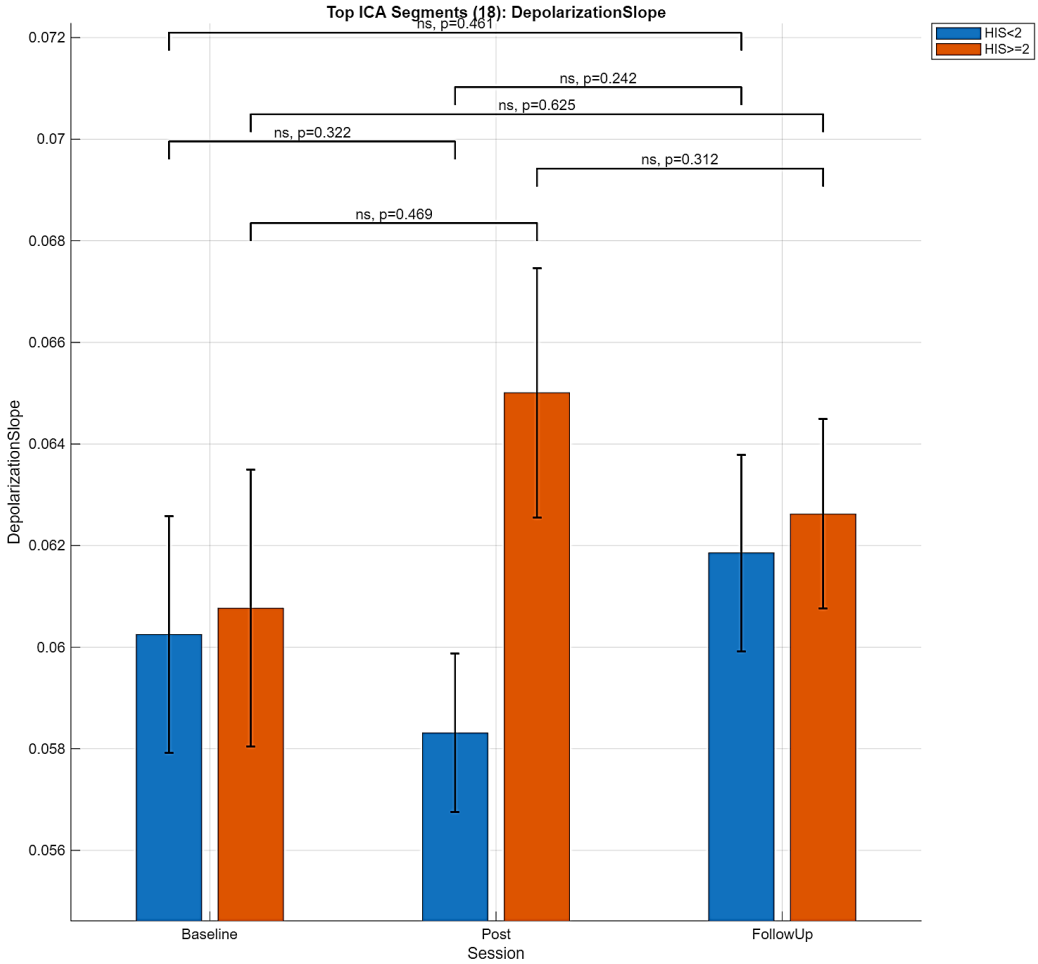

Figure 28. Depolarization Slope. ICA trend analysis of Depolarization Slope under sham tACS+CE. Mean Depolarization Slope values from the top 18 ICA-selected segments are shown across baseline, post-treatment, and follow-up sessions for HIS < 2 and HIS ≥ 2 groups. Error bars

represent standard error. The list of selected segments and their IC1 loadings are provided in Appendix D, Table D.1.

For depolarization slope, the HIS < 2 group demonstrated a slight decrease at post-treatment followed by recovery at follow-up, whereas the HIS ≥ 2 group showed a marked increase at post-treatment that remained elevated at follow-up. This divergence suggests that participants with higher cerebrovascular burden exhibit stronger modulation in depolarization dynamics during cognitive exercise, although these changes did not reach statistical significance.

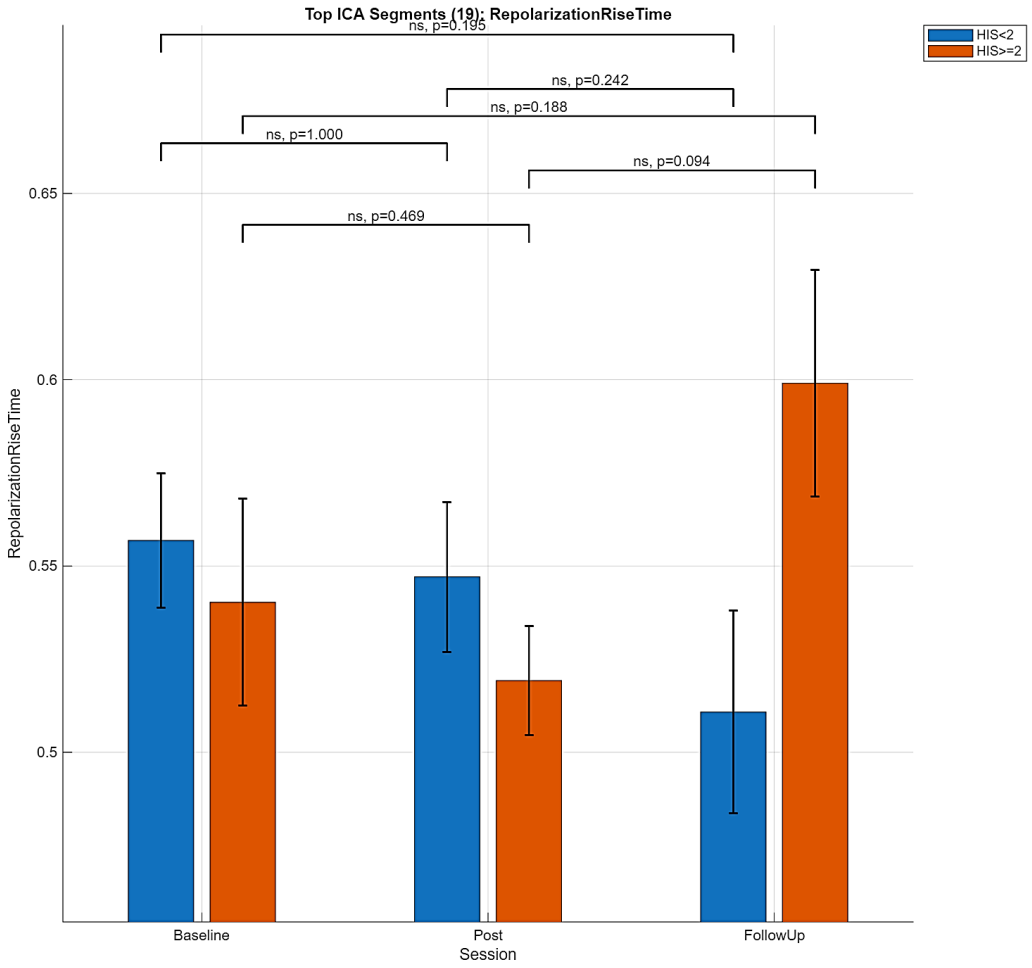

Figure 29. Repolarization Rise Time. ICA trend analysis of Repolarization Rise Time under sham tACS+CE. Mean Repolarization Rise Time values from the top 19 ICA-selected segments are shown across baseline, post-treatment, and follow-up sessions for HIS < 2 and HIS ≥ 2 groups. Error bars represent standard error. The list of selected segments and their IC1 loadings are provided in Appendix D, Table D.1.

For repolarization rise time, the HIS < 2 group showed a gradual decrease across sessions, whereas the HIS ≥ 2 group demonstrated a marked increase at follow-up. This opposing trend suggests differential recovery or adaptation mechanisms in repolarization dynamics, although the changes were not statistically significant.

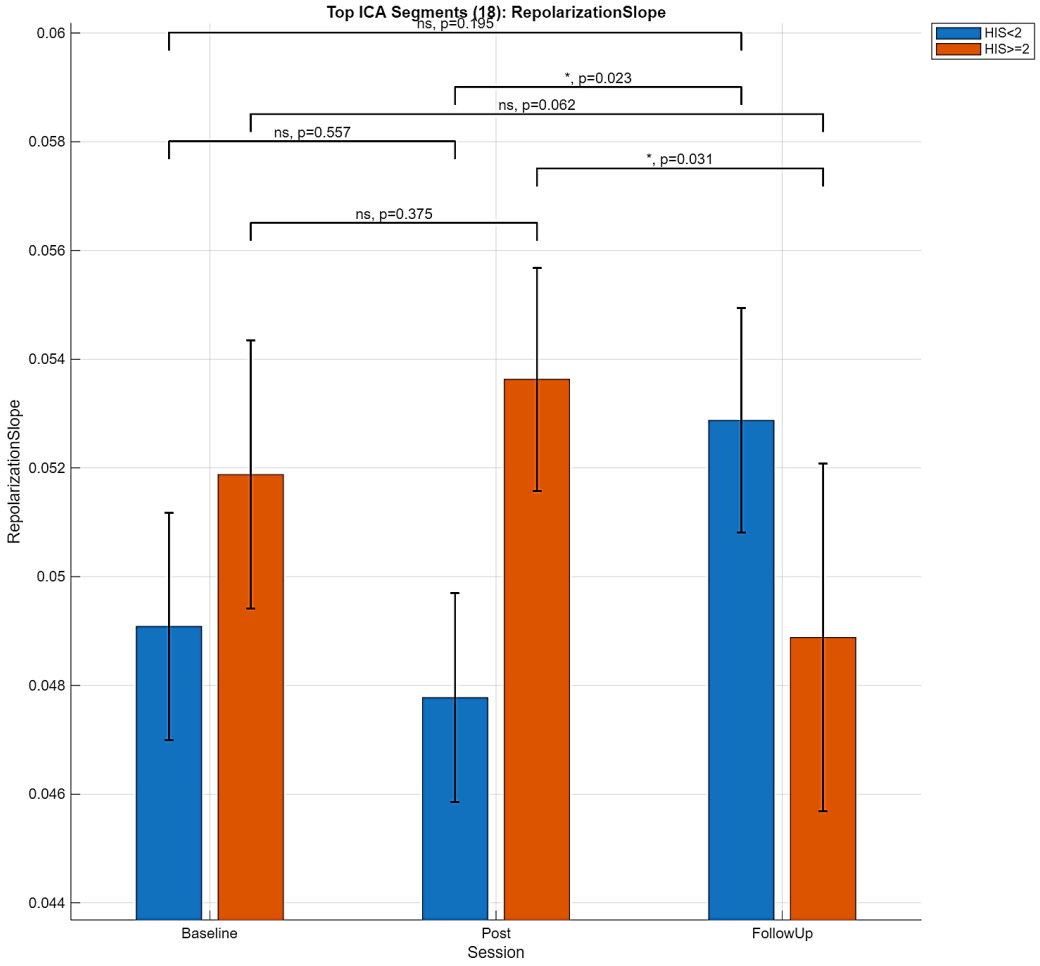

Figure 30. Repolarization Slope. ICA trend analysis of Repolarization Slope under sham tACS+CE. Mean Repolarization Slope values from the top 18 ICA-selected segments are shown across baseline, post-treatment, and follow-up sessions for HIS < 2 and HIS ≥ 2 groups. Error bars represent standard error. The list of selected segments and their IC1 loadings are provided in Appendix D, Table D.1.

For repolarization slope, the HIS < 2 group exhibited a gradual increase across sessions, while the HIS ≥ 2 group showed an increase at post-treatment followed by a decrease at follow-up. Notably, significant differences were observed in comparisons involving follow-up ($p \approx 0.023$ and $p \approx$

0.031), indicating that repolarization dynamics are particularly sensitive to group differences at later stages.

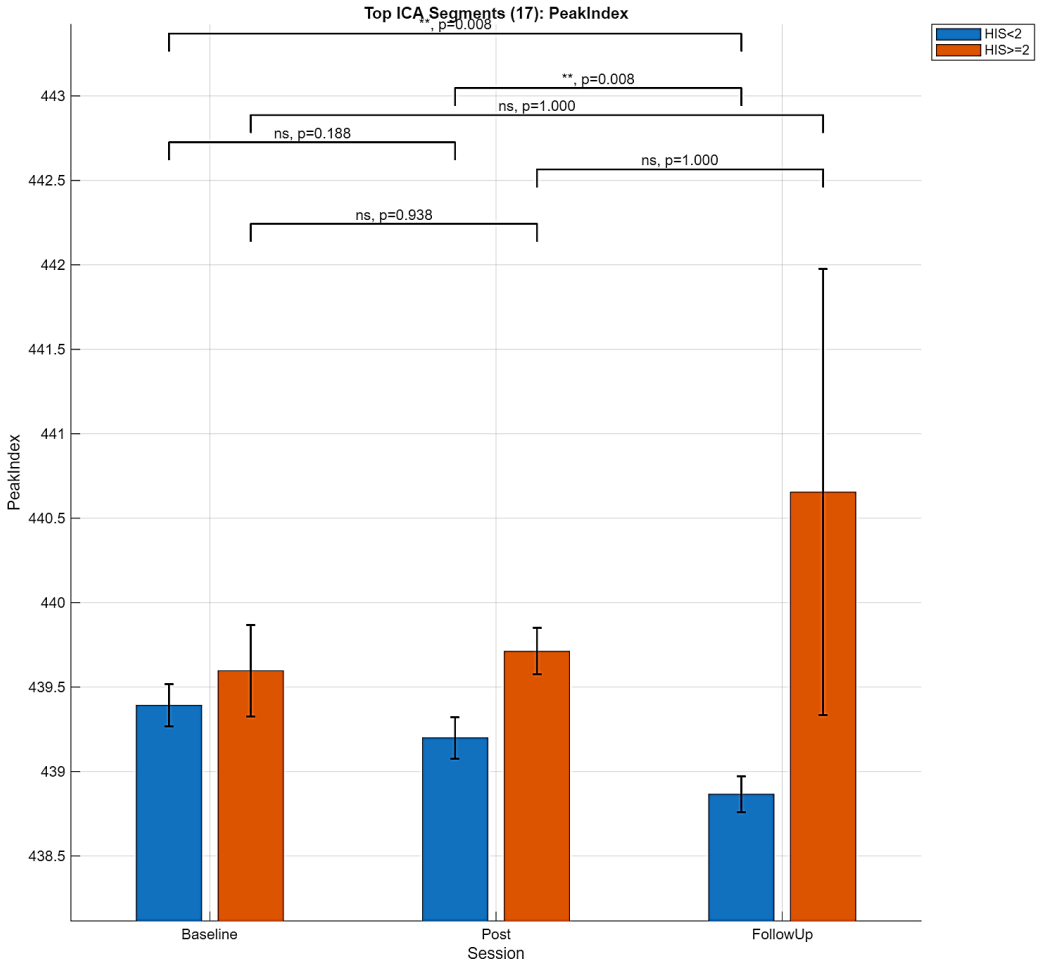

Figure 31. Peak Index. ICA trend analysis of Peak Index under sham tACS+CE. Mean Peak Index values from the top 17 ICA-selected segments are shown across baseline, post-treatment, and follow-up sessions for HIS < 2 and HIS ≥ 2 groups. Error bars represent standard error. The list of selected segments and their IC1 loadings are provided in Appendix D, Table D.1.

The most pronounced group difference was observed for Peak Index. While the HIS < 2 group showed a gradual decrease across sessions, the HIS ≥ 2 group exhibited a substantial increase,

particularly at follow-up. This difference was statistically significant ($p \approx 0.008$), indicating a strong divergence in peak timing characteristics between the two groups over time.

These ICA-based trend analyses demonstrate that, while both groups exhibit temporal changes in EVestG features, participants with higher cerebrovascular burden show greater variability, delayed responses, and stronger divergence across features, particularly in peak timing and repolarization dynamics, highlighting distinct underlying neural adaptation patterns following cognitive exercises.

4.3 Summary of Results

This section draws the individual analyses together into a single narrative. The AP-area analysis proceeded in stages: AP area was first averaged across all 42 left-ear segments for the whole sample (Figure 4), which revealed no clear session-to-session pattern and motivated two refinements — separating motion-evoked (dynamic) from stationary (static) segments, and classifying participants by cerebrovascular burden (HIS < 2 vs HIS ≥ 2). The classified AP-area trends (Figures 5–6), the cognitive trajectories (Figure 7), and the PCA/ICA decompositions of the full feature set (Figures 8–31) together support four main observations, all of which are reported as non-significant trends given the small subgroup sizes and overlapping distributions.

4.3.1 Effect of Active versus Sham tACS

Active tACS + CE was associated with more structured and temporally consistent EVestG patterns than sham. Under active stimulation, both PCA and ICA were dominated by timing-related features — depolarization and repolarization rise times and peak index — and showed more stable evolution across sessions, consistent with enhanced temporal synchronization of vestibular-related neural firing. Sham was instead dominated by recovery- and slope-related features and showed

greater variability and more feature-specific fluctuation, consistent with less coordinated modulation. These effects were clearest in the left ear, consistent with left-DLPFC stimulation preferentially engaging left-sided vestibulo-cortical circuits.

4.3.2 Influence of cerebrovascular burden (HIS)

HIS level changed both the direction and the stability of the response. In the dynamic condition, the HIS < 2 subgroup showed a sustained narrowing of AP area across sessions and a more distributed pattern of feature importance, consistent with a more adaptable neural system, alongside an improving ADAS-Cog trajectory. The HIS ≥ 2 subgroup instead showed an initial narrowing at post-treatment followed by a rebound widening at follow-up, was dominated by AP area and slope-based features and paralleled a partial loss of cognitive gain — consistent with a more rigid, less adaptable response associated with higher vascular burden.

4.3.3 Most sensitive features and segments

Across analyses, AP area served as the most interpretable summary feature, indexing overall narrowing and widening of the waveform, while depolarization and repolarization rise times and peak index were the features most responsive to active stimulation. At the segment level, motion-evoked dynamic segments (OnBB and RTC-OnAA), recorded predominantly in supine and vertical tilt orientations, were more sensitive to treatment-related change than stationary segments, and were also the segments most consistently identified as dominant by both PCA and ICA. Notably, dynamic and static AP areas tended to move in opposite directions, suggesting that evoked and spontaneous activity reflect different facets of the same circuit's response to stimulation.

4.3.4 How the findings fit together

Taken as a whole, the results indicate that EVestG-derived AP features — particularly dynamic AP area together with timing-related measures — may be able to track neurophysiological change associated with gamma tACS + CE, and that this change depends on cerebrovascular status. Lower-burden participants trend toward a narrower, more control-like waveform that is sustained through follow-up and accompanied by cognitive improvement, whereas higher-burden participants show only a transient narrowing before reverting toward their broader baseline morphology. This convergence of the AP-area trends, the feature-level patterns, and the cognitive trajectories — interpreted alongside HIS classification — forms the basis for the mechanistic discussion that follows. All observations remain trend-level and hypothesis-generating and require confirmation in larger cohorts.

Chapter 5: Discussion

This study investigated the temporal evolution of EVestG-derived AP features following real and/or sham tACS combined with cognitive exercises, with participants classified based on cerebrovascular burden. Using both PCA and ICA, the results indicated that EVestG features may capture distinct and evolved neural response patterns across sessions, with apparent differences between stimulation conditions and participant groups. Building on prior EVestG work relating waveform-feature changes to cognitive performance [33], and on the left–right asymmetry observed here (Section 4.1), the present study shows how both dominant and independent neural components evolve over time under different intervention conditions and reflect underlying differences in neural adaptability associated with cerebrovascular burden.

Before these patterns are interpreted, an important caveat must be emphasized. The subgroup analyses in this study are based on small samples — particularly the higher-cerebrovascular-burden group (HIS ≥ 2), which contained only six participants in the active condition and seven in the sham condition — and the box-and-whisker distributions show substantial overlap in their error bars across sessions. With the exception of some single pairwise comparison, none of the within- or between-subgroup changes reached statistical significance. Accordingly, all subgroup differences discussed in this chapter should be regarded as non-significant trends that are hypothesis-generating rather than confirmatory. They are interpreted here for their direction and physiological plausibility, and to motivate replication in larger cohorts, but no claim of a statistically established treatment effect is intended. This caution applies throughout the sections that follow.

5.1 PCA versus ICA

PCA and ICA were applied to the EVestG feature space with different objectives, and the distinction between them is important for interpreting the results rather than treating the two as interchangeable. PCA is a second-order method: it finds orthogonal directions that successively capture the maximum variance in the data, so its components are, by construction, uncorrelated and ranked by how much overall variability they explain. It therefore answers the question of which features and segments dominate the aggregate signal structure. ICA makes a different assumption. It models the recorded EVestG signal as a linear mixture of underlying sources and seeks components that are statistically independent — using higher-order statistics and non-Gaussianity rather than variance — without imposing orthogonality or any ranking by magnitude. It therefore answers a separate question: which underlying sources are mixed together in the measurement, regardless of how much variance each contributes. Because a low-variance source can be physiologically meaningful, a process that PCA folds into a minor component may emerge as a distinct independent component under ICA. PCA and ICA are thus not redundant or simply complementary; they recover different aspects of the same data, and using both provides a fuller account than either alone.

The rationale for applying ICA to EVestG rests on the assumption that the recorded field potential is not the expression of a single neural process but a mixture of several that are at least partially independent. Plausible contributing sources include the activity of functionally distinct afferent populations responding to the different motion phases (acceleration, deceleration, and stationary background), efferent vestibular modulation descending from brainstem and cortical regions, vascular- and perfusion-related contributions that differ with cerebrovascular burden, and non-neural components such as recording artifact [11, 12]. These processes are summed at the electrode

and are not expected to covary in a simple, variance-aligned way, which is precisely the situation ICA is designed to address: where PCA would distribute a shared source across several correlated components, ICA can isolate it as a single independent component. This is why ICA, in the present analysis, recovered feature-specific and sometimes oppositely directed temporal trends that were not apparent in the variance-ranked PCA components, and why it is retained alongside PCA rather than replaced by it.

An important finding of this study is the variability in temporal dynamics between the post-treatment and follow-up intervals. The correlation analysis revealed that, while some features exhibited moderate positive correlations, indicating consistent behavior over time, others showed weak or even strong negative correlations, suggesting substantial changes or reversals in the underlying signal patterns (see Appendix A to D for detailed correlation values). These findings indicate that EVestG responses do not follow a simple linear progression after intervention but instead reflect dynamic and evolving neural processes. The presence of strong negative correlations ($r < -0.7$ in several cases) suggests that initial responses may undergo systematic reorganization or compensatory adaptation during follow-up, rather than simple decay or maintenance of treatment effects. This highlights the importance of considering longer-term temporal effects when evaluating neural responses to stimulation. This dynamic behavior was consistently more pronounced in ICA results across all conditions and consistent with the view that independent component analysis better captures the complex, multi-source nature of vestibular neural adaptations to stimulation.

5.2 Feature-Level Interpretation

The observed changes across EVestG features provide insight into different aspects of neural response dynamics. Depolarization-related features, including depolarization slope and rise time,

reflect the initial activation of neural responses and are indicative of how rapidly neural elements respond to vestibular stimulation. In contrast, repolarization-related features, such as repolarization rise time and slope, represent recovery processes and the return of neural activity toward baseline. Features related to signal timing, particularly peak index, reflect the temporal coordination and synchronization of neural responses. The differential behavior of these features across groups and conditions suggests that both activation and recovery mechanisms are modulated by stimulation and are affected by cerebrovascular burden, with timing-related features showing sensitivity to group differences. Notably, while some features may exhibit mathematical interdependencies (e.g., AP area and rise times), PCA and ICA analyses account for these relationships by identifying orthogonal and independent components, respectively.

Across all subgroup analyses, a consistent pattern emerged regarding the relative importance of EVestG-derived AP features under different stimulation conditions and levels of cerebrovascular burden. In participants who first received active tACS combined with cognitive exercises the dominant features identified through both PCA and ICA were primarily related to temporal characteristics of the AP waveform, particularly depolarization and repolarization rise times as well as peak index. These timing-related features reflect the temporal organization and synchronization of neural responses, suggesting that tACS is associated with more structured and coordinated modulation of neural activity. The prominence of these features indicates that active stimulation may enhance the temporal precision of vestibular-related neural firing patterns.

In contrast, participants who first received sham tACS + cognitive exercises demonstrated a different feature profile, with dominant contributions arising mainly from repolarization-related measures and slope-based features. These features describe the recovery dynamics and rate of change of the neural response rather than its timing. The increased importance of repolarization

slope and rise time in this group suggests that, in the absence of active stimulation, neural responses are characterized by less coordinated and more variable recovery processes. This pattern is consistent with weaker or less organized neural modulation, where the system does not converge toward a dominant temporally synchronized response.

Further differentiation was observed when participants were classified based on cerebrovascular burden. In individuals with higher modified HIS (HIS ≥ 2), features such as AP area and slope-based measures consistently showed dominant contributions across both PCA and ICA analyses. The AP area reflects the overall magnitude of the neural response, while slope features capture rapid changes in activation and recovery phases. The dominance of these features, along with the higher variance explained by PC1 and stronger IC contributions, indicates that neural activity in this group is governed by a more pronounced but less flexible dominant pattern. This suggests reduced adaptability and increased rigidity in neural response dynamics, potentially reflecting underlying cerebrovascular-related impairments in neural regulation.

In contrast, participants with lower cerebrovascular burden (HIS < 2) exhibited a more distributed pattern of feature importance, with no single feature consistently dominating across analyses. Instead, multiple features, including both timing- and amplitude-related measures, contributed to the observed patterns. This distributed representation suggests a more adaptive and flexible neural system, where multiple underlying processes interact to shape the EVestG signal. Such variability may reflect a greater capacity for neural modulation and reorganization in response to stimulation and cognitive engagement.

Taken together, these findings demonstrate that EVestG-derived AP features capture distinct aspects of neural dynamics that vary systematically with both intervention type and cerebrovascular status. The dominance of timing-related features in the tACS + cognitive exercises

condition highlights the role of stimulation in enhancing neural synchronization, whereas the prevalence of recovery-related features in the sham tACS + cognitive exercises condition reflects less structured neural responses. Moreover, the contrast between HIS ≥ 2 and HIS < 2 groups underscores the influence of cerebrovascular burden on the balance between dominant and distributed neural patterns, providing further evidence for altered neural adaptability in populations with higher vascular impairment. These feature-level insights provide the foundation for the comparative analyses presented in the following sections.

5.3 Real versus Sham tACS + cognitive exercises

The comparison between active tACS + cognitive exercises and sham tACS + cognitive exercises revealed clear differences in the structure and evolution of EVestG features. To assess the clinical relevance of the observed neurophysiological trends, the temporal patterns of EVestG-derived features were compared with ADAS-Cog score trajectories at the group level. This comparison was intended to evaluate whether the direction and pattern of neurophysiological changes were consistent with cognitive outcomes, rather than to establish a formal statistical association between the two measures. In the active stimulation condition, both PCA and ICA results demonstrated more structured and consistent patterns across features and sessions, with clearer dominance of specific segments and more stable temporal evolution. In contrast, the sham condition showed greater variability, less consistent feature trends, and more pronounced feature-specific differences, particularly in ICA results. These findings suggest that active tACS contributes to the modulation of neural activity in a more organized manner, potentially enhancing the coherence of vestibular-related neural responses.

To further interpret these findings, the trend plots of key features, including depolarization and repolarization rise times, were examined alongside the AP area to provide an overall view of AP

waveform changes. Focusing on the HIS < 2 subgroup, the results for the tACS + cognitive exercises condition (Figures. 9, 11, 15 and 17) from both PCA and ICA analyses showed a gradual decrease in both depolarization and repolarization rise times across sessions. This suggests that, from baseline to post-treatment, both the depolarization phase and the recovery phase of the AP became faster, and this effect persists during the wash-out period from post-treatment to follow-up. In addition, the AP area trends (Figures. 8 and 14) exhibited a similar gradual decrease from baseline to follow-up in both PCA and ICA results. Together, these observations suggest that active tACS combined with cognitive exercises leads to a narrowing of the AP waveform. This finding is consistent with previous studies indicating that a narrower AP segment in EVestG averaged FPs reflects faster depolarization and repolarization of vestibular afferent neurons, potentially associated with increased Na^+ channel activity and reduced pre- and post-potential hyperpolarization [14].

In contrast, the HIS < 2 subgroup in the sham tACS + cognitive exercises condition showed a different pattern (Figures. 21, 23, 27, and 29). Depolarization rise time increased from baseline to post-treatment and then decreased slightly, though not significantly, during the follow-up period. Meanwhile, repolarization rise time continued to show a gradual decrease from baseline to follow-up. The AP area trends derived from both PCA and ICA analyses in this group (Figures. 20, 26) followed a pattern similar to that of depolarization rise time. Overall, these trends suggest that the absence of active tACS is associated with slower depolarization dynamics, potentially reflecting reduced Na^+ channel activity. However, the recovery phase still became faster over time, although to a lesser extent than in the real condition. This implies that sham condition may influence repolarization mechanisms, possibly related to K^+ channel activity, whereas enhancement of the depolarization phase appears to require the additional effect of active tACS.

Focusing on the HIS ≥ 2 subgroup, the results for the active tACS + cognitive exercises condition from both PCA and ICA analyses showed a different temporal pattern compared to the HIS < 2 group. Depolarization rise time (Figure. 9) generally remained steady from baseline to post-treatment, followed by an increase during the follow-up period, indicating a partial reversal or recovery of the depolarization dynamics. In Figure. 11, repolarization rise time exhibited an increase from post-treatment to follow-up, suggesting a delayed enhancement of the recovery phase. In addition, the AP area trends derived from both PCA and ICA analyses (Figures 8 and 14) showed a decrease from baseline to post-treatment followed by a marked increase at follow-up. Together, these observations suggest a widening of the AP waveform over time rather than a sustained narrowing. This pattern is consistent with the known neurovascular characteristics of AD-CVD and the temporal dynamics of tACS-induced modulation reported in EVestG studies [6, 14]. From baseline to post-treatment, the application of real tACS combined with cognitive exercises induces an immediate, hemisphere-specific entrainment effect that transiently accelerates both depolarization and repolarization phases, resulting in a narrower AP waveform, as reflected by the reduced AP area [6]. This effect is consistent with prior findings in populations with lower vascular burden, where subthreshold electric fields enhance the excitability of vestibular afferents [6]. However, from post-treatment to follow-up, a different pattern emerges in participants with higher cerebrovascular burden. In this group, the EVestG signal is influenced by the inherently slower and broader AP waveform associated with AD-CVD, characterized by delayed depolarization dynamics [6, 14]. The delayed increase in depolarization and repolarization rise times and the rebound widening of the AP area therefore may reflect vascular-mediated adaptive processes that emerge after stimulation. Recent evidence suggests that the effects of transcranial electrical stimulation extend beyond direct neural entrainment and include primary

vascular responses, such as improved perfusion and neurovascular coupling [31, 32]. In particular, 40 Hz tACS has been shown to increase cerebral blood flow in the temporal lobes and hippocampi of AD patients [31]. These vascular pathways may be especially relevant in participants with higher cerebrovascular burden, where the indirect, perfusion-mediated effects of active tACS could predominate over the immediate neural entrainment observed in participants with lower HIS. Consequently, while the initial narrowing of the AP waveform represents the direct neurophysiological effect of active tACS, the subsequent widening during follow-up likely reflects the re-emergence of the underlying vascular-constrained neural dynamics. These findings indicate that EVestG-derived shape metrics, particularly AP area and rise times, when interpreted alongside HIS classification, may capture both the acute neural modulatory effects of active tACS and the delayed, vascular-related adaptations characteristic of AD and AD-CVD.

The HIS ≥ 2 subgroup in the sham tACS + cognitive exercises condition showed a distinct pattern compared to the active stimulation condition (Figures. 21, 23, 27, and 29). Depolarization rise time generally decreased from baseline to post-treatment and then increased again during the follow-up period, indicating a partial recovery toward baseline levels. In contrast, repolarization rise time exhibited a more stable or slightly increasing trend from post-treatment to follow-up, suggesting a delayed or less consistent recovery dynamic. The AP area trends derived from both PCA and ICA analyses in this group (Figures. 20, 26) showed a gradual increase at follow-up after an initial reduction or stabilization post-treatment, reflecting a widening of the AP waveform over time. Overall, these trends suggest that, in the absence of active tACS, neural responses in participants with higher cerebrovascular burden are characterized by less stable and more fluctuating dynamics. The depolarization phase showed an initial decrease in rise time at post-treatment that reversed at follow-up, rather than a sustained acceleration, suggesting limited long-term enhancement of Na^+

channel-related activity. The recovery phase showed a slight slowing of repolarization rise time from baseline to post-treatment with limited change at follow-up, suggesting only partial modulation of K^+ channel mechanisms. This pattern implies that sham tACS combined with cognitive exercises is insufficient to induce consistent or sustained improvements in both activation and recovery phases in this subgroup, and that active tACS may be necessary to achieve more stable and coordinated neural modulation. While these interpretations are consistent with known tACS mechanisms and neurovascular physiology, direct measurement of cerebral blood flow or ion channel activity would be needed to confirm the proposed vascular-mediated pathways in future studies.

5.4 Lower versus higher HIS scores (HIS < 2 vs HIS ≥ 2)

One consideration when interpreting the HIS subgroup trajectories is that the two subgroups did not begin from the same baseline, and their baselines also differed from the pooled (combined) values. This was most pronounced in the dynamic condition under active stimulation, where the mean baseline AP-dynamic area was 26.24 for HIS < 2 but only 21.08 for HIS ≥ 2 — a difference of roughly five units — with both referenced against a dynamic control mean of 19.84. Because the HIS < 2 subgroup was larger (N = 11 versus N = 6), the pooled baseline (a weighted mean of approximately 24.4) sat closer to the HIS < 2 value, so the combined analysis (Figure 4) masked subgroup-specific starting points that became apparent only after classification. In the static condition, by contrast, the two subgroup baselines were much closer together (22.96 versus 23.46 under active stimulation), indicating that the baseline divergence was largely specific to the motion-evoked segments. This heterogeneity carries two implications for interpretation. First, the apparent convergence of the HIS < 2 subgroup toward the control mean across sessions partly reflects its elevated starting point and the correspondingly greater room to decrease; regression

toward the mean therefore cannot be excluded, and the trajectories are best read relative to each subgroup's own baseline rather than in absolute terms. Second, the fact that the baseline difference was confined to the dynamic segments is consistent with the interpretation developed in Section 5.5, that motion-evoked and stationary segments index different aspects of vestibular function. A comparable baseline imbalance was already noted for the ADAS-Cog scores, where the HIS < 2 participants assigned to sham began with higher baseline cognitive impairment. Together, these observations indicate that baseline differences — both between subgroups and between subgroups and the combined sample — represent an important caveat on the present trend-level interpretations.

Having established the effects of the presence and absence of active tACS, the differences in responses between participants with HIS < 2 and HIS ≥ 2 under active stimulation can be further examined. As discussed in the previous subsection, participants with HIS ≥ 2 showed dominant contributions primarily from AP area and slope-based features across both PCA and ICA analyses, whereas participants with HIS < 2 exhibited a more distributed contribution involving both timing- and amplitude-related features. Accordingly, the analysis of slope-based measures provides further insight into these group-specific responses. In both PCA and ICA results (Figures 10, 16), depolarization slope in the HIS ≥ 2 group became steeper from baseline to post-treatment, followed by a reduction in steepness at the follow-up session. In contrast, the HIS < 2 group demonstrated the opposite trend, with an initial reduction in slope followed by an increase at follow-up. For repolarization slope, PCA results (Figure 12) showed both groups exhibiting a similar pattern of slight increase followed by stability. However, ICA results (Figure 18) revealed divergent trends, with the HIS < 2 group showing a slight increase while the HIS ≥ 2 group showed a gradual decrease, suggesting that the independent component structure of repolarization slope differs

between groups. These observations suggest that the primary difference between the two groups lies in the depolarization dynamics, potentially reflecting differential modulation of Na^+ channel activity in response to active tACS. Repolarization mechanisms showed more consistent behavior at the dominant variance level (PCA), but group-specific differences emerged at the independent component level (ICA), indicating that K^+ channel-related recovery dynamics may be more subtly affected by cerebrovascular burden than the depolarization phase.

The observed divergence in depolarization slope trends between the HIS ≥ 2 and HIS < 2 groups can be explained by underlying differences in baseline cerebrovascular dynamics. EVestG studies have consistently shown that participants with higher cerebrovascular burden (HIS $\geq$ 2), representative of AD-CVD, exhibit broader AP waveforms and slower depolarization phases, whereas those with lower HIS demonstrate narrower APs and faster rise dynamics [6, 14]. Consequently, prior to stimulation, the HIS $\geq$ 2 group is characterized by a relatively flatter depolarization slope. We propose that the observed changes in AP waveform are consistent with alterations in ion channel dynamics based on the following reasoning: (1) tACS at gamma frequency (40 Hz) has been shown to modulate cortical excitability [28]; (2) vestibular pathways project through the brainstem to cortical regions [11]; (3) prior EVestG studies have interpreted waveform narrowing as reflecting Na^+ channel upregulation [6, 14]. However, this interpretation remains indirect, as the present study did not measure ion channel activity or cortical excitability directly. Alternative explanations, including changes in neural synchronization or synaptic efficacy, cannot be ruled out. In participants with lower vascular burden, this results in a sustained increase in depolarization speed, reflected as a steeper slope from baseline to post-treatment. In contrast, in the HIS ≥ 2 group, the same stimulation initially compensates for the inherently slower depolarization dynamics, producing a transient steepening of the slope at post-treatment. However,

during the follow-up period, delayed vascular-mediated processes, such as improved cerebral perfusion or neurovascular coupling, contribute to a re-emergence of the underlying AD-CVD physiology. This is reflected as a reduction in depolarization steepness, corresponding to slower Na^+ channel kinetics and a broader AP waveform. In comparison, repolarization slope trends were more consistent across both groups at the dominant variance level (PCA), although ICA revealed some divergence, suggesting that K^+ channel-related recovery dynamics may be more uniformly influenced by chronic vascular conditions at the population level but exhibit group-specific differences when examined through independent component structures.

Across both PCA and ICA analyses, the HIS ≥ 2 group generally exhibited a stronger dominance of the primary signal patterns, as reflected by higher variance explained and larger component contributions. However, this was accompanied by greater variability in temporal dynamics, including fewer positive correlations between post-treatment and follow-up intervals and more feature-specific fluctuations. In contrast, participants with HIS < 2 showed more consistent and transient changes, with clearer progression from baseline to post-treatment and stabilization at follow-up. These findings suggest that while neural responses in the HIS ≥ 2 group may be more strongly driven by dominant patterns, they are also less stable over time, potentially reflecting reduced neural adaptability associated with increased cerebrovascular burden and altered neurovascular coupling.

5.5 Dynamic versus Static conditions

Examination of the top five dominant segments identified in both PCA and ICA analyses revealed clear convergence in their spatial distribution across tilt orientations. Supine and vertical positions were repeatedly represented among the highest-ranking segments, whereas lateral or rotational tilts appeared less consistently. This pattern aligns with the pilot study [27], which showed that

vestibular stimuli engaging the otolithic organs—particularly supine and vertical tilts—produce the most distinctive EVestG responses for differentiating AD from AD-CVD. Corresponding PCA and ICA outcomes in the present study also demonstrate strong agreement between dynamic AP features and the dominant patterns identified by both methods. Specifically, the temporal evolution of AP-dynamic areas mirrors the features and segments most frequently identified as dominant contributors. The recurrent detection of motion-related phases (OnBB and RTC-OnAA) and the comparatively lower representation of static phases (BGi and RTC-BGi) suggests that dynamic components of the EVestG signal more accurately reflect the neural changes associated with intervention. Collectively, these observations reinforce that movement-evoked vestibular responses, particularly those elicited in supine and vertical orientations, are optimal for capturing disease-specific or stimulation-induced electrophysiological effects.

The stronger representation of dynamic segments in both the statistical analyses and the observed AP-area trends indicates that neural responses are more sensitive to vestibular stimulation during movement-related phases than during stationary conditions. Dynamic segments reflect evoked vestibular activity and thus more readily exhibit pronounced changes in AP characteristics after intervention, whereas static segments primarily capture baseline or spontaneous activity, which appears less responsive to modulation.

Overall, these findings show that dynamic EVestG features offer greater sensitivity for detecting treatment-related neural changes and correspond more closely with the dominant variance and independent signal structures identified through PCA and ICA. This supports the interpretation that movement-related vestibular responses play a central role in mediating the neurophysiological effects of tACS and cognitive exercises.

A central question raised by these findings is why the dynamic and static AP-area trends did not move in the same directions during the treatment interval, rather than simply differing in magnitude. Although the present study did not measure ion-channel activity or cortical excitability directly, this opposition is consistent with the two segment types reflecting functionally distinct states of the same vestibular afferent population. The dynamic segments (OnBB and RTC-OnAA) capture the motion-evoked response, in which afferents fire in a phase-locked manner temporally coupled to the stimulus. Gamma tACS is thought to act preferentially on this driven activity: by entraining endogenous oscillations during active firing, stimulation can enhance the synchronization and temporal precision of the evoked discharge, which would be expected to sharpen the depolarization–repolarization cycle and thereby reduce the evoked AP area (a narrower waveform). The static segments (BGi and RTC-BGi), by contrast, are recorded in the absence of motion and reflect spontaneous, tonic firing that indexes the resting excitability of the same circuit.

A plausible mechanism for the opposite direction of change is homeostatic regulation of the excitation–inhibition (E/I) balance. When the evoked response is up-regulated and more tightly synchronized, the network may compensate by shifting its resting set-point in the opposite direction, such that an increase in evoked phase-locking (narrowing of the dynamic AP area) is accompanied by a transient broadening of the spontaneous baseline (widening of the static AP area). This interpretation is consistent with evidence that tACS can exert simultaneously excitatory and inhibitory effects on the same cortical target, with the net direction depending on the ongoing E/I state of the stimulated circuit [28]. Under this view, the dynamic and static segments sample the same stimulation at two different points on the E/I curve — one during active, stimulus-driven firing and one at rest — so that a single intervention can drive them in opposite directions. Notably,

this opposition was most pronounced in the HIS < 2 subgroup, whereas in the HIS ≥ 2 subgroup the two trends ran more nearly in parallel (Figures 5 and 6), suggesting that the capacity for this evoked-versus-resting trade-off depends on intact neurovascular regulation, which is compromised under higher cerebrovascular burden. Direct measurement of cortical excitability or cerebral perfusion would be required to confirm this proposed mechanism.

The results highlight the potential of EVestG-derived features as non-invasive biomarkers for monitoring neural responses to intervention. The complementary strengths of PCA and ICA in capturing structured and evolving patterns suggest that EVestG is sensitive to subtle neural changes tied to both stimulation and cognitive engagement. In particular, group-dependent differences in EVestG dynamics and their association with cognitive performance suggest utility in assessing treatment responsiveness and tracking disease progression. Incorporating ICA further enhances this potential by isolating functionally relevant but statistically independent neural components not evident through variance-based analyses alone.

Together, these observations suggest that active tACS amplifies phase-specific vestibular synchronization, whereas cerebrovascular pathology constrains long-term neural plasticity.

5.6 Comparison with Prior EVestG Classification Studies

The present study builds directly on the EVestG classification work of [6], and several points of comparison clarify how the two studies relate. In [6], cerebrovascular burden was operationalized with a modified HIS using a cutoff of 3 as the highest acceptable score for AD and a range of ≥4 to ≤7 for AD-CVD (mean HIS 1.8 ± 1.2 for AD and 5.6 ± 1.4 for AD-CVD). Its central finding was that EVestG averaged field potential (FPave) waveform-shape features could separate AD from AD-CVD, and both from healthy controls, with AD presenting a narrower, smaller FPave and AD-CVD a wider, larger one (≥80% accuracy for One-vs-All and 78% for AD vs AD-CVD).

The discriminating feature was not an individual AP parameter but a correlation-based measure of whole-FPave shape similarity, computed over the regions of statistically significant separation between populations, with the AP defined as the full V-shaped waveform from baseline through the negative peak and back. For AD-versus-AD-CVD separation specifically, the most informative segment was a stationary one — the supine-average BGi and RTC-BGi of the left ear. The present study differs from [6] in four respects, discussed below: the HIS threshold (2 rather than 3), the AP feature definition (six discrete physiological parameters rather than whole-waveform shape correlation), the segment emphasis (motion-evoked OnBB and RTC-OnAA, plus PCA/ICA across all 84 segments, rather than stationary BGi), and the analytical objective (longitudinal treatment monitoring rather than cross-sectional diagnosis).

The main finding of [6] was that AD participants exhibited narrower AP and smaller averaged FP waveforms compared to both AD-CVD and healthy controls, while AD-CVD participants showed wider AP and larger waveforms — reflecting faster and slower depolarization/repolarization dynamics, respectively. These patterns achieved classification accuracies of ≥80% for One-vs-All and 78% for AD vs AD-CVD separation. Notably, the EVestG features used in that study were correlation-based measures of whole FPave waveform shape similarity, rather than the individual AP waveform parameters (slopes, rise times, peak index, and AP area) extracted in the present study.

In [6], the AP was defined as the full V-shaped waveform extending from baseline through the negative peak and back, and the extracted features were based on correlation differences of the entire FP waveform shape within regions of statistically significant separation between populations. The most informative segments for AD vs AD-CVD classification were predominantly stationary segments — specifically, the averaged supine BGi and RTC-BGi from

the left ear. This contrasts with the present study, which extracted six individual AP waveform parameters (depolarization and repolarization slopes and rise times, peak index, and AP area) and found that dynamic, motion-evoked segments (OnBB and RTC-OnAA from the Supine-up tilt) were more sensitive to treatment-related changes.

This difference in segment sensitivity is not a contradiction but reflects the distinct objectives of the two studies. The other study [6] sought to identify stable diagnostic biomarkers that distinguish disease states — a static, trait-like contrast between AD and AD-CVD populations. For this purpose, stationary BGi segments provide a clean baseline neural fingerprint with minimal motion artifact, making them ideal for classification. In contrast, the present study sought to detect treatment-induced changes over time — a dynamic, state-dependent question. Motion-evoked segments capture the vestibular system's active neural response, which is more likely to exhibit plasticity-related modulation following neuromodulatory intervention. The fact that the AP area narrowed in our dynamic condition while showing opposite patterns in the static condition further supports this interpretation: spontaneous baseline activity (static) and evoked neural responses (dynamic) are governed by different physiological mechanisms and respond differently to tACS. Consequently, the optimal EVestG segment depends on the question being asked — BGi for diagnosis, dynamic segments for treatment monitoring. This distinction is itself a methodological contribution of the present work.

A related question concerns the interpretation of AP narrowing in the present study. Because [6] found that AD participants have narrower AP waveforms than both healthy controls and AD-CVD participants, it might appear that AP narrowing following tACS reflects worsening — the signal becoming “more AD-like” rather than improvement. This concern, however, conflates two distinct axes. The AD-versus-AD-CVD distinction in [6] is a diagnostic contrast describing which

pathophysiological profile a participant most resembles; it is not a severity ordering in which the AD profile represents a worse cognitive state than the AD-CVD profile. Once these axes are separated, the direction of change observed here is consistent with improvement rather than decline.

The framework provided by [33] makes this explicit. There, normalized probability (NP) values — NP_AD, NP_AD-CVD, and NP_C — were derived from EVestG features to estimate, on a continuous scale, how strongly each participant's signals align with the AD, AD-CVD, and healthy-control profiles, allowing diagnostic certainty to be tracked across sessions. Following rTMS, cognitively improved participants showed a decrease in NP_AD-CVD with a slight increase in NP_AD, whereas non-improved and declined participants showed the opposite pattern; regression analyses confirmed that increasing NP_AD-CVD was associated with cognitive decline and increasing NP_AD with cognitive improvement. The authors interpreted cognitive improvement as arising primarily from a reduction in cerebrovascular symptomology — plausibly mediated by increased cerebral blood flow — rather than from a change in core AD pathology and reported that participants with higher certainty of an AD (versus AD-CVD) diagnosis were the most likely to benefit.

Applying this framework to the present data, the present results are coherent. The HIS < 2 subgroup corresponds to the low-cerebrovascular-burden, high-AD-certainty participants that [33] identifies as most responsive, and these participants showed a sustained AP narrowing across sessions alongside the improving ADAS-Cog trajectory. Rather than indicating a shift toward more severe AD pathology, this narrowing represents movement away from the broad, vascular-constrained AD-CVD profile and toward a more normative waveform — the change that [33] associates with benefit. Conversely, the HIS ≥ 2 subgroup showed an initial narrowing at post-treatment followed

by a rebound widening at follow-up: a re-emergence of the broad AD-CVD-type waveform that parallels the partial loss of cognitive gain in this subgroup and is consistent with the NP_AD-CVD increase that [33] links to decline. It should be noted that [33] examined rTMS rather than tACS, so this framework is applied here by analogy; nevertheless, the convergence of the AP-area trends and the NP-based findings on the cerebrovascular component as the locus of change strengthens the interpretation that EVestG-derived AP narrowing reflects treatment-related improvement, not worsening, when interpreted alongside HIS classification.

5.7 Improved versus Non-Improved Subgroup Analysis

To further explore whether specific AP features differentiate treatment responders from non-responders, participants were classified as improved (ADAS-Cog decreased by one point or more from baseline to post-treatment) or non-improved (ADAS-Cog changed by less than one point or increased), following the responder definition used in the related EVestG study [33]. AP area, averaged across the 42 left-ear segments, was used as a single representative feature and examined with and without HIS classification. Descriptively, improved participants showed a gradual, sustained reduction in AP area across sessions, most clearly in the active tACS+CE condition, whereas non-improved participants remained elevated and showed no comparable decline. This is consistent with the interpretation developed in Section 5.6 — that treatment-related narrowing of the AP reflects movement away from the broad AD-CVD-type waveform — and suggests that AP area may carry some information about neurophysiological response status. However, when the improved and non-improved subgroups were further divided by the HIS threshold, the resulting cells contained very few participants (N = 2 to 7, with one cell reduced to a single valid baseline value), and no pattern of sufficient magnitude or consistency emerged to support statistical analysis or reliable interpretation. The response-based grouping was therefore not carried forward as a

primary analysis; AP area served as a gating feature, and because the differences it revealed were modest and underpowered once classified, the remaining waveform features were not pursued within this framework. This limitation is inherent to the sample size of the present study and underscores the need for larger cohorts in future work. The detailed AP-area comparisons for improved versus non-improved participants, with and without HIS stratification, are provided in Appendix E.

Chapter 6: Conclusion

6.1 Summary and Contributions

This study investigated the temporal evolution of EVestG-derived action potential features following active tACS combined with cognitive exercises and sham tACS combined with cognitive exercises in participants with AD, classified by cerebrovascular burden using the modified Hachinski Ischemic Score.

The results demonstrate that EVestG-derived AP features capture distinct neural response patterns across treatment conditions. Under active tACS + cognitive exercises, both PCA and ICA analyses revealed more structured and consistent feature evolution across sessions, whereas the sham condition showed greater variability and less coherent temporal trends. Timing-related features, particularly depolarization and repolarization rise times, were especially sensitive to intervention effects, while AP area provided a complementary measure of overall waveform change.

Subgroup analysis revealed that participants with lower cerebrovascular burden (HIS < 2) exhibited sustained AP narrowing from baseline through follow-up, consistent with progressive neural modulation. In contrast, participants with higher cerebrovascular burden (HIS ≥ 2) showed an initial narrowing at post-treatment followed by a rebound widening at follow-up, suggesting that vascular-constrained neural dynamics re-emerge after the stimulation period. These group-specific trajectories highlight the role of cerebrovascular status in shaping neurophysiological response to neuromodulation.

The combined application of PCA and ICA provided complementary insights: PCA identified dominant shared variance patterns across features and segments, while ICA isolated statistically independent signal components that revealed feature-specific dynamics not apparent from

variance-based analyses alone. Across both methods, dynamic movement phases — particularly those recorded during supine and vertical tilts engaging the otolithic organs — consistently contributed most to the observed patterns, indicating that motion-evoked EVestG responses provide the most informative markers of treatment-related neural change.

The main contributions of this thesis are as follows. First, it extends previous EVestG research from cross-sectional disease classification toward longitudinal treatment-response monitoring in dementia, representing the first systematic application of EVestG for evaluating tACS intervention effects. Second, it evaluated both magnitude-based and timing-based EVestG-derived AP features as candidate neurophysiological biomarkers, providing a more comprehensive characterization of AP waveform dynamics than prior studies. Third, PCA and ICA were applied in a complementary framework, enabling the detection of structured treatment effects that are not apparent from conventional univariate analyses. Fourth, it demonstrated that HIS-based subgroup stratification reveals distinct neurophysiological trajectories, highlighting the importance of accounting for cerebrovascular burden when evaluating treatment response.

While these contributions are exploratory given the limited sample size, they established a methodological framework and provided initial evidence that EVestG-derived AP features warrant further investigation as candidate biomarkers for monitoring neurophysiological responses to neuromodulation. With validation in larger independent cohorts, such biomarkers could contribute to objective treatment evaluation and support more individualized approaches to intervention in populations with varying levels of cerebrovascular burden.

6.2 Limitations

Several limitations should be considered when interpreting the results of this study. First, the sample size was relatively limited, which may affect the generalizability of the findings and the

statistical power to detect subtle effects. Second, the crossover design, while beneficial for reducing inter-subject variability, introduces complexity in isolating long-term effects and potential carryover influences between conditions. A further limitation concerns the demographic balance between groups. Age and sex were not fully matched across the active and sham conditions, nor between the patient groups and the healthy control reference (Table 1), and both factors can influence EVestG-derived AP characteristics. Because of the limited sample size, age and sex were not included as covariates in the present analysis; the ANOVA of the tACS effect was therefore not adjusted for these variables. As a result, the possibility that part of the observed between-group differences reflects demographic imbalance rather than treatment cannot be excluded. Future studies with larger samples should incorporate age and sex as covariates — for example, through an analysis of covariance (ANCOVA) — to formally separate treatment-related effects from demographic influences. Third, although PCA and ICA provided valuable insights into dominant and independent signal patterns, these methods are inherently data-driven and do not directly identify underlying physiological mechanisms. Fourth, although the EVestG feature-selection procedure was first conducted independently of the present treatment outcome analysis and was based on the previously established study [6], both studies were conducted within the same research group using the same EVestG recording system and partially overlapping clinical populations. While this separation reduces the likelihood of circular reasoning, the shared research environment represents a potential limitation, and confirmation of these biomarkers through external validation with an independent cohort would strengthen their generalizability. Finally, the present study did not perform direct statistical correlations between EVestG features and ADAS-Cog scores at the individual participant level. This was a deliberate methodological choice rather than an oversight. ADAS-Cog scores were used as an independent reference to assess whether the

direction and temporal pattern of neurophysiological changes observed in EVestG features were consistent with the expected cognitive outcomes. This interpretive alignment approach was adopted because the small sample size and the exploratory nature of the multivariate analyses would make individual-level correlations statistically unreliable. Future studies with larger cohorts should formally examine the relationship between EVestG-derived features and cognitive endpoints to determine whether these neurophysiological measures can serve as validated predictors of treatment response.

Future studies incorporating larger participant samples, multimodal neuroimaging, and extended monitoring periods will be essential to validate EVestG-based biomarkers and to clarify how electrophysiological dynamics mediate behavioral improvements after tACS and cognitive interventions. In addition, direct measurement of ion channel activity and cerebral blood flow would further strengthen the mechanistic interpretation of the observed neurophysiological changes.

6.3 Future Work

Several directions may extend and strengthen the findings of this study. First, future studies should include larger sample sizes to improve statistical power and enable more robust subgroup analyses, as many of the current trends appeared meaningful but did not reach statistical significance. A larger cohort would also permit examination of potential modifiers such as sex, age, medication use, and disease severity.

Second, the relationship between EVestG-derived features and cognitive outcomes should be examined more directly through correlation and predictive modeling within a larger dataset, clarifying which waveform features are most strongly associated with cognitive change over time.

Third, the influence of cerebrovascular burden on neurophysiological response patterns warrants further investigation using multimodal measures, such as neuroimaging or cerebral blood flow assessment, to determine whether the altered PCA and ICA patterns observed in participants with higher HIS reflect impaired neurovascular coupling, delayed neural adaptation, or compensatory mechanisms.

Fourth, future studies may build on the multivariate decomposition approach used here by applying additional machine learning techniques — such as clustering, nonlinear manifold learning, or predictive classifiers — to detect treatment-responsive EVestG signatures more accurately and to identify responders and non-responders before intervention.

Fifth, expanding the EVestG feature set to include spectral and firing-interval-based measures, alongside the AP waveform characteristics examined here, may improve sensitivity to subtle treatment-related changes. In addition, given the finding that dynamic vestibular segments appear more sensitive to intervention than static segments, future work should investigate optimal tilt directions and movement phases in greater detail, potentially enabling a more targeted and time-efficient EVestG protocol for clinical applications.

Finally, future studies should investigate longer-term effects of repeated gamma tACS through extended longitudinal monitoring to determine whether EVestG-derived biomarkers can track sustained neural changes and guide personalized neuromodulation strategies in dementia populations.

Bibliography

[1] Long, S., Benoist, C., & Weidner, W. (2023). World Alzheimer Report 2023: Reducing dementia risk: never too early, never too late. Alzheimer's Disease International. https://www.alzint.org/resource/world-alzheimer-report-2023/

[2] Xavier, C., & Pinto, N. (2025). Navigating the blurred boundary: Neuropathologic changes versus clinical symptoms in Alzheimer's disease, and its consequences for research in genetics. Journal of Alzheimer S Disease, 104(3), 611–626. https://doi.org/10.1177/13872877251317543

[3] Giacomo Koch, Daniele Altomare, Alberto Benussi, Lucie Bréchet, Elias P Casula, Alessandra Dodich, Michela Pievani, Emiliano Santarnecchi, Giovanni B Frisoni, The emerging field of non-invasive brain stimulation in Alzheimer's disease, Brain, Volume 147, Issue 12, December 2024, Pages 4003–4016, https://doi.org/10.1093/brain/awae292

[4] Moussavi, Z., Kimura, K., Kehler, L., de Oliveira Francisco, C., & Lithgow, B. (2021). A Novel Program to Improve Cognitive Function in Individuals with Dementia Using Transcranial Alternating Current Stimulation (tACS) and Tutored Cognitive Exercises. Frontiers in aging, 2, 632545. https://doi.org/10.3389/fragi.2021.632545

[5] Uehara, M. A., Kalia, S., Campuzano, M. G., Jafari-Jozani, M., Lithgow, B., & Moussavi, Z. (2025). Cognitive and Neuropsychiatric Effects of 40 Hz tACS Simultaneously with Cognitive Exercises for Dementia: A Randomized, Crossover, Double-Blind, Sham-Controlled Study. Medicina, 61(4), 757. https://doi.org/10.3390/medicina61040757

[6] Dastgheib, Zeinab A., et al. "An Unbiased Algorithm for Objective Separation of Alzheimer's, Alzheimer's Mixed with Cerebrovascular Symptomology, and Healthy Controls

from One Another Using Electrovestibulography (EVestG).” Medical & Biological Engineering & Computing, vol. 60, no. 3, 2022, pp. 797–810, https://doi.org/10.1007/s11517-022-02507-1

[7] Hachinski, Vladimir C., et al. “Cerebral Blood Flow in Dementia.” Archives of Neurology (Chicago), vol. 32, no. 9, 1975, pp. 632–37, https://doi.org/10.1001/archneur.1975.00490510088009.

[8] Román, G. C., Tatemichi, T. K., Erkinjuntti, T., Cummings, J. L., Masdeu, J. C., Garcia, J. H., Amaducci, L., Orgogozo, J. M., Brun, A., & Hofman, A. (1993). Vascular dementia: diagnostic criteria for research studies. Report of the NINDS-AIREN International Workshop. Neurology, 43(2),250 260. https://doi.org/10.1212/wnl.43.2.250

[9] Lithgow, B. J., Saha, C., Dastgheib, Z., & Moussavi, Z. (2025). Surface Versus Penetrative rTMS Stimulation May Be More Effective for AD Patients with Cerebrovascular Disease. *Neuroscience Insights*, *20*, 26331055251328355. https://doi.org/10.1177/26331055251328355

[10] Rosen, W. G., Mohs, R. C., & Davis, K. L. (1984). A new rating scale for Alzheimer's disease. The American journal of psychiatry, 141(11), 1356–1364. https://doi.org/10.1176/ajp.141.11.1356

[11] Hitier, M., Besnard, S., & Smith, P. F. (2014). Vestibular pathways involved in cognition. Frontiers in integrative neuroscience, 18, 59. https://doi.org/10.3389/fnint.2014.00059

[12] Lithgow, B. (2012). A methodology for detecting field potentials from the external ear canal: NEER and EVestG. Annals of Biomedical Engineering, 40(8), 1835-1850. https://doi.org/10.1007/s10439-012-0526-3

[13] Zeinab A. Dastgheib, Chathura Kumaragamage, Brian J. Lithgow, Zahra K. Moussavi, The evolution of Electrovestibulography technique and safety considerations, Biomedical Engineering Advances, Volume 9, 2025, 100157, ISSN 2667-0992, https://doi.org/10.1016/j.bea.2025.100157.

[14] Lithgow, B. J., Dastgheib, Z., Anssari, N., Mansouri, B., Blakley, B., Ashiri, M., & Moussavi, Z. (2021). Physiological separation of Alzheimer's disease and Alzheimer's disease with significant levels of cerebrovascular symptomology and healthy controls. Medical & biological engineering & computing, 59(7-8), 1597–1610. https://doi.org/10.1007/s11517-021-02409-8

[15] Jacobson N, Lithgow B, Jafari Jozani M, Moussavi Z. The Effect of Transcranial Alternating Current Stimulation With Cognitive Training on Executive Brain Function in Individuals With Dementia: Protocol for a Crossover Randomized Controlled Trial JMIR Res Protoc 2022;11(4):e37282 https://www.researchprotocols.org/2022/4/e37282 DOI: 10.2196/37282

[16] Beach TG, Monsell SE, Phillips LE, Kukull W (2012) Accuracy of the clinical diagnosis of Alzheimer disease at National Institute on Aging Alzheimer Disease Centers, 2005–2010. J NeuropatholExp Neurol 71:266–273. https://doi.org/10.1097/NEN.0b013e31824b211b

[17] Neuling, T., Rach, S., & Herrmann, C. S. (2013). Orchestrating neuronal networks: sustained after-effects of transcranial alternating current stimulation depend upon brain states. Frontiers in human neuroscience, 17, 161. https://doi.org/10.3389/fnhum.2013.00161

[18] Bland, N. S., & Sale, M. V. (2019). Current challenges: the ups and downs of tACS. Experimental brain research, 237(12), 3071–3088. https://doi.org/10.1007/s00221-019-05666-0

[19] Elyamany, O., Leicht, G., Herrmann, C. S., & Mulert, C. (2021). Transcranial alternating current stimulation (tACS): from basic mechanisms towards first applications in psychiatry. European archives of psychiatry and clinical neuroscience, 271(1), 135–156. https://doi.org/10.1007/s00406-020-01209-9

[20] Goldberg, J. M., Wilson, V. J., Cullen, K. E., Angelaki, D. E., Broussard, D. M., Buttner-Ennever, J., Fukushima, K., & Minor, L. B. (2012). The Vestibular System: A Sixth Sense. Oxford University Press. https://doi.org/10.1093/acprof:oso/9780195167085.001.0001

[21] Bigelow, R. T., Semenov, Y. R., du Lac, S., Hoffman, H. J., & Agrawal, Y. (2016). Vestibular vertigo and comorbid cognitive and psychiatric impairment: the 2008 National Health Interview Survey. Journal of neurology, neurosurgery, and psychiatry, 87(4), 367–372. https://doi.org/10.1136/jnnp-2015-310319

[22] Wei, E. X., Oh, E. S., Harun, A., Ehrenburg, M., Xue, Q.-L., Simonsick, E., & Agrawal, Y. (2019). Increased Prevalence of Vestibular Loss in Mild Cognitive Impairment and Alzheimer's Disease. *Current Alzheimer Research*, 16(12), 1143–1150. https://doi.org/10.2174/1567205016666190816114838

[23] Agrawal, Y., Smith, P. F., & Rosenberg, P. B. (2020). Vestibular impairment, cognitive decline and Alzheimer's disease: Balancing the evidence. *Aging & Mental Health*, 24(5), 705–708. https://doi.org/10.1080/13607863.2019.1566813

[24] Nasreddine, Z. S., Phillips, N. A., Bédirian, V., Charbonneau, S., Whitehead, V., Collin, I., Cummings, J. L., & Chertkow, H. (2005). The Montreal Cognitive Assessment, MoCA: a brief screening tool for mild cognitive impairment. Journal of the American Geriatrics Society, 53(4), 695–699. https://doi.org/10.1111/j.1532-5415.2005.53221.x

[25] Moussavi, Z. MindTriggers. 2020. Available online: https://apps.apple.com/us/app/mind-triggers/id1508008769 (accessed on 20 January 2025).

[26] Kumaragamage, C., Lithgow, B. & Moussavi, Z. A new low-noise signal acquisition protocol and electrode placement for electrocochleography (ECOG) recordings. Med Biol Eng Comput 53, 499–509 (2015). https://doi.org/10.1007/s11517-015-1251-5

[27] Marzban, S., Dastgheib, Z., Lithgow, B. *et al.* Using principal component analysis to determine which vestibular stimuli provide best biomarkers for separating Alzheimer's from mixed Alzheimer's disease. *Med Biol Eng Comput* **63**, 1943–1953 (2025). https://doi.org/10.1007/s11517-024-03110-2

[28] Khatoun, A., Asamoah, B., & Mc Laughlin, M. (2017). Simultaneously Excitatory and Inhibitory Effects of Transcranial Alternating Current Stimulation Revealed Using Selective Pulse-Train Stimulation in the Rat Motor Cortex. The Journal of neuroscience: the official journal of the Society for Neuroscience, 37(39), 9389–9402. https://doi.org/10.1523/JNEUROSCI.1390-17.2017

[29] Jolliffe, I. T. (2002). *Principal Component Analysis* (2nd ed.). Springer-Verlag. https://doi.org/10.1007/b98835

[30] Hyvärinen, A., & Oja, E. (2000). Independent component analysis: algorithms and applications. *Neural Networks*, 13(4–5), 411–430. https://doi.org/10.1016/S0893-6080(00)00026-5

[31] Sprugnoli, G., Munsch, F., Cappon, D., et al. (2021). Impact of multisession 40Hz tACS on hippocampal perfusion in patients with Alzheimer's disease. Alzheimer's Research & Therapy, 13, 203. https://doi.org/10.1186/s13195-021-00922-4

[32] Bahr-Hosseini, M., & Bikson, M. (2021). Neurovascular modulation: A review of primary vascular responses to transcranial electrical stimulation as a mechanism of action. Brain Stimulation, 14(4), 837–847. https://doi.org/10.1016/j.brs.2021.04.015

[33] Dastgheib, Z.A., Lithgow, B.J. & Moussavi, Z.K. Differential impact of repetitive transcranial magnetic stimulation on alzheimer's disease symptomology: evidence from

electrovestibulography. *Cogn Neurodyn* **19**, 120 (2025). https://doi.org/10.1007/s11571-025-10310-5

Appendices

Appendix A PCA results for active tACS + cognitive exercises

A.1 PCA results for active tACS + cognitive exercises in low HIS scores

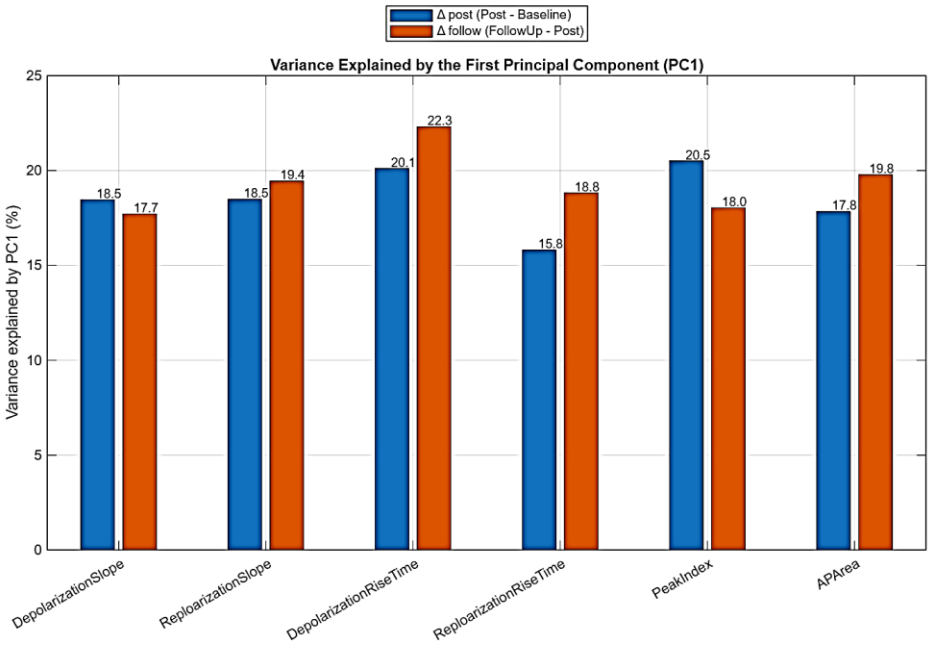

Figure A. 1 Variance explained by PC1. This shows the percentage of variance explained by PC1 for each feature during Δpost and Δfollow.

Across the analyzed features, PC1 explained approximately 16–21% of the variance during Δpost and 18–22% during Δfollow.

The highest variance contribution during Δpost was observed for Peak Index (20.5%), followed by Depolarization Rise Time (20.1%). During Δfollow, the highest contribution was observed for Depolarization Rise Time (22.3%), indicating that its dominant variance pattern became more pronounced during follow-up.

In contrast, Repolarization Rise Time showed the lowest PC1 variance contribution during Δpost (15.8%), although its variance contribution increased during follow-up (18.8%). Overall, the variance explained by PC1 remained relatively consistent across features, indicating moderate stability of the dominant AP pattern.

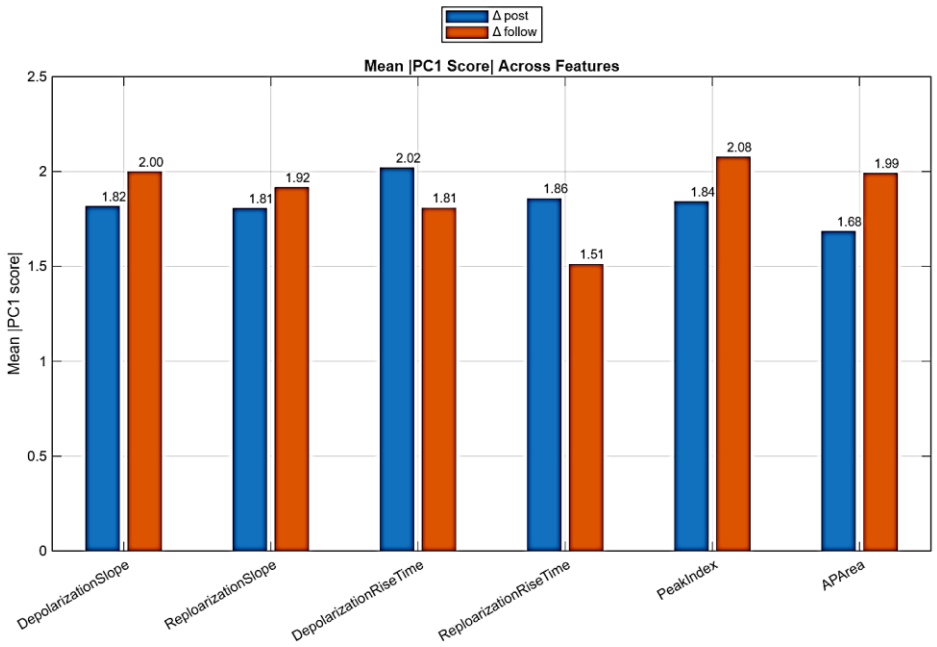

Figure A. 2 Mean Magnitude of PC1 scores. The mean absolute PC1 scores

The mean absolute PC1 scores for each feature were presented in Figure A.2 These values represent the magnitude of PC1 expression in the EVestG-derived AP changes.

Across most features, the magnitude of PC1 scores was comparable between Δpost and Δfollow. However, some features demonstrated notable differences between the two periods. For example, Peak Index exhibited a larger mean PC1 score during follow-up (2.08) compared to Δpost (1.84), suggesting stronger expression of the dominant EVestG pattern at follow-up for this feature. Similarly, AP Area increased from 1.68 during Δpost to 1.99 during Δfollow.

In contrast, Depolarization Rise Time showed a decrease in PC1 magnitude from Δpost (2.02) to Δfollow (1.81), indicating a reduction in the dominant pattern strength for this feature during follow-up.

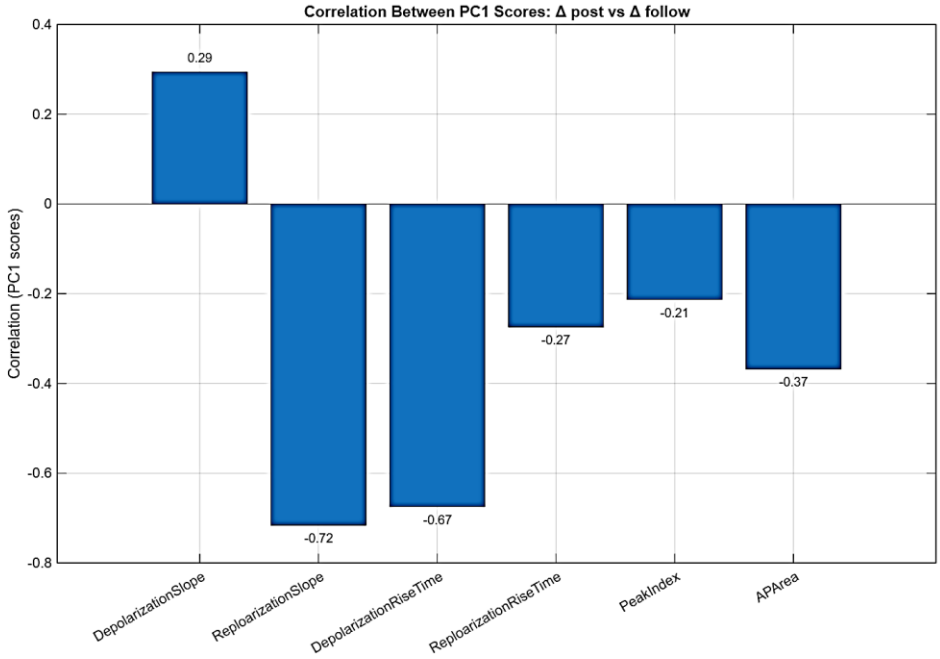

Figure A. 3 Correlation of PC1 scores between Δpost and Δfollow

Figure A.3 illustrates the correlation between PC1 scores obtained from Δpost and Δfollow for each feature. This correlation reflects the similarity of the dominant PCA patterns between the time intervals.

The results indicate that most features exhibited negative correlations between Δpost and Δfollow, suggesting that the dominant patterns observed immediately after treatment were altered during the follow-up period. For instance, Repolarization Slope (−0.72) and Depolarization Rise Time (−0.67) showed strong negative correlations, indicating significant changes in the dominant component structure between the two intervals.

Similarly, AP Area (-0.37), Repolarization Rise Time (−0.27), and Peak Index (−0.21) demonstrated moderate negative correlations. In contrast, Depolarization Slope showed a weak positive correlation (0.29), suggesting relative stability of the dominant pattern for this feature across time.

Overall, these findings indicate that the principal EVestG-derived AP patterns associated with most features underwent substantial changes between the immediate post-treatment period and the follow-up measurement.

Feature	Top 5 segments - Δpost	Top 5 segments - Δfollow
Depolarization Slope	CAL_RTConBB | IAR_BG | IAR_RTConBB | IAR_RTConAA | RAL_onAA	CAR_RTConAA | CAR_RTCBG | UAL_onBB | PUR_RTCBG | BAR_RTConBB
Repolarization Slope	UAL_onBB | RAL_onAA | PUR_RTConBB | PUL_RTConAA | UAL_RTConAA	IAR_onBB | PRR_onAA | BAR_RTCBG | PRL_onAA | PRR_BG
Depolarization Rise Time	CAL_RTConBB | BAL_RTConBB | RAL_onAA | PRR_RTConAA | PUR_RTCBG	CAR_RTCBG | CAL_onBB | BAR_RTCBG | PRR_onAA | PRR_RTCBG
Repolarization Rise Time	PUR_RTConBB | BAR_RTConBB | PRR_BG | IAL_RTCBG | BAR_BG	UAR_RTConBB | UAL_onBB | CAL_onBB | PRL_onAA | RAR_BG
Peak Index	BAL_RTConBB | UAR_onAA | CAL_RTConBB | BAR_RTConBB | BAL_onAA	IAR_RTCBG | PUR_RTConBB | UAL_RTConAA | PUR_RTCBG | IAR_onBB
AP Area	UAL_RTConAA | RAR_RTConAA | UAL_onBB | BAL_BG | RAL_onAA	RAR_RTConAA | PRL_RTConBB | PRR_RTCBG | UAL_onBB | PUR_RTCBG

Table A. 1 Dominant segments contributing to PC1
Legend: Segment labels follow the format: [Tilt Direction][Ear]_[Movement Phase]
Tilt Direction: BA = Backward, CA = Contralateral, IA = Ipsilateral, PR = Prone (Supine) Rotation, PU = Prone (Supine) Up, RA = Right Rotation, UA = Up/Down

Ear: L = Left, R = Right
Movement Phase: BG = Stationary (BGi), onAA = Acceleration, onBB = Deceleration, RTCBG = Return-to-Center Stationary, RTConAA = Return-to-Center Acceleration, RTConBB = Return-to-Center Deceleration
Example: CAL_RTConBB = Contralateral tilt, Left ear, Return-to-Center Deceleration phase

The five segments with the highest contributions to PC1 for each feature are summarized in Table A.1. These segments represent the primary contributors to the dominant variance pattern captured by PCA. Across the analyzed features, several segments appeared repeatedly among the top contributors. For example, segments such as UAL_onBB, PUR_RTCBG, RAL_onAA, and BAR_RTConBB were frequently observed among the dominant contributors across multiple features and time intervals.

The frequency analysis of dominant segments further revealed that certain tilts appeared more often within the top ones. As shown in the above table, UAL was the most frequent occurrence (8 occurrences), followed by PRR and PUR (7 occurrences each). Other commonly appearing orientations included BAR, IAR, and CAL.

Overall, the PCA results demonstrate that the PC1 captured a moderate proportion of the variance in EVestG-derived AP features across both Δpost and Δfollow intervals. While the magnitude of the dominant component remained relatively stable across features, the correlations between Δpost and Δfollow PC1 scores suggest that the spatial structure of the dominant AP patterns changed for several features during the follow-up period.

Additionally, the dominant PCA patterns were consistently influenced by a limited set of EVestG segments and tilts, indicating that specific vestibular response segments contributed to the principal variance patterns.

A.2 PCA results for active tACS + cognitive exercises in high HIS scores

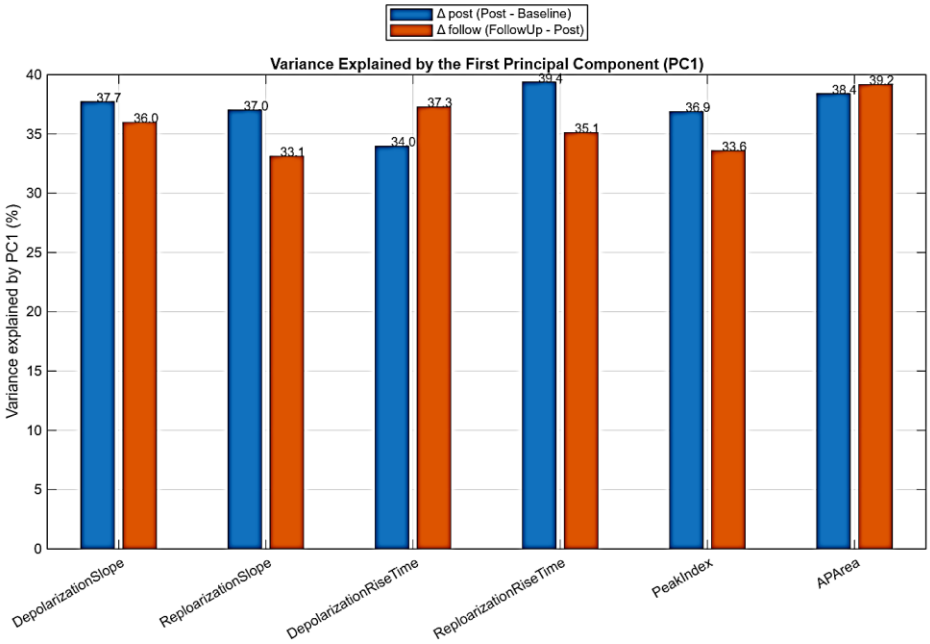

Figure A. 4 Variance explained by PC1

The percentage of variance explained by PC1 for each feature is shown in Figure A.4. For this group, PC1 explained a relatively larger proportion of the variance compared with the HIS < 2 group, ranging approximately from 33% to 39% across the AP features.

Among the features, AP Area showed the largest variance explained during Δfollow (39.2%), while Repolarization Rise Time exhibited the highest variance during Δpost (39.4%). In contrast, Repolarization Slope showed the lowest PC1 variance contribution during Δfollow (33.1%).

Overall, these values indicate that the PC1 captured a substantial proportion of the variability, suggesting that a dominant signal pattern strongly influenced the EVestG responses within this participant group.

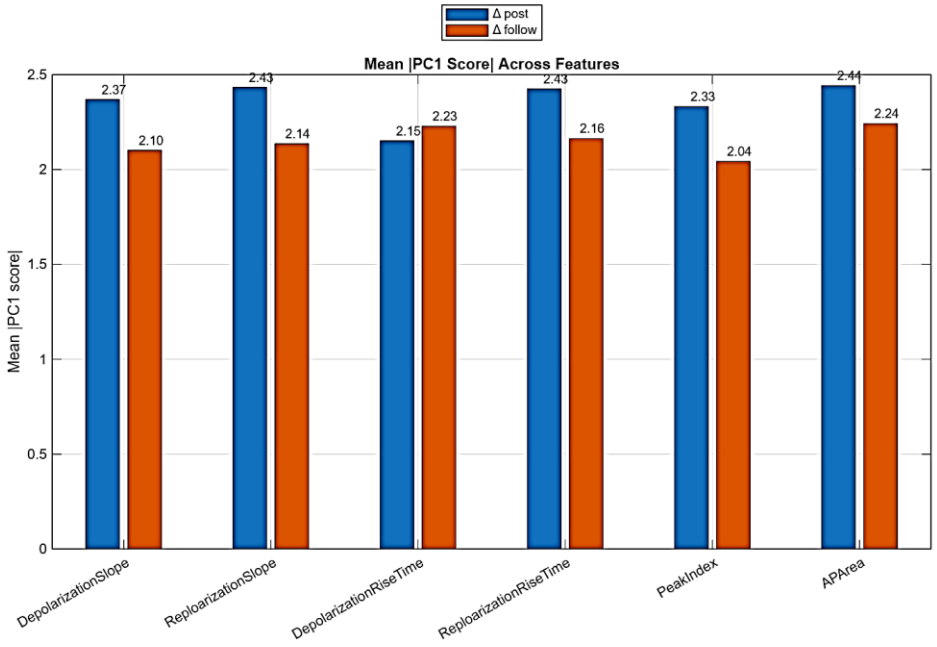

Figure A. 5 Magnitude of PC1 scores

Figure A.5 presents the mean absolute PC1 scores for each feature during Δpost and Δfollow. These values reflect the magnitude of the dominant AP pattern captured by PC1.

Across all features, the mean absolute PC1 scores were consistently higher during Δpost compared with Δfollow. For example, AP Area exhibited the highest mean PC1 magnitude during Δpost (2.44), which decreased slightly during Δfollow (2.24). Similarly, Repolarization Rise Time showed a reduction from 2.43 during Δpost to 2.16 during Δfollow. A similar pattern was observed across other features, indicating that the dominant AP component was more pronounced immediately after treatment and slightly reduced at follow-up.

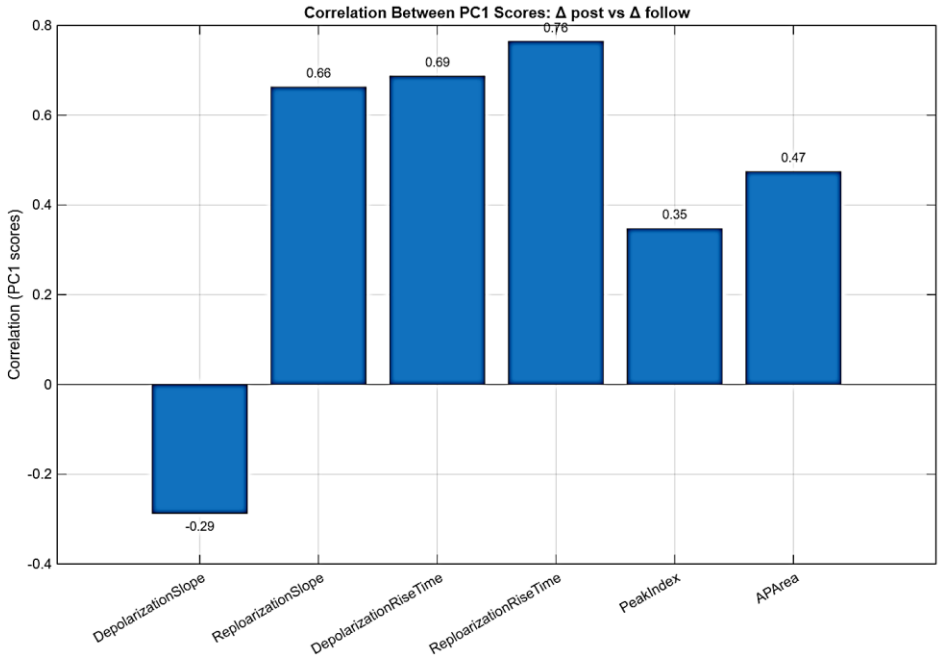

Figure A. 6 Correlation of PC1 scores between Δpost and Δfollow

The correlation between PC1 scores obtained from Δpost and Δfollow is shown in Figure A.6. In contrast to the HIS < 2 group, the majority of EVestG features in the HIS ≥ 2 group demonstrated moderate to strong positive correlations between Δpost and Δfollow.

Strong positive correlations were observed for Repolarization Rise Time (r = 0.76), Depolarization Rise Time (r = 0.69), and Repolarization Slope (r = 0.66). Moderate correlations were also observed for AP Area (r = 0.47) and Peak Index (r = 0.35).

Only Depolarization Slope exhibited a negative correlation (r = −0.29), indicating a reversal of the dominant PCA pattern between the two intervals for this feature.

Overall, these results suggest that the dominant AP patterns captured by PC1 were more consistent between the post-treatment and follow-up periods for participants with HIS ≥ 2 compared with those with HIS < 2.

Feature	Top 5 segments - Δpost	Top 5 segments - Δfollow
Depolarization Slope	PRL_onBB | BAR_RTConBB | IAR_RTCBG | IAL_onAA | PUR_RTConAA	CAR_onBB | UAR_RTCBG | PUR_onBB | RAR_onBB | CAL_RTCBG
Repolarization Slope	IAL_onAA | BAR_RTConBB | PUL_RTConBB | IAL_BG | IAR_onAA	PUR_onBB | IAL_onBB | UAR_onAA | PRL_RTConBB | PRR_onBB
Depolarization Rise Time	BAR_RTConBB | PRL_onAA | IAR_RTConAA | PUR_RTConAA | UAR_RTCBG	PUR_onBB | UAR_RTCBG | CAR_onBB | RAR_onBB | IAR_RTCBG
Repolarization Rise Time	CAR_BG | IAR_RTConAA | PRL_RTCBG | PUR_RTConAA | PUL_RTConBB	IAL_onBB | PUR_onBB | PRL_RTConBB | RAR_BG | BAR_RTConBB
Peak Index	UAR_RTConBB | UAR_onBB | PUL_RTConBB | IAL_BG | IAL_RTConBB	RAR_BG | IAR_RTCBG | CAR_onBB | RAR_onBB | PUR_onBB
AP Area	BAR_RTConBB | IAL_onAA | RAR_onAA | BAR_RTCBG | IAL_RTCBG	PUR_onBB | UAR_RTCBG | CAR_onBB | PRR_onBB | BAR_RTConBB

Table A. 2 Dominant EVestG segments contributing to PC1

The EVestG segments with the largest contributions to PC1 are summarized in Table A.2. These segments represent the components of the AP that most strongly influenced the dominant PCA pattern.

Several segments appeared repeatedly across multiple features, including BAR_RTConBB, PUR_onBB, CAR_onBB, and UAR_RTCBG, suggesting that these segments consistently contributed to the primary variance structure of the EVestG signals.

A frequency analysis of the dominant segments further revealed that specific tilts occurred more frequently among the top ones. As shown in the second table, the most common tilts included IAL

and PUR (9 occurrences each), followed by BAR and UAR (7 occurrences each). Other frequently observed tilts included IAR, RAR, and CAR.

Overall, the PCA results indicate that a dominant variance pattern captured by PC1 explains a meaningful portion of the variability in the EVestG-derived AP features. The higher proportion of variance explained in the HIS ≥ 2 group suggests that the vestibular responses in this group are more strongly dominated by a single underlying AP pattern. These findings indicate that cerebrovascular burden may influence the structure and stability of the dominant AP patterns following stimulation.

Appendix B ICA results for active tACS + cognitive exercises

B.1 ICA results for active tACS + cognitive exercises in low HIS scores

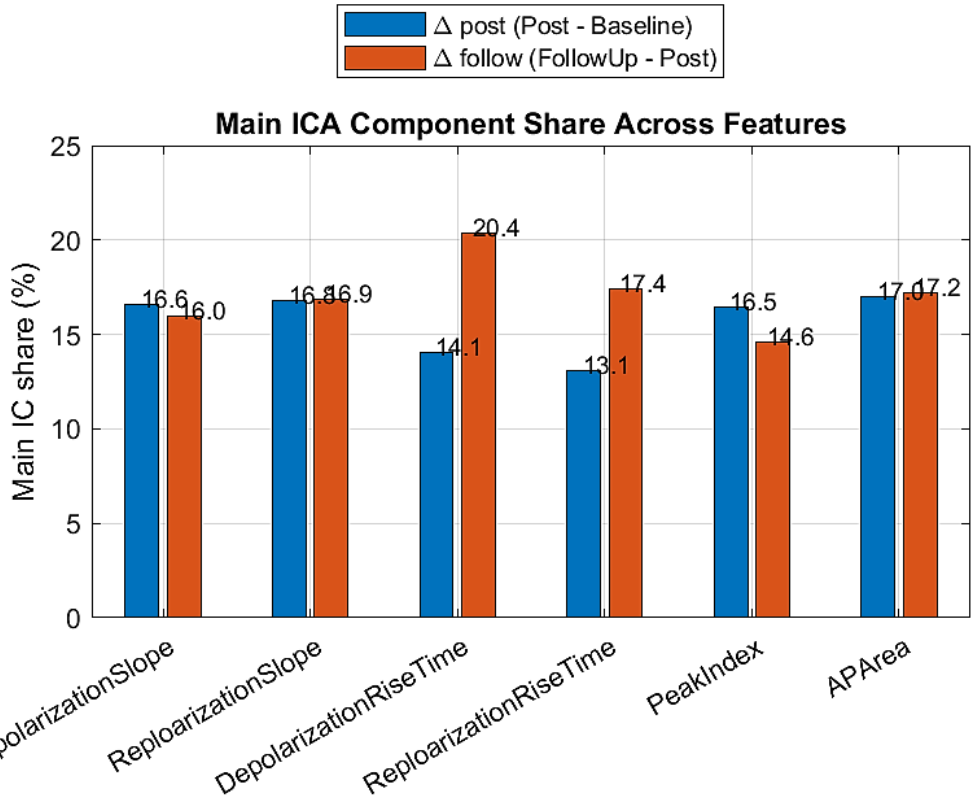

Figure B. 1 Contribution of the main IC. The proportion of variance in AP features captured by the dominant IC.

Figure B.1 shows the proportion of variance in AP features captured by the dominant independent component (IC) across EVestG features. Overall, the dominant IC accounted for approximately 13–17% of the variability during Δpost and 15–20% during Δfollow.

Among the features, Depolarization Rise Time showed the largest increase in component contribution during the follow-up interval, rising from approximately 14.1% during Δpost to 20.4% during Δfollow. A similar trend occured for Repolarization Rise Time, increasing from 13.1% to 17.4%.

In contrast, Peak Index showed a decrease in the main IC contribution during follow-up (from 16.5% to 14.6%), while Depolarization Slope remained relatively stable between the two intervals. Overall, these findings indicate that the dominant independent patterns associated with rise-time features became more pronounced during the follow-up period.

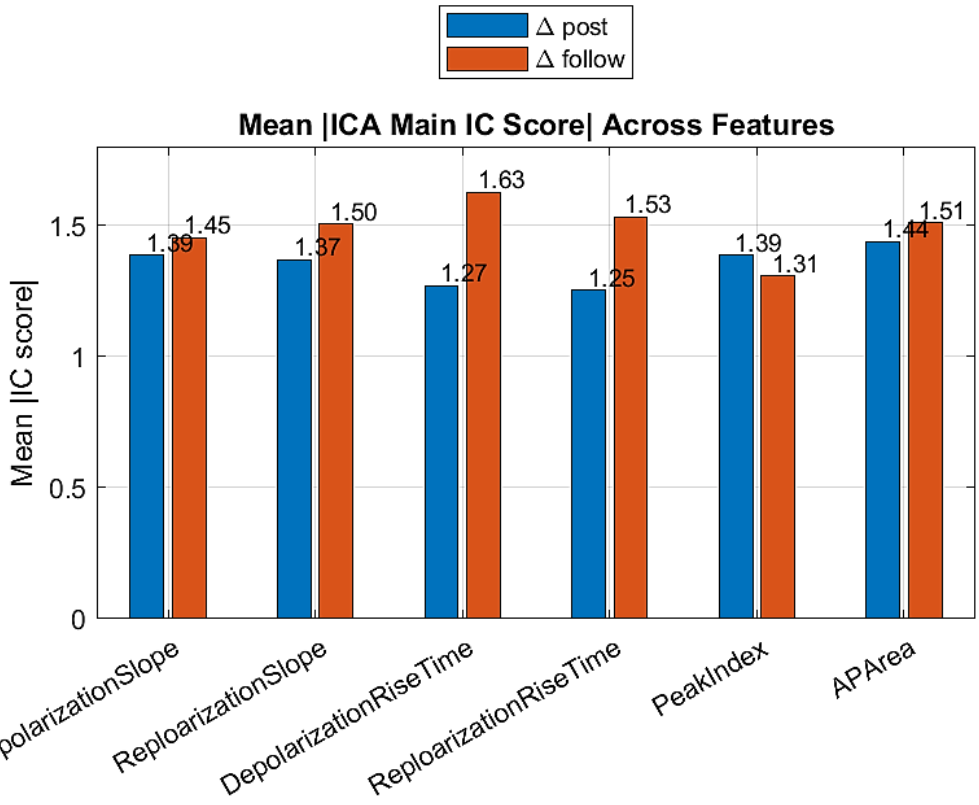

Figure B. 2 Magnitude of ICA component scores

The mean absolute values of the ICA component scores for each feature are presented in Figure B.2. These scores represent the strength of the dominant independent signal pattern captured by ICA.

For most features, the magnitude of the ICA component scores was higher during Δfollow compared with Δpost, indicating a stronger expression of the independent pattern during the

follow-up interval. For example, Depolarization Rise Time increased from 1.27 during Δpost to 1.63 during Δfollow, and Repolarization Rise Time increased from 1.25 to 1.53.

Similarly, Depolarization Slope and Repolarization Slope also exhibited moderate increases in score magnitude during follow-up. In contrast, Peak Index showed a slight decrease in magnitude between Δpost and Δfollow, while AP Area showed a small increase.

These results suggest that the dominant independent EVestG patterns became more strongly expressed during the follow-up interval for several features.

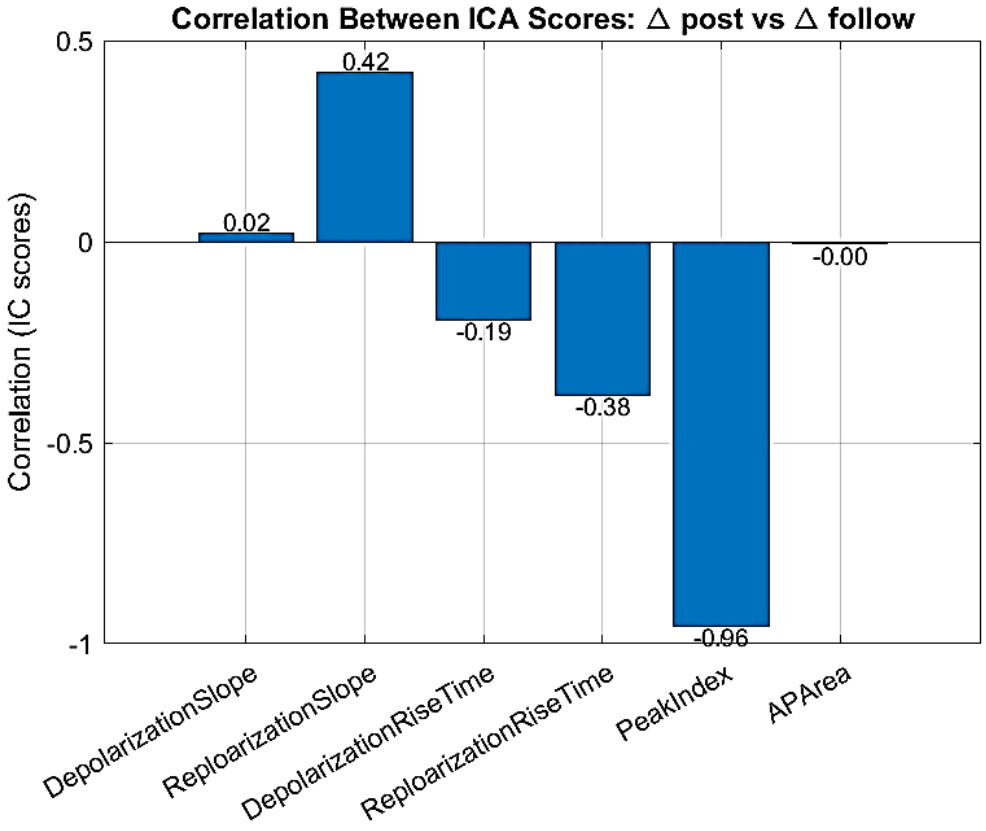

Figure B. 3 Correlation between ICA scores in Δpost and Δfollow

The correlation between ICA component scores obtained from Δpost and Δfollow is illustrated in Figure B.3. The correlations varied across features, indicating differences in the stability of the independent patterns between the two intervals.

A moderate positive correlation was observed for Repolarization Slope (r = 0.42), suggesting that the dominant independent pattern for this feature remained relatively consistent between the post-treatment and follow-up intervals. Depolarization Slope showed a near-zero correlation (r ≈ 0.02), indicating minimal similarity between the two intervals.

In contrast, several features exhibited negative correlations, including Depolarization Rise Time (r = −0.19) and Repolarization Rise Time (r = −0.38). The strongest negative correlation was observed for Peak Index (r = −0.96), indicating a substantial change in the dominant independent pattern between Δpost and Δfollow.

AP Area showed a near-zero correlation, suggesting little similarity in the independent component structure between the two intervals.

Overall, these findings indicate that the independent patterns extracted by ICA were less stable across time compared with the PCA components, particularly for several features.

Feature	Top 5 segments - Δpost	Top 5 segments - Δfollow
Depolarization Slope	BAL_RTConBB | RAL_onAA | IAR_BG | RAL_BG | CAL_RTConBB	CAR_RTConAA | RAR_BG | PUR_onAA | BAL_BG | PUL_RTConBB
Repolarization Slope	UAL_onBB | PUL_RTConAA | PUL_BG | UAL_RTConAA | IAL_BG	PRR_BG | BAR_RTCBG | PUR_BG | PRL_onAA | BAL_BG
Depolarization Rise Time	IAL_BG | BAL_RTConAA | IAR_onBB | UAL_BG | PUR_onAA	PRR_RTCBG | PUR_onAA | PRR_RTConAA | BAR_RTCBG | PRL_onAA
Repolarization Rise Time	PRR_RTConAA | PRL_RTCBG | UAR_RTConBB | RAL_onBB | RAL_RTConBB	CAL_RTConBB | IAR_onAA | CAR_RTConBB | PUL_BG | BAR_RTCBG
Peak Index	UAR_onAA | UAL_BG | RAR_BG | RAR_RTConAA | IAR_onBB	PUR_RTConBB | IAR_RTCBG | PUR_RTCBG | RAR_onAA | IAL_BG
AP Area	RAR_RTConAA | PUL_RTConAA |	PRL_RTConBB | RAR_RTConAA |

	UAL_RTConAA | PUR_RTConBB | BAL_BG	CAR_RTConBB | RAL_RTCBG | PUR_BG

Table B. 1 Dominant segments contributing to the ICA components

The EVestG segments with the largest contributions to the dominant ICA component are summarized in Table B.1. These segments represent the independent signal sources that most strongly influenced the extracted components. Across the analyzed features, several segments appeared repeatedly among the dominant contributors. For example, BAL_BG, BAR_RTCBG, IAL_BG, PUR_onAA, and RAR_RTConBB were among the segments most frequently identified across features.

A frequency analysis of the dominant segments also revealed recurring vestibular tilt orientations. The most frequent orientations included PUR (8 occurrences) and RAR (6 occurrences), followed by BAL, IAR, PUL, and RAL, each appearing multiple times among the dominant components. These results indicate that the independent patterns identified by ICA were influenced by a subset of segments associated with specific vestibular tilts.

Overall, the ICA analysis revealed that the dominant independent component captured a moderate proportion of the AP features variability. In contrast to the PCA results, the ICA component correlations between Δpost and Δfollow varied substantially across features, indicating that the independent patterns often changed between the immediate post-treatment and follow-up intervals. Furthermore, the ICA analysis identified a consistent subset of EVestG segments and tilts contributing to the independent AP components, suggesting that specific vestibular response patterns underlie the independent structure of the EVestG signals in this participant group.

B.2 ICA results for active tACS + cognitive exercises in high HIS scores

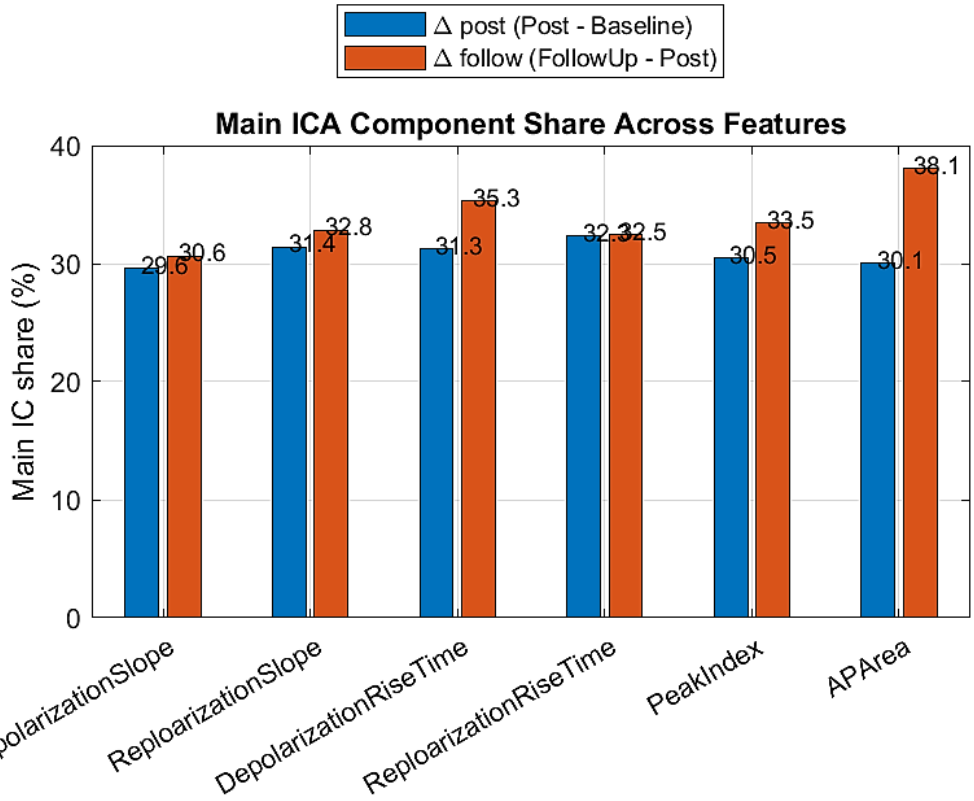

Figure B. 4 Contribution of the main IC

The proportion of signal variability explained by the dominant independent component across the AP features is illustrated in Figure B.4. Overall, the dominant component accounted for approximately 29–32% of the signal variability during Δpost and 31–38% during Δfollow, indicating that a single independent component captured a substantial portion of the feature variation.

Across the features, a modest increase in component contribution was observed during the follow-up interval. The most pronounced increase occurred for AP Area, which rose from approximately 30.1% during Δpost to 38.1% during Δfollow, suggesting that this feature became more strongly dominated by a single independent pattern over time. Depolarization Rise Time and Peak Index

also showed marked increases during follow-up, reaching 35.3% and 33.5%, respectively. In contrast, Repolarization Rise Time remained relatively stable between the two intervals, with contributions of approximately 32.3%–32.5%.

Figure B. 5 Magnitude of ICA component scores

The average magnitude of the dominant ICA scores across features is shown in Figure B.5. The mean absolute IC scores ranged from approximately 1.9 to 2.2, indicating a relatively consistent AP contribution across features.

For several features, including Repolarization Slope, Peak Index, and AP Area, the magnitude of the IC scores increased slightly during the follow-up interval compared with Δpost. In contrast, Depolarization Slope and Repolarization Rise Time showed a small decrease in IC magnitude during follow-up. These variations suggest that although the dominant independent component

remained strong across features, its relative influence evolved differently across the AP metrics over time.

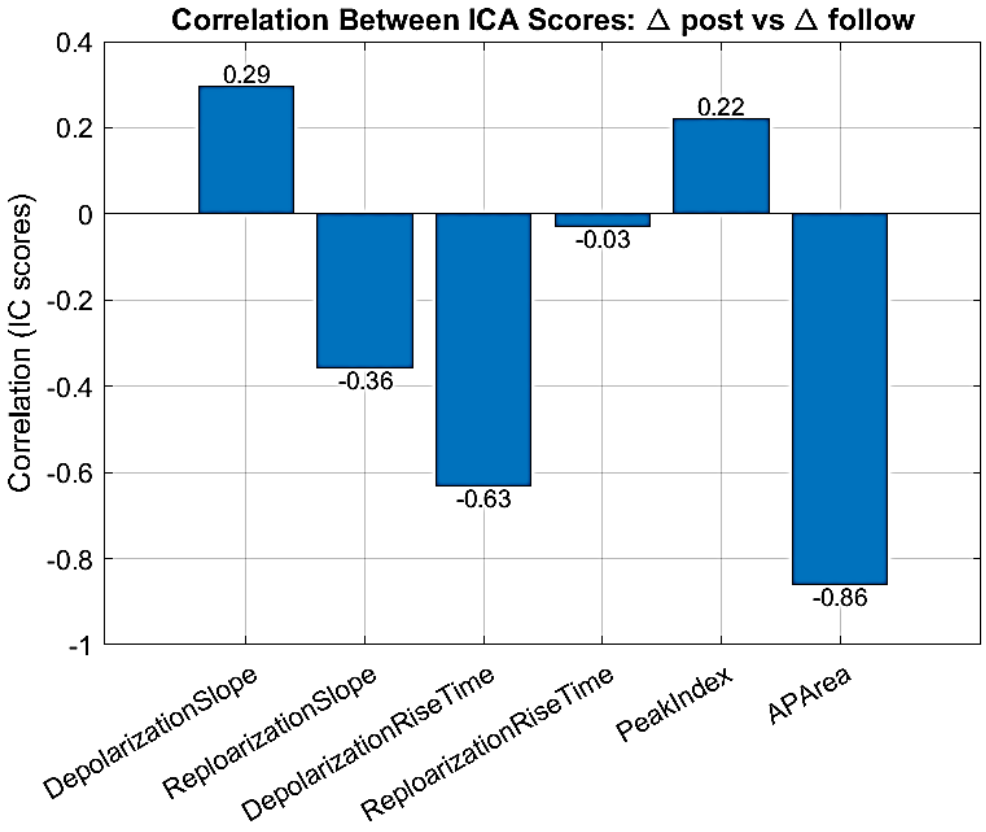

Figure B. 6 Correlation between post-treatment and follow-up ICA patterns

To assess whether the independent patterns observed immediately after treatment persisted at follow-up, correlations were calculated between the dominant ICA scores obtained during Δpost and Δfollow for each feature (Figure B.6).

The results revealed weak to moderate negative correlations for several features, including AP Area ($r \approx -0.86$), Depolarization Rise Time ($r \approx -0.63$), and Repolarization Slope ($r \approx -0.36$). These negative correlations suggest that the dominant signal patterns associated with treatment-related changes often reversed or evolved between the post-treatment and follow-up periods. In contrast, Depolarization Slope ($r \approx 0.29$) and Peak Index ($r \approx 0.22$) showed weak positive

correlations, indicating partial stability of the dominant patterns for these features across time. Repolarization Rise Time showed almost no correlation between intervals ($r \approx -0.03$), suggesting that the independent signal structure for this feature changed substantially between post-treatment and follow-up.

Feature	Top 5 segments - Δpost	Top 5 segments - Δfollow
Depolarization Slope	BAR_RTConBB | IAR_onAA | IAL_RTConBB | UAL_RTConAA | IAR_onBB	PUR_onBB | RAR_onBB | UAR_RTCBG | PUL_RTConAA | IAL_onBB
Repolarization Slope	BAR_RTConBB | CAR_BG | PUR_BG | UAL_RTConAA | PRL_RTCBG	PUR_onBB | IAL_onBB | UAR_onAA | BAR_RTConBB | CAR_onBB
Depolarization Rise Time	UAR_onBB | BAR_RTConBB | IAL_onAA | IAR_RTCBG | CAL_onAA	CAR_onBB | UAR_RTCBG | RAR_onBB | PUR_onBB | RAR_BG
Repolarization Rise Time	PUL_RTConBB | CAL_onAA | RAR_RTConBB | IAR_RTConAA | BAL_onBB	PUR_onBB | PRL_RTConBB | BAR_RTConBB | RAR_BG | PRL_onAA
Peak Index	PRL_BG | BAR_RTConBB | UAR_RTConBB | PUL_RTConBB | BAR_RTCBG	RAR_BG | CAR_onBB | IAR_RTCBG | PUR_onBB | RAR_onBB
AP Area	PRL_onAA | BAR_RTConAA | IAR_RTCBG | IAL_onAA | PUL_RTConBB	PUR_onBB | UAR_RTCBG | CAR_onBB | BAR_RTConBB | RAR_onBB

Table B. 2 Distribution of dominant segments and tilts

The segments contributing most frequently to the dominant ICA patterns are summarized in Table B.2. For Δpost, dominant segments were most frequently associated with BAR_RTConBB, UAR_onBB, and PUL_RTCon segments across multiple features. In contrast, the follow-up interval was primarily dominated by PUR_onBB segments across several AP features, suggesting a shift in the underlying independent features' structure between the immediate treatment response

and longer-term follow-up. When examined by tilts, BAR, RAR, and PUR tilts occurred most frequently among the dominant ICA components, followed by IAR and UAR tilts.

Overall, the ICA analysis indicates that the EVestG-derived AP features in participants with HIS ≥ 2 exhibit structured but evolving independent patterns following real tACS treatment. While a strong dominant component explains a substantial portion of the variability across features, the correlation analysis suggests that the underlying independent AP component structure changes between the post-treatment and follow-up periods.

Appendix C PCA results for sham tACS + cognitive exercises

C.1 PCA results for sham tACS + cognitive exercises in low HIS scores

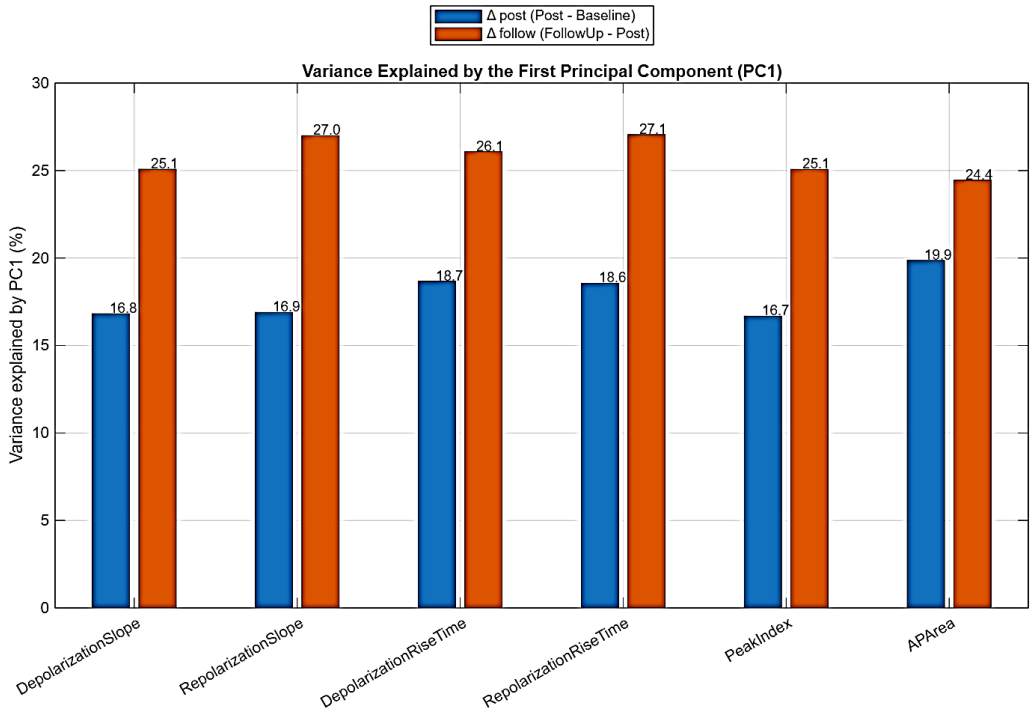

Figure C. 1 Contribution of the PC1

The proportion of variance in the EVestG-derived AP features explained by the PC1 is shown in Figure C.1.

Overall, PC1 accounted for a moderate proportion of the variability, explaining approximately 16.7% to 19.9% of the variance during Δpost and 24.4% to 27.1% during Δfollow. Across all features, the variance explained by PC1 was consistently higher during the follow-up interval compared with the post-treatment interval.

Among the features, Repolarization Rise Time and Repolarization Slope exhibited the highest contributions during Δfollow (approximately 27.1% and 27.0%, respectively), while AP area showed the lowest increase from Δpost to Δfollow, rising from approximately 19.9% to 24.4%.

These findings indicate that the dominant variance pattern became more pronounced during the follow-up interval, suggesting a stronger consolidation of EVestG signal structure over time in this group.

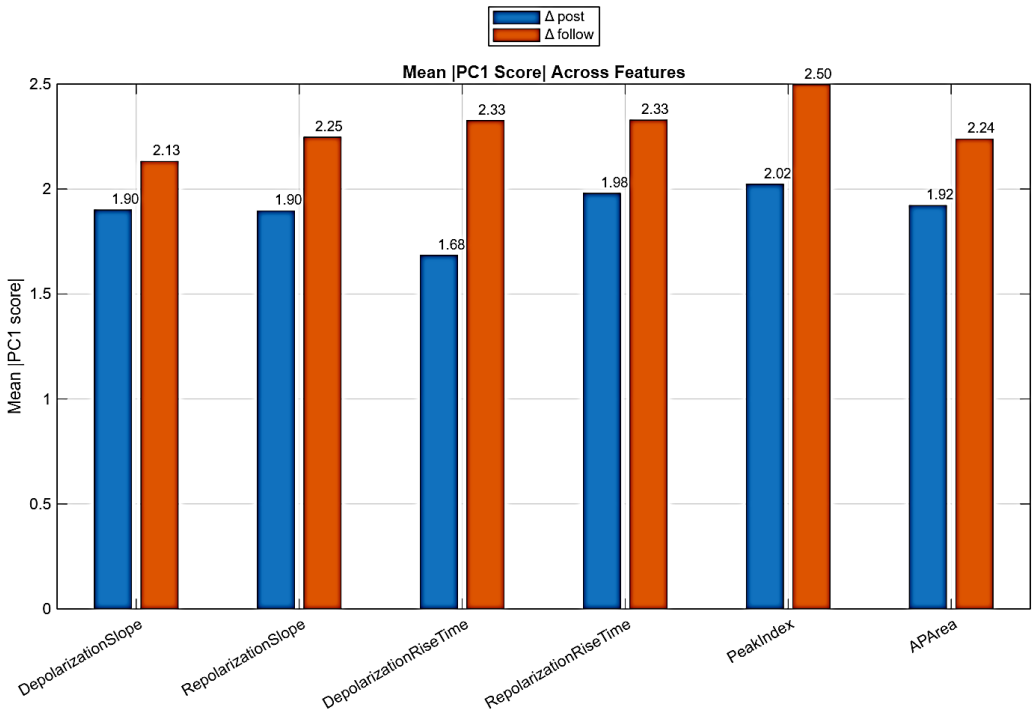

Figure C. 2 Magnitude of PC1 Scores

The mean absolute values of the PC1 scores for each feature are presented in Figure C.2. Across all features, the magnitude of the PC1 scores was consistently higher during Δfollow compared with Δpost, indicating an increased strength of the dominant signal pattern during the follow-up interval.

For example, Peak Index increased from approximately 2.02 during Δpost to 2.50 during Δfollow, while Depolarization Rise Time increased from 1.68 to 2.33. Similarly, Repolarization Rise Time and Repolarization Slope showed notable increases in score magnitude during follow-up.

These results suggest that the dominant EVestG pattern identified by PCA became more strongly expressed after the follow-up period in participants receiving sham tACS + cognitive exercises treatment.

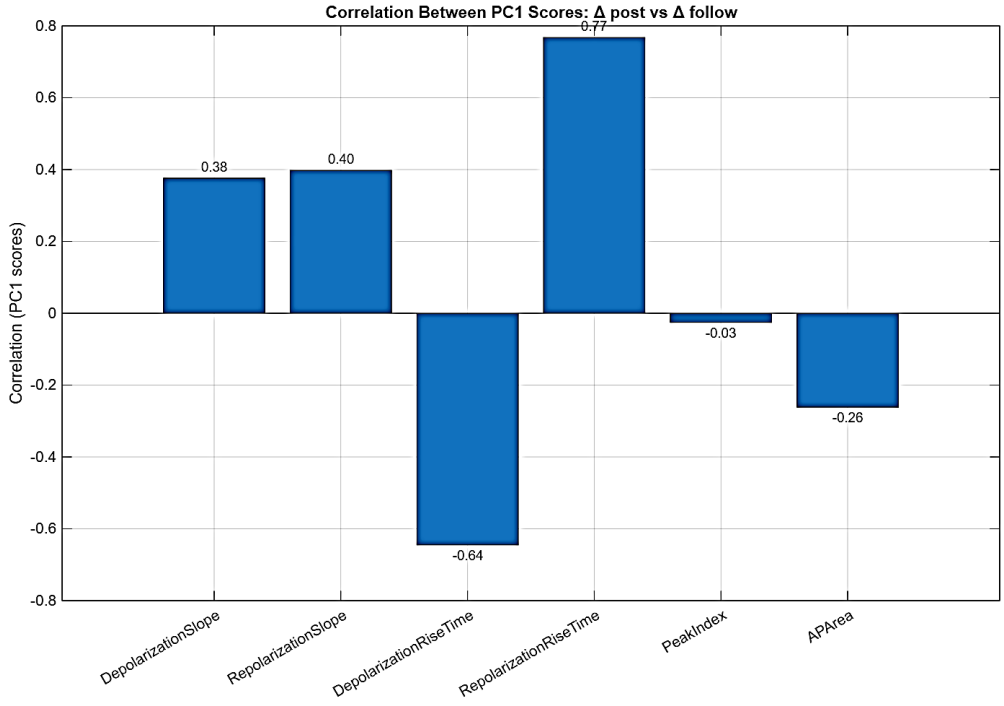

Figure C. 3 Correlation Between PC1 Scores (Δpost vs Δfollow)

The correlation between PC1 scores obtained from Δpost and Δfollow is illustrated in Figure C.3.

The correlations varied substantially across features, indicating differences in the temporal stability of the dominant patterns.

Moderate positive correlations were observed for Repolarization Rise Time ($r = 0.77$), Repolarization Slope ($r = 0.40$), and Depolarization Slope ($r = 0.38$), suggesting that the dominant patterns for these features remained relatively consistent between post-treatment and follow-up.

In contrast, Depolarization Rise Time showed a strong negative correlation ($r = -0.64$), indicating a reversal or substantial change in the dominant pattern between the two intervals. AP Area also exhibited a negative correlation ($r = -0.26$), while Peak Index showed a near-zero correlation ($r \approx -0.03$), suggesting minimal similarity between Δpost and Δfollow.

Overall, these findings indicate that while some EVestG features maintained stable dominant patterns over time, others exhibited considerable variability between the immediate post-treatment and follow-up intervals.

Feature	Top 5 segments - Δpost	Top 5 segments - Δfollow
Depolarization Slope	PRR_RTConBB | IAR_RTConBB | PUL_RTCBG | RAR_RTConAA | CAL_RTCBG	UAR_onBB | PRR_onBB | PUL_onAA | PRR_RTConAA | UAL_RTConAA
Repolarization Slope	CAR_BG | CAL_RTConBB | UAR_RTConBB | PRR_onAA | IAL_BG	BAL_onAA | IAL_BG | RAL_BG | BAL_RTConAA | CAR_BG
Depolarization Rise Time	PUR_onBB | BAL_RTConAA | CAL_RTCBG | BAR_RTConBB | CAR_RTCBG	CAR_BG | UAR_RTCBG | IAR_BG | IAL_onBB | UAL_RTConAA
Repolarization Rise Time	RAR_RTConBB | PRR_RTConBB | PRR_onBB | CAR_BG | UAR_RTConBB	BAL_onAA | RAL_BG | UAR_RTCBG | IAR_BG | BAL_RTConAA
Peak Index	IAL_onAA | CAL_RTCBG | BAR_BG | CAR_RTConBB | IAR_RTCBG	CAR_onBB | CAR_BG | IAR_RTConBB | RAL_BG | IAR_BG

AP Area	CAL_RTConAA | PRR_RTConBB | UAR_RTConBB | CAR_BG | PRL_RTCBG	IAL_BG | IAR_BG | BAL_onAA | CAR_onBB | PRL_RTConBB

Table C. 1 Dominant Segments Contributing to PC1

The EVestG segments with the largest contributions to PC1 are summarized in Table C.1.

Across the analyzed features, several segments appeared repeatedly among the dominant contributors. Notably, segments such as PRR_RTConBB, IAR_RTConBB, CAR_BG, and UAL_RTConAA were frequently identified across multiple features and time intervals.

A frequency analysis of the dominant segments further revealed recurring vestibular tilt directions. As shown in the corresponding table, the most frequent tilts included CAR, IAR, and PRR, followed by BAL, UAR, and CAL, indicating that specific directional movements contributed more strongly to the dominant variance patterns.

These results suggest that the PCA-derived dominant patterns were driven by a subset of EVestG segments associated with particular tilt directions and temporal phases of the vestibular response.

Overall, the PCA analysis demonstrated that PC1 captured a moderate but increasing proportion of the EVestG signal variability from post-treatment to follow-up.

The increased variance explained and higher PC1 score magnitudes during the follow-up interval indicate that the dominant signal pattern became more pronounced over time in participants receiving sham tACS + cognitive exercises.

However, the correlation analysis revealed that the stability of this dominant pattern varied across features, with some features showing consistent behavior over time and others exhibiting substantial changes between Δpost and Δfollow.

Furthermore, the PCA results identified a consistent subset of EVestG segments and tilt directions contributing to the dominant patterns, suggesting that specific vestibular response components play a key role in shaping the overall EVestG signal structure in this participant group.

C.2 PCA results for sham tACS + cognitive exercises in high HIS scores

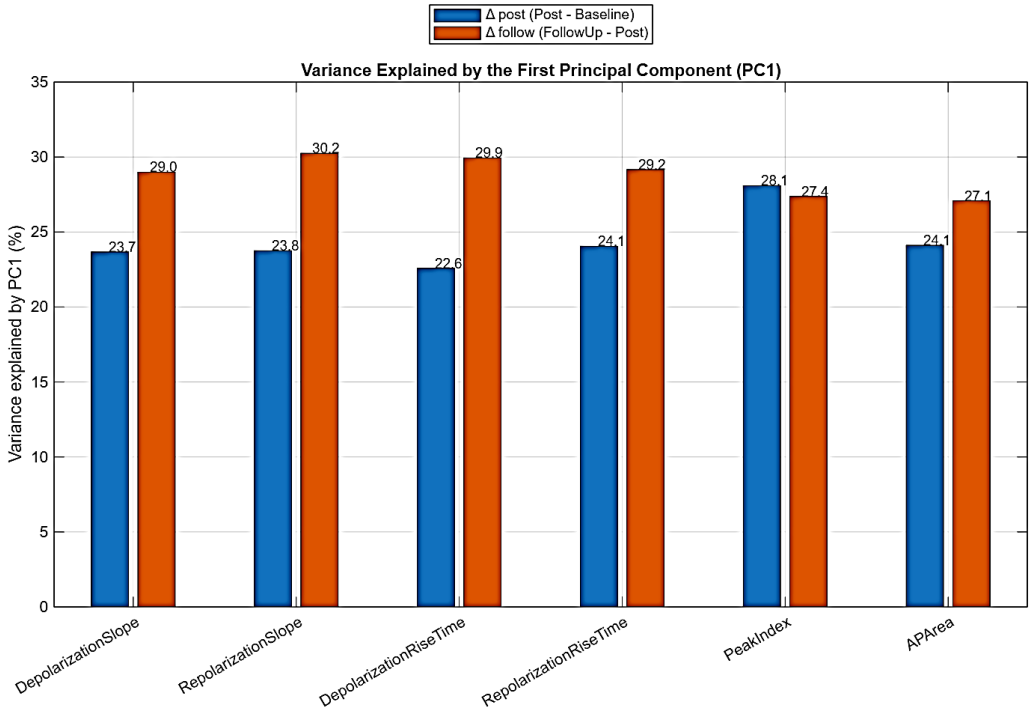

Figure C. 4 Contribution of the PC1

The proportion of variance in the EVestG-derived AP features explained by the PC1 is shown in Figure C.4.

Overall, PC1 accounted for a relatively higher proportion of the variability compared with the HIS < 2 group, explaining approximately 22.6% to 28.1% of the variance during Δpost and 27.1% to 30.2% during Δfollow. Across most features, the variance explained by PC1 remained consistently high in both intervals, with a slight increase during the follow-up period.

Among the features, Repolarization Slope and Depolarization Slope exhibited the highest contributions during Δfollow (approximately 30.2% and 29.0%, respectively). In contrast, Peak Index showed a slight decrease from Δpost (28.1%) to Δfollow (27.4%), indicating a minor reduction in the dominance of the principal pattern for this feature.

These findings indicate that the dominant variance pattern captured by PC1 was strong and relatively stable across sessions in participants with higher cerebrovascular burden.

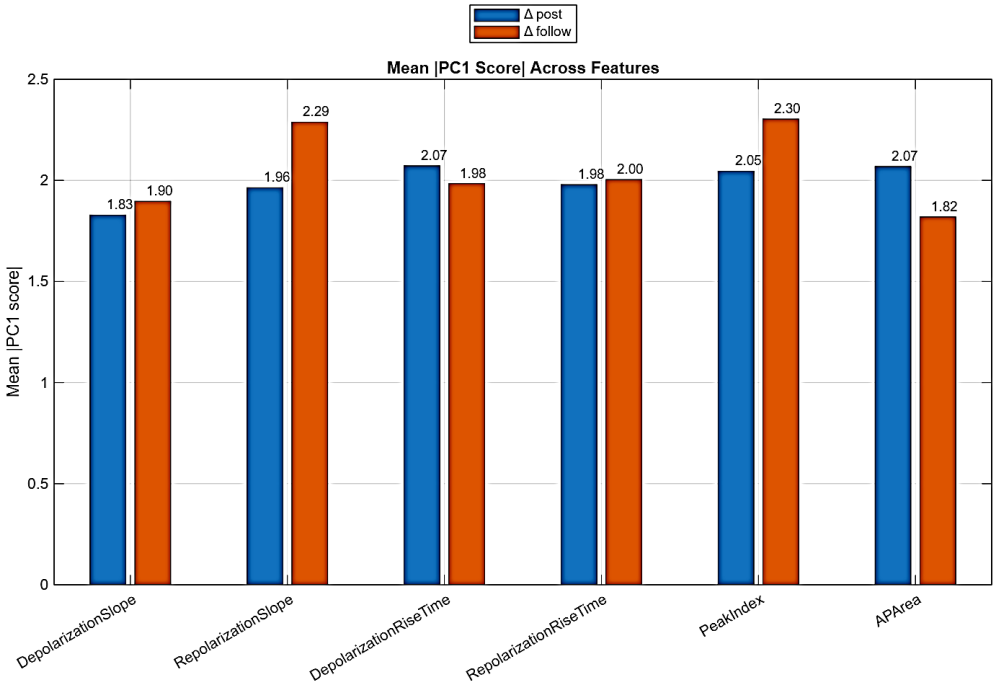

Figure C. 5 Magnitude of PC1 Scores

The mean absolute values of the PC1 scores for each feature are presented in Figure C.5.

In contrast to the HIS < 2 group, the magnitude of the PC1 scores in the HIS ≥ 2 group showed more variable trends across features, rather than a consistent increase during follow-up.

For example, Repolarization Slope increased from approximately 1.96 during Δpost to 2.29 during Δfollow, while Peak Index increased from 2.05 to 2.30. In contrast, AP area decreased from 2.07

during Δpost to 1.82 during Δfollow, and Depolarization Rise Time showed a slight decrease from 2.07 to 1.98.

These mixed trends suggest that, although the dominant component remains strong, the expression of this pattern across features varies over time in this group.

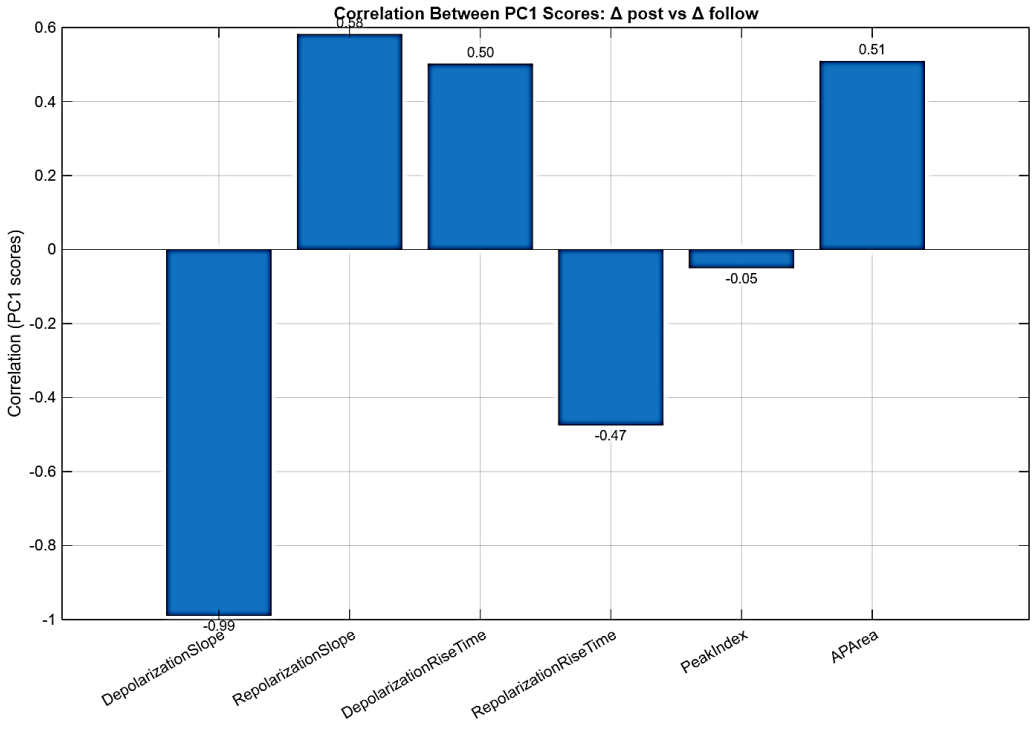

Figure C. 6 Correlation Between PC1 Scores (Δpost vs Δfollow)

The correlation between PC1 scores obtained from Δpost and Δfollow is illustrated in Figure C.6. The correlations varied substantially across features, indicating differences in the temporal stability of the dominant patterns.

Moderate positive correlations were observed for Repolarization Slope (r = 0.58), AP Area (r = 0.51), and Depolarization Rise Time (r = 0.50), suggesting that the dominant patterns for these features remained relatively consistent between post-treatment and follow-up.

In contrast, Depolarization Slope exhibited a very strong negative correlation (r = −0.99), indicating a near-complete reversal of the dominant pattern between the two intervals. Repolarization Rise Time also showed a negative correlation (r = −0.47), while Peak Index showed a near-zero correlation (r ≈ −0.05), suggesting minimal similarity across time.

Overall, these findings indicate that although some features maintain stable dominant patterns, others exhibit substantial temporal reorganization in participants with higher cerebrovascular burden.

Feature	Top 5 segments - Δpost	Top 5 segments - Δfollow
Depolarization Slope	PRL_onBB | RAL_BG | RAL_onBB | PRL_RTConAA | UAR_RTConAA	UAR_RTConAA | CAR_onAA | RAR_RTConBB | BAL_RTCBG | UAR_RTConBB
Repolarization Slope	UAL_BG | UAL_RTCBG | BAR_RTConBB | PRL_RTConAA | UAR_onAA	RAR_onAA | RAR_RTConBB | CAR_onAA | IAR_RTConAA | IAR_RTCBG
Depolarization Rise Time	UAR_RTConAA | PUR_onBB | CAR_onAA | RAL_RTConAA | UAL_onAA	UAL_RTConBB | CAL_BG | UAR_RTConAA | PUL_BG | IAL_onBB
Repolarization Rise Time	UAR_RTConAA | PRL_RTConAA | PUL_onAA | IAR_RTConBB | RAL_onBB	UAL_RTConBB | CAL_BG | RAR_onAA | RAR_RTConAA | RAR_RTConBB
Peak Index	UAL_RTCBG | CAL_RTConBB | BAR_BG | RAL_BG | PUL_onAA	PUR_onBB | PUL_RTConAA | PRR_RTConAA | CAL_BG | PRL_onBB
AP Area	PRL_onBB | RAL_onBB | IAL_RTConAA | CAL_BG | PRR_RTConBB	UAL_RTConBB | UAL_RTCBG | RAR_onAA | RAR_RTConBB | PRR_RTCBG

Table C. 2 Dominant Segments Contributing to PC1

The EVestG segments with the largest contributions to PC1 are summarized in Table C.2. Across the analyzed features, several segments appeared repeatedly among the dominant contributors. Notably, segments such as UAR_RTConAA, UAL_RTConAA, RAL_onBB, and PRL_RTConAA were frequently identified across multiple features and time intervals.

A frequency analysis of the dominant segments further revealed recurring vestibular tilt directions. The most frequent tilts included RAR, UAL, and UAR, followed by PRL, RAL, and CAL, indicating that these directional movements contributed most strongly to the dominant PCA patterns.

These results suggest that the dominant variance patterns in this group were driven by a consistent subset of EVestG segments associated with specific tilt directions and phases of the vestibular response.

Overall, the PCA analysis demonstrated that the PC1 captured a substantial proportion of the EVestG signal variability in participants with HIS ≥ 2.

Compared with the HIS < 2 group, the variance explained by PC1 was consistently higher, indicating a stronger dominance of a single underlying signal pattern. However, the correlation analysis revealed that the temporal stability of this dominant pattern varied across features, with some features showing consistent behavior and others exhibiting pronounced changes between Δpost and Δfollow.

Furthermore, the PCA results identified a recurring subset of EVestG segments and tilt directions contributing to the dominant patterns, suggesting that specific vestibular response components play a key role in shaping the EVestG signal structure in this group.

Appendix D ICA results for sham tACS + cognitive exercises

D.1 ICA results for sham tACS + cognitive exercises in low HIS scores

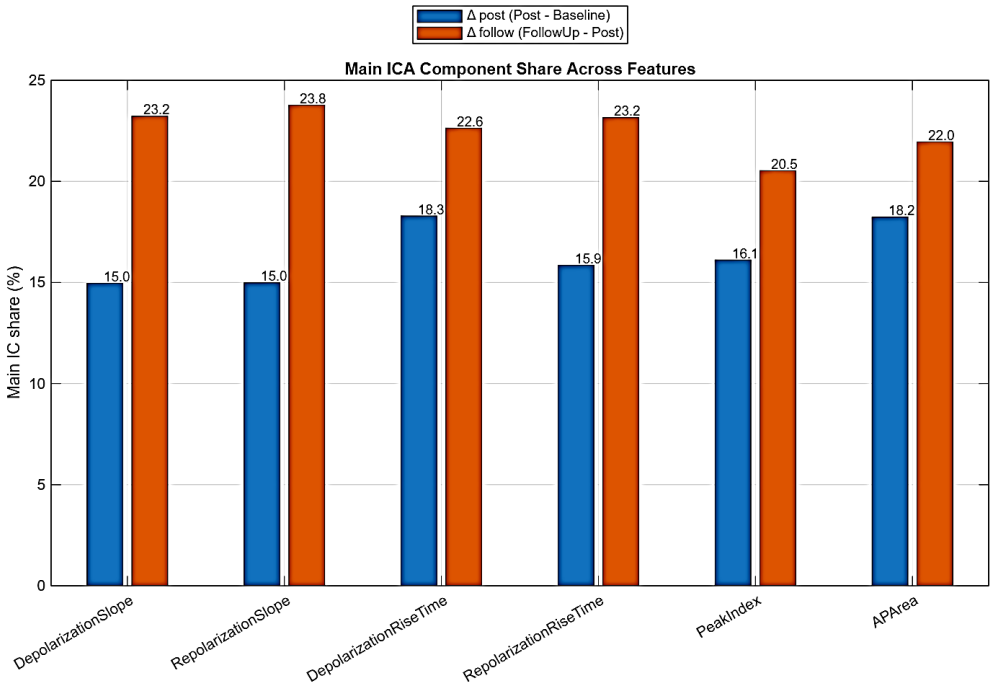

Figure D. 1 Contribution of the main IC

Overall, the dominant IC accounted for a moderate proportion of the signal variability across features, with a consistent increase observed from Δpost to Δfollow. Specifically, the IC contribution ranged from approximately 15–18% during Δpost and increased to approximately 20–24% during Δfollow across all features. This indicates that independent signal structures became more pronounced during the follow-up period.

Among the features, depolarization rise time and AP area showed the highest IC contributions, suggesting that these features carry stronger independent signal components thsn others. In contrast, depolarization and repolarization slopes exhibited relatively lower contributions, indicating a more distributed or less independent signal structure.

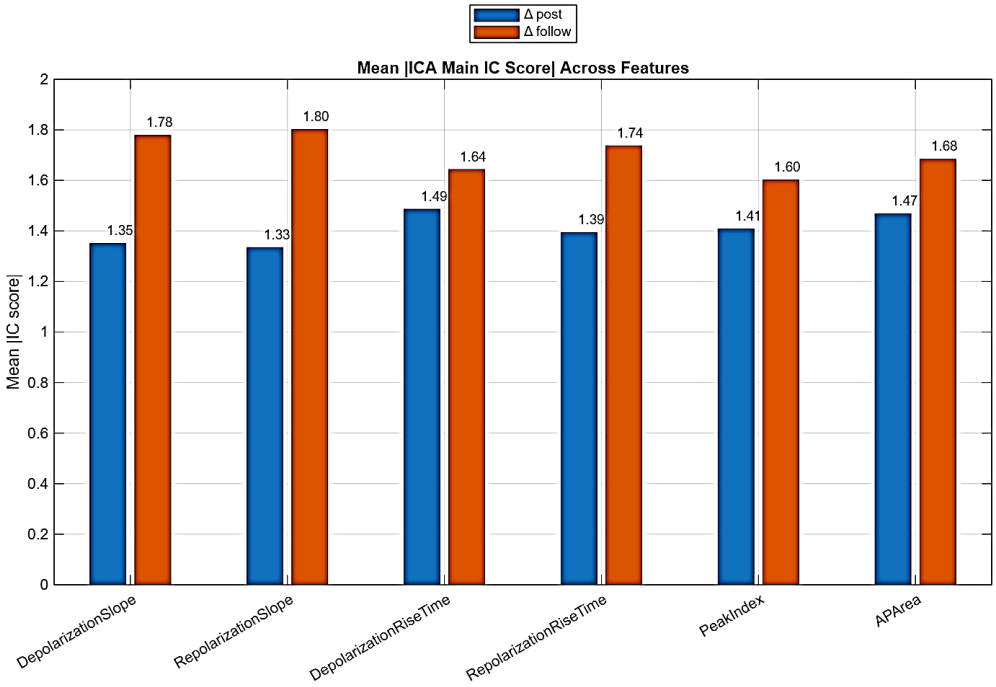

Figure D. 2 Magnitude of ICA component scores

The magnitude of the IC scores, represented by the mean absolute IC values, also increased consistently from Δpost to Δfollow for all features. This trend suggests that the strength of the independent neural patterns became more pronounced over time, even in the absence of active stimulation.

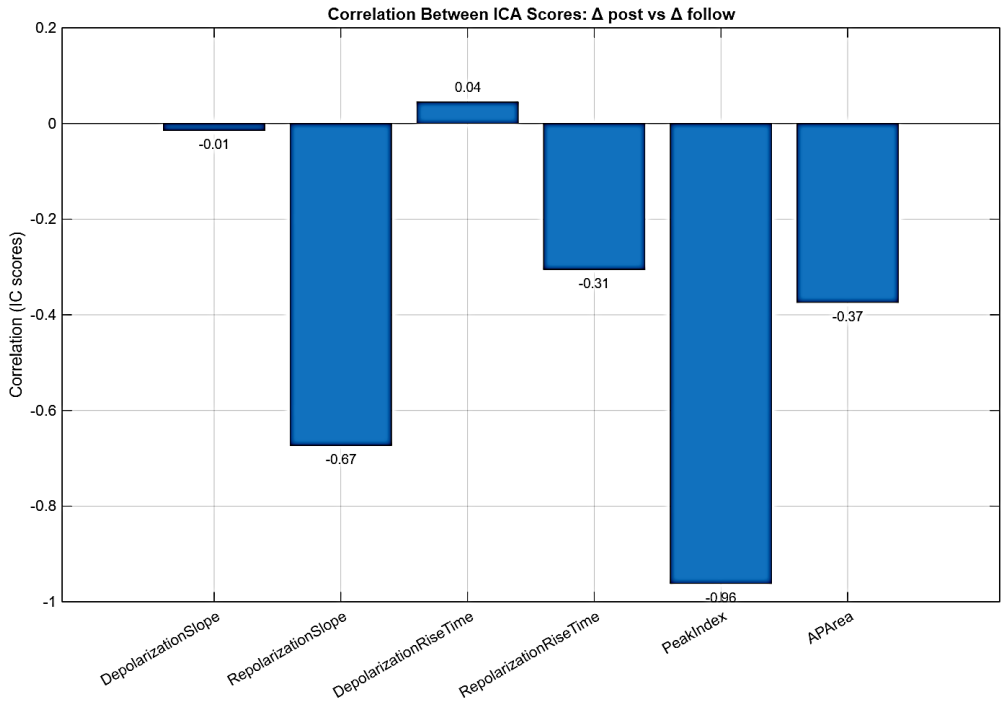

Figure D. 3 Correlation between post-treatment and follow-up ICA patterns

The correlation between IC scores derived from Δpost and Δfollow revealed predominantly weak to moderate negative relationships across features. In particular, peak index demonstrated a strong negative correlation ($r \approx -0.96$), while repolarization slope also showed a substantial negative correlation ($r \approx -0.67$). Other features, such as AP area and repolarization rise time, exhibited moderate negative correlations, whereas depolarization rise time showed near-zero correlation. These findings indicate that the independent patterns identified immediately after treatment were not preserved at follow-up and, in some cases, evolved in opposite directions.

Feature	Top 5 segments - Δpost	Top 5 segments - Δfollow
Depolarization Slope	PRR_RTConBB | PUL_RTConAA | RAR_RTConAA | RAL_BG | IAR_RTCBG	UAR_RTCBG | UAR_onBB | PUL_onAA | BAR_RTConBB | PUL_onBB
Repolarization Slope	RAR_RTConBB | PRR_onAA | PUL_RTCBG | IAL_BG | CAL_RTConBB	BAL_RTConAA | BAL_onAA | BAR_onAA | UAL_onAA | BAL_BG

Depolarization Rise Time	BAL_RTConAA | PUR_onBB | RAR_onBB | PUR_RTConAA | CAR_RTCBG	UAR_RTCBG | RAL_BG | CAR_BG | IAL_onBB | RAL_RTCBG
Repolarization Rise Time	PRR_onBB | RAL_RTConBB | PUL_RTCBG | PUR_onBB | BAL_RTConBB	BAR_onAA | PUL_RTConBB | BAL_BG | BAL_RTConAA | PUR_onBB
Peak Index	CAL_RTConAA | RAR_RTConAA | PUL_RTConAA | RAR_onBB | PRR_BG	PUR_onBB | IAR_BG | PRR_RTConBB | PUL_RTConAA | BAR_RTConBB
AP Area	PUL_RTCBG | RAR_RTConBB | PRR_RTConBB | PRR_onAA | PUL_RTConAA	IAL_BG | PUR_onBB | PUR_RTConBB | PUL_RTConAA | IAR_BG

Table D. 1 Distribution of dominant segments and tilts

Analysis of the most dominant segments contributing to the independent components further revealed that the informative segments were not uniformly distributed across all movement phases. Instead, segments associated with RTC phases, particularly acceleration and deceleration phases, appeared more frequently among the top contributors. In terms of tilt directions, posterior and vertical tilts (e.g., PUL, BAL, PRR) were more prominently represented, suggesting that these movements may elicit stronger independent vestibular responses.

These results suggest that, in participants with lower cerebrovascular burden, independent EVestG signal patterns continue to evolve over time following cognitive exercise alone, with increasing strength but limited temporal stability.

D.2 ICA results for sham tACS + cognitive exercises in high HIS scores

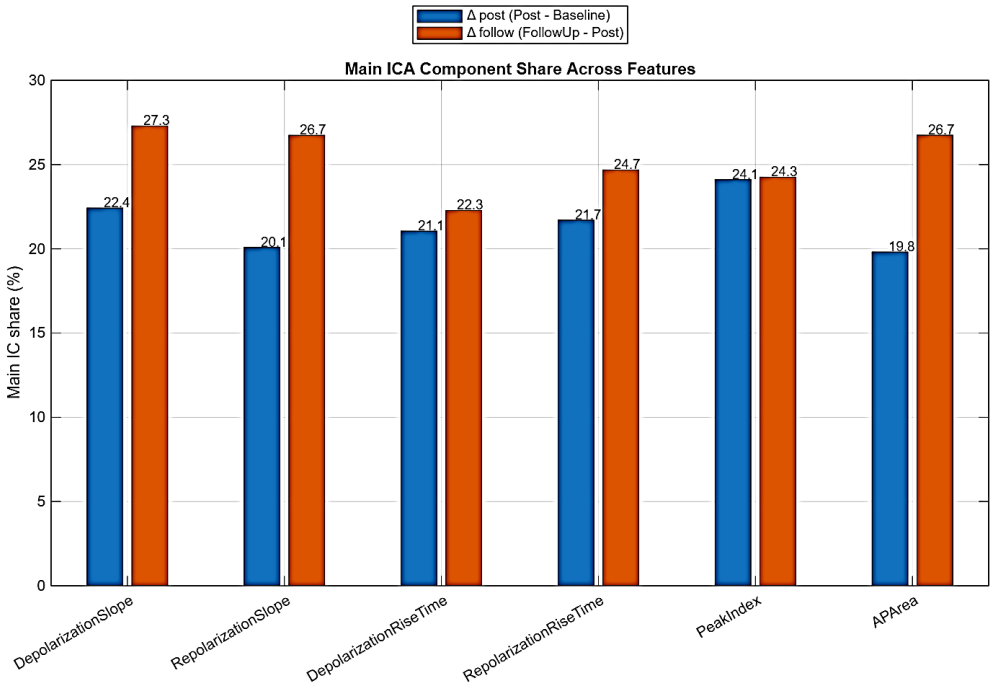

Figure D. 4 Contribution of the main IC

Overall, the dominant IC accounted for a larger proportion of the signal variability than the HIS < 2 group. The IC contribution ranged from approximately 20–24% during Δpost and increased to approximately 22–27% during Δfollow across features. This indicates that independent signal structures were more strongly represented in participants with higher cerebrovascular burden, particularly during the follow-up period.

Across features, depolarization slope, repolarization slope, and AP area demonstrated the highest IC contributions, while depolarization rise time showed comparatively lower contributions. Unlike the HIS < 2 group, the distribution of IC contribution across features appeared more uniform, suggesting a more globally organized independent signal structure rather than feature-specific dominance.

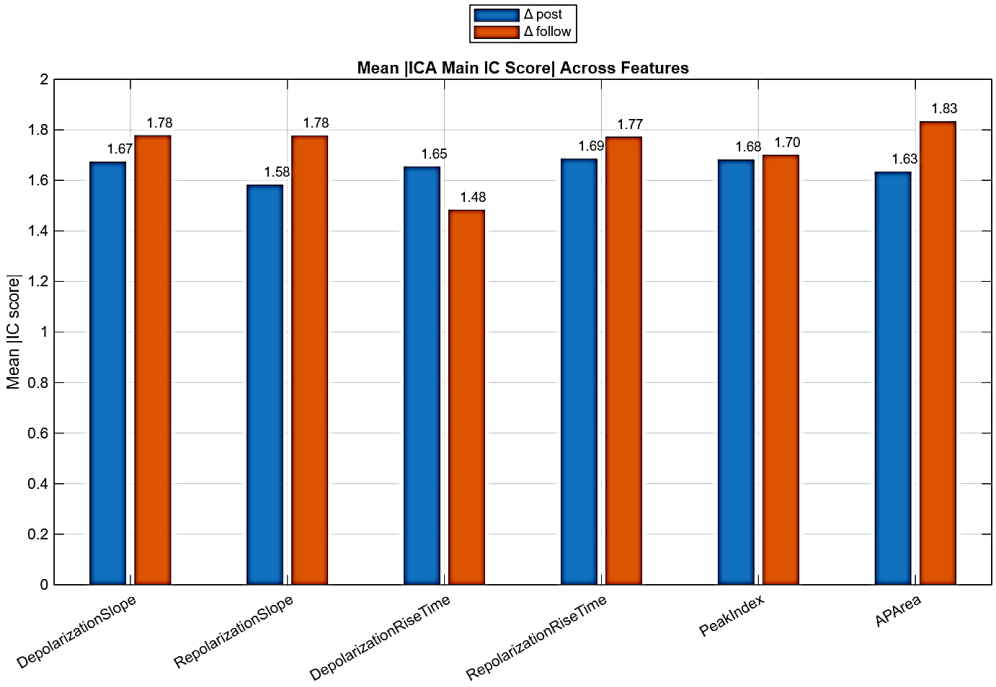

Figure D. 5 Magnitude of ICA component scores

The magnitude of the IC scores, reflected by the mean absolute IC values, showed a consistent increase from Δpost to Δfollow for most features. This trend indicates that the strength of the independent neural patterns continued to increase over time. Relative to the HIS < 2 group, the IC scores were generally higher, suggesting stronger and more pronounced independent signal components in this group.

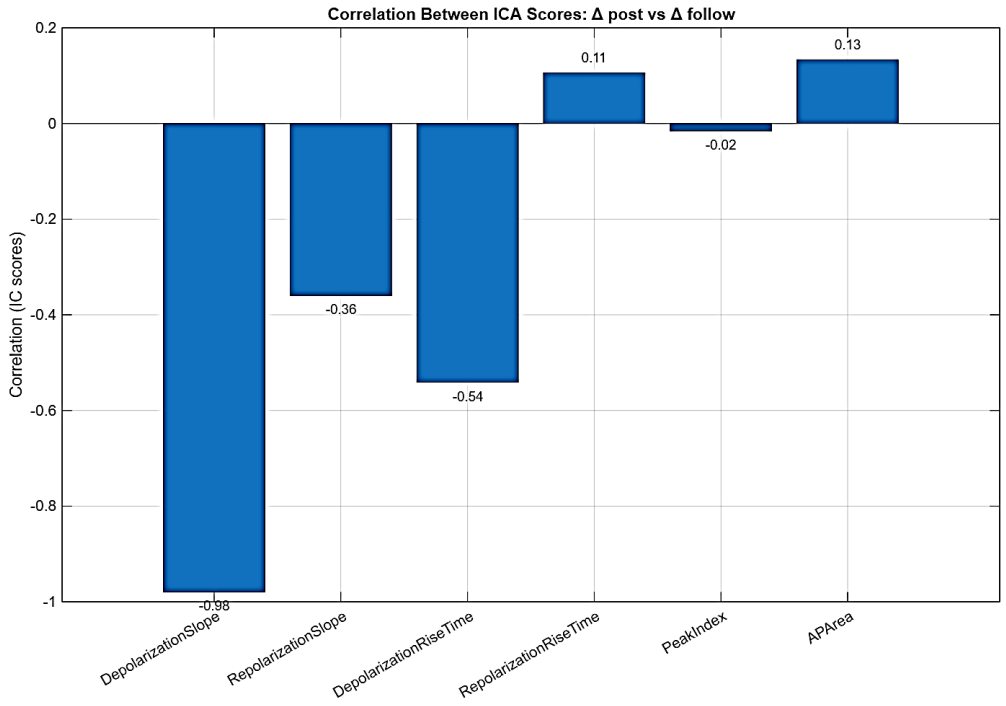

Figure D. 6 Correlation between post-treatment and follow-up ICA patterns

The correlation analysis between IC scores from Δpost and Δfollow revealed a mixed pattern. A strong negative correlation was observed for depolarization slope ($r \approx -0.98$), indicating a reversal in the dominant independent pattern over time. Moderate negative correlations were also present for depolarization rise time ($r \approx -0.54$) and repolarization slope ($r \approx -0.36$). In contrast, repolarization rise time and AP area exhibited weak positive correlations, while peak index remained near zero. These findings suggest that, although independent components are stronger in this group, their temporal stability varies across features, with some features showing persistence and others showing substantial reorganization.

Feature	Top 5 segments - Δpost	Top 5 segments - Δfollow
Depolarization Slope	RAL_onBB | RAL_BG | PRL_RTConBB | PRL_onBB | PRL_RTConAA	UAR_RTConAA | CAR_onAA | PUR_onBB | BAL_RTConAA | IAR_RTCBG

Repolarization Slope	IAL_onAA | BAR_BG | IAL_RTCBG | UAL_RTCBG | PRL_RTConAA	UAL_RTCBG | RAR_onAA | RAR_RTConBB | PRR_RTCBG | CAR_onAA
Depolarization Rise Time	BAR_RTConAA | PUR_onBB | PUL_onAA | UAR_RTConAA | UAR_RTConBB	UAR_RTConAA | CAR_onAA | CAR_BG | UAR_RTCBG | PUL_RTConAA
Repolarization Rise Time	PRL_onBB | RAL_onBB | CAL_onBB | IAL_RTConAA | IAR_RTConBB	PUL_RTConAA | PUL_BG | BAR_RTConBB | UAL_RTCBG | CAL_RTConBB
Peak Index	BAR_BG | IAL_onBB | RAL_BG | PRR_RTConBB | UAR_onAA	PUR_onBB | PRL_onBB | IAR_RTConAA | PRR_RTConAA | UAR_RTConAA
AP Area	BAR_RTConBB | PUL_onAA | CAR_RTConBB | UAR_RTCBG | CAR_RTCBG	UAL_RTConBB | RAR_RTConBB | CAR_onBB | PRR_RTCBG | PRR_RTConAA

Table D. 2 Distribution of dominant segments and tilts

Examination of the dominant contributing segments revealed that the most informative segments were again primarily associated with RTC phases, particularly acceleration and deceleration components. However, compared to the HIS < 2 group, there was a stronger representation of supine position tilts, especially PUL and PRR movements, indicating a shift toward posterior vestibular dominance in participants with higher cerebrovascular burden.

These results suggest that, in participants with higher cerebrovascular burden, independent EVestG signal patterns are stronger and more globally distributed, but exhibit feature-dependent temporal stability, reflecting a more complex and dynamic reorganization of vestibular-related neural activity following cognitive exercises.

Appendix E Improved versus Non-Improved

This appendix presents the averaged AP area for participants separated into improved and non-improved subgroups based on their ADAS-Cog response. Participants were classified as improved if their ADAS-Cog total score decreased by one point or more from baseline to post-treatment, and as non-improved otherwise (no change or an increase). This ≥1-point threshold, and the inclusion of "no change" within the non-improved group, follow the responder definition used in the related EVestG study [33], adopted here for methodological consistency. AP area was averaged across all 42 left-ear segments for each participant at each session.

AP area is presented as a single representative feature rather than the full feature set. It was used as a gating feature: because AP area provides an interpretable, general indicator of waveform narrowing and widening, it was examined first to determine whether response-based grouping produced differences large enough to justify analyzing additional features. As shown below, the differences were modest, which is why the remaining waveform features were not pursued within this framework. All comparisons in this appendix are descriptive and exploratory; given the small per-cell sample sizes, no inferential claims are made.

E.1 Improved versus non-improved (no HIS subgrouping)

In the active tACS+CE condition, improved participants (N = 8) showed a gradual decrease in mean AP area across sessions (22.54 → 21.26 → 20.96), whereas non-improved participants (N = 9) remained elevated and showed no comparable decline across all sessions (24.14 → 24.35 → 23.76). In the sham tACS+CE condition, improved participants (N = 8) showed a small, steady decrease (21.28 → 20.96 → 20.75), while non-improved participants (N = 9) showed a reduction at post-treatment followed by a partial rebound at follow-up (21.57 → 19.40 → 20.84). Across both conditions, improved participants tended toward lower and more consistently declining AP-

area values than non-improved participants, the effect being clearest in the active condition. To assess whether these differences were statistically reliable, improved and non-improved participants were compared at each session using a two-way ANOVA (treatment response group × session) and independent-samples comparisons at each timepoint. None of the comparisons reached statistical significance in either condition. The only comparison approaching significance was at post-treatment in the active tACS+CE condition, where the improved subgroup showed a lower mean AP area than the non-improved subgroup (21.26 vs 24.35; $p = 0.054$). The two groups did not differ at baseline in either condition, or significant differences were observed at follow-up. Although these differences did not reach significance, the direction of the trends was consistent across sessions in the active condition, with improved participants showing lower AP-area values. Given the small subgroup sizes, these results are reported as exploratory and descriptive only and motivated the further HIS subdivision reported next.

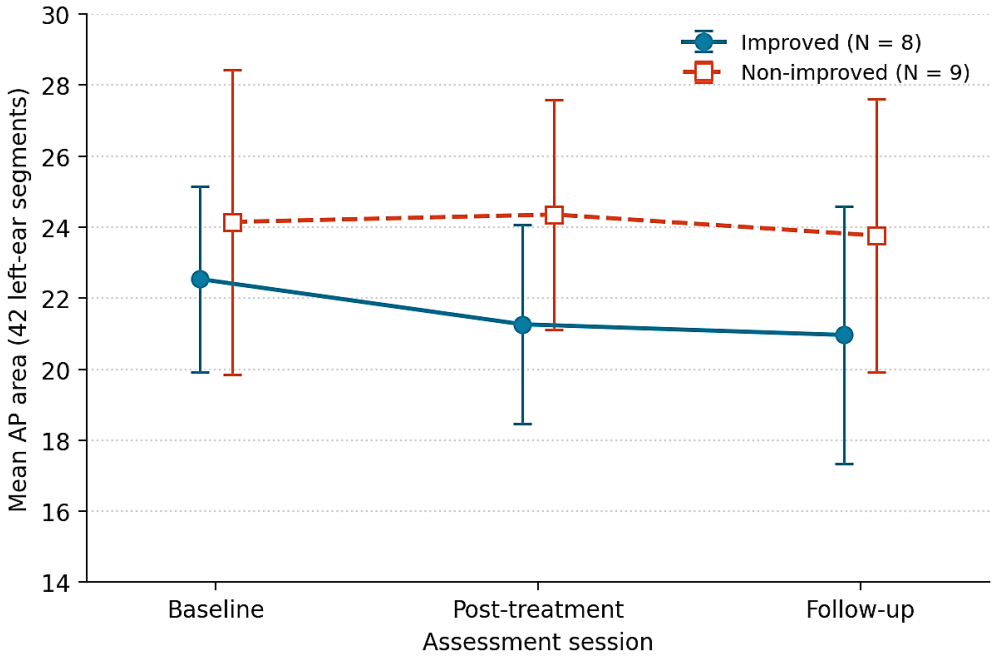

Figure E. 1 Mean AP area (averaged across 42 left-ear segments) for improved (N = 8) and non-improved (N = 9) participants in the active tACS+CE condition, across baseline, post-treatment, and follow-up sessions. Error bars represent standard deviation.

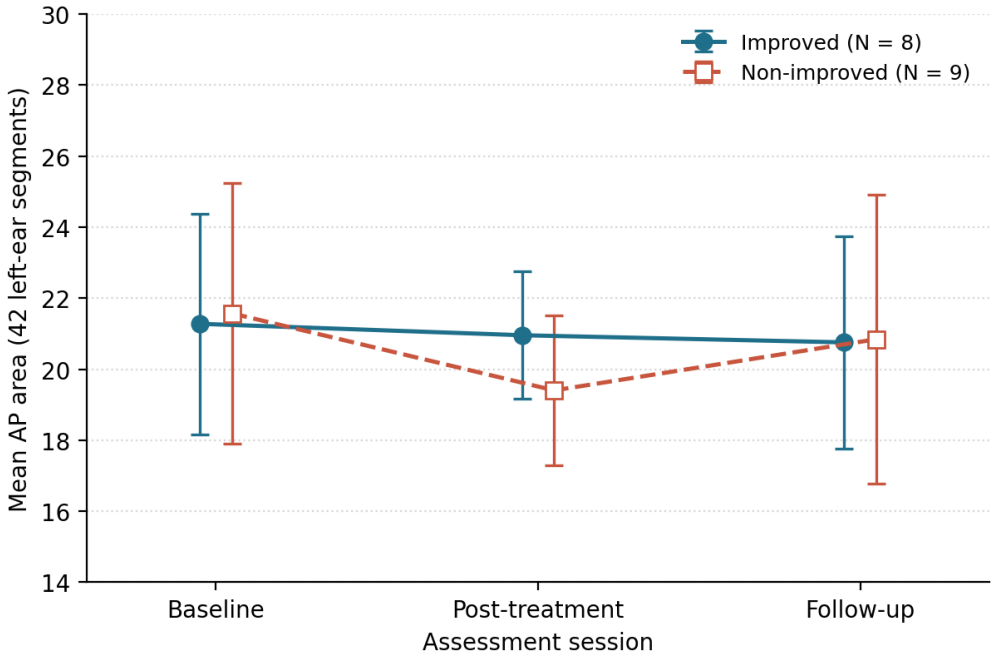

Figure E. 2 Mean AP area (averaged across 42 left-ear segments) for improved (N = 8) and non-improved (N = 9) participants in the sham tACS+CE condition, across baseline, post-treatment, and follow-up sessions. Error bars represent standard deviation

E.2 Improved versus non-improved, with HIS subgrouping

When the improved and non-improved subgroups were further divided by the HIS threshold (HIS < 2 vs HIS ≥ 2), the per-cell sample sizes became very small (N = 2 to 7; Table E.1), with one cell reduced to a single valid baseline value. The corresponding AP-area means are reported in Table E.1 for completeness. No consistent or sufficiently large pattern emerged across these cells, and the limited cell sizes preclude any statistical analysis or reliable interpretation. This underpowering is the reason the HIS-classified responder analysis was not carried forward in the main results; it is shown here to document that the response-based grouping was investigated both with and without HIS stratification. The HIS-based classification used throughout the main analysis proved the more informative grouping, as reflected in the results of Chapters 4 and 5.

Condition	Group	HIS	N	Baseline	Post-treatment	Follow-up
Active	Improved	< 2	4	23.07 (1.78)	21.10 (2.06)	19.28 (3.18)
Active	Improved	≥ 2	4	22.14 (3.32)	20.91 (3.86)	24.37 (1.26)
Active	Non-improved	< 2	7	23.93 (4.41)	24.49 (3.45)	23.03 (3.90)
Active	Non-improved	≥ 2	2	21.09 (—)*	22.38 (1.36)	20.36 (4.10)
Sham	Improved	< 2	4	20.06 (1.12)	21.60 (1.42)	20.00 (2.97)
Sham	Improved	≥ 2	4	22.49 (4.16)	20.31 (2.10)	21.50 (3.26)
Sham	Non-improved	< 2	7	21.87 (3.76)	19.94 (1.99)	20.17 (2.10)
Sham	Non-improved	≥ 2	2	20.98 (4.19)	18.32 (2.30)	22.19 (8.03)

Table E. 1 Mean AP area (averaged across 42 left-ear segments) for improved and non-improved participants Classified by HIS, under active and sham tACS+CE, at baseline, post-treatment, and follow-up. Values are means with standard deviations in parentheses where computable. All cells are descriptive only; no inferential statistics were applied.

*SD not computable (single valid value at baseline).